Properties of transcranial electrical stimulation artifacts in EEG and MEG recordings

Dissertation

zur Erlangung des Grades eines

Doktors der Naturwissenschaften

der Mathematisch-Naturwissenschaftlichen Fakultät

und

der Medizinischen Fakultät

der Eberhard-Karls-Universität Tübingen

vorgelegt

von

Nima Noury

aus Teheran, Iran

April 2017

Tag der mündlichen Prüfung:	8. Oktober 2018
Dekan der Math.-Nat. Fakultät:	Prof. Dr. W. Rosenstiel
Dekan der Medizinischen Fakultät:	Prof. Dr. I. B. Autenrieth
1. Berichterstatter:	Dr. Markus Siegel
2. Berichterstatter:	Prof. Dr. Christoph Braun

Prüfungskommission:

Prof. Dr. Christoph Braun
Dr. Markus Siegel
Prof. Dr. Peter Thier
Dr. Andreas Bartels

Declaration:

I hereby declare that I have produced the work entitled “Properties of transcranial electrical stimulation artifacts in EEG and MEG recordings”, submitted for the award of a doctorate, on my own (without external help), have used only the sources and aids indicated and have marked passages included from other works, whether verbatim or in content, as such. I swear upon oath that these statements are true and that I have not concealed anything. I am aware that making a false declaration under oath is punishable by a term of imprisonment of up to three years or by a fine.

Tübingen, ...

Date Signature

Table of contents

Abstract 1

1 Introduction 3

2 Brain Stimulation 5

2.1 Invasive stimulation techniques 6

2.2 Non-invasive stimulation techniques 7

2.3 Transcranial Electrical Stimulation (tES) 9

3 Electrophysiological recordings during tES 12

3.1 Available methods for simultaneous tES and M/EEG 13

4 Our results: tES artifacts in EEG and MEG 16

4.1 First paper: amplitude of stimulation artifacts 17

4.2 Second paper: phase of stimulation artifacts 18

4.3 Third paper: reply and physics behind stimulation artifacts 20

5 Summary and discussion 21

5.1 Invasive recordings 21

5.2 Discontinuous closed-loop approaches 22

5.3 Cross-frequency approaches 23

5.4 Accounting for residual artifacts 23

5.5 Computer simulations 25

5.6 Other stimulation methods 25

References 27

6 Manuscripts included in this thesis 36

6.1 Paper 1 36

6.2 Paper 2 53

6.3 Paper 3 70

Acknowledgment 101

Abstract

Transcranial electrical stimulation (tES) is a non-invasive neuromodulation technique applicable to healthy and diseased subjects that can manipulate brain activity for both therapeutic and research purposes. Simultaneous combination of tES with non-invasive brain imaging techniques might be useful for guiding stimulation parameters to influence brain activity efficiently, and for closed-loop stimulation of the brain. Moreover, such a simultaneous observation is necessary to understand mechanisms underlying tES effects at the network level. However, strong stimulation artifacts at the stimulation frequency make such a simultaneous monitoring by means of MEG or EEG (M/EEG) challenging. At commonly used tES strengths, these artifacts are about 1000 times bigger than brain signals recorded by M/EEG. Therefore, sub-optimal removal of stimulation artifacts leads to residual artifacts that could be mistakenly taken as brain signals. Designing optimal artifact-removal methods requires detailed knowledge about properties of artifacts. In this dissertation, we provide this missing fundamental information by carefully analyzing M/EEG signals during tES. We show that, in contrast to previous assumptions, tES artifacts are non-linearly transformed versions of stimulation currents. This non-linearity manifests itself in both the amplitude and the phase of tES artifacts, and is partly dependent on the stimulation frequency. Specifically, we show that each heartbeat and every respiratory breath strongly modulates both the amplitude and the phase of stimulation artifacts, which makes artifacts dependent on the physiological state of the subject. Due to these modulations, tES artifacts are not narrow band, but contaminate recorded signals even 8 Hz beyond the stimulation frequency. Moreover, the spatial pattern of artifacts continuously varies over time, which decreases the performance of artifact-removal methods based on PCA, ICA or beamforming. In light of our findings, we evaluate available artifact-removal pipelines and show that their outputs are contaminated with residual artifacts, which could have potentially driven biological conclusions made using these pipelines. Finally, we discuss consequences of our findings and provide some ideas for future research regarding how to investigate brain activity during tES. In sum, this dissertation reconsiders assumptions regarding tES artifacts in M/EEG and provides missing fundamental information about their properties. Our results could be used to prevent pitfalls of simultaneous tES and M/EEG and to design and evaluate new artifact-removal pipelines.

1 Introduction

Our brains are encased in thick skulls. This is beneficial to protect them, but at the same time makes it challenging for scientists to non-invasively monitor and manipulate brain activity. Nowadays, neuroscientists are equipped with various non-invasive brain imaging techniques that provide different levels of spatial and temporal resolution. Over the last decades, brain imaging techniques like electroencephalography (EEG) and magnetoencephalography (MEG) have been widely used for understanding different aspects of brain function through mainly correlative approaches (Baillet, 2017; Baillet et al., 2001). To further our understanding, new causal approaches are required. For instance, it has been shown that features of neuronal oscillations correlate with different cognitive states (Donner and Siegel, 2011; Siegel et al., 2012). Whether or not neuronal oscillations causally contribute to cognition should be investigated with causal approaches, which requires brain stimulation tools to manipulate brain activity in a controlled manner (Dayan et al., 2013).

Transcranial electrical stimulation (tES) is one of few non-invasive brain stimulation techniques that could be employed to manipulate brain activity in both healthy and diseased subjects (Fertonani and Miniussi, 2016). In this technique, weak, temporally patterned electrical currents are applied to the subject's head. Although most of these currents run through the skin, part of them reach the brain (Huang et al., 2017; Opitz et al., 2016). There is accumulating evidence that tES is capable of modulating different aspects of brain activity, including neuronal oscillations (Vossen et al., 2015; Woods et al., 2016). Online monitoring of brain activity during tES is necessary to understand its immediate neuronal effects. Moreover, simultaneous brain imaging can be used to stimulate the brain in a closed-loop manner to manipulate healthy and diseased brain states (Bergmann et al., 2016). However, strong stimulation artifacts make the simultaneous monitoring of brain activity challenging (Thut et al., 2017).

Despite several attempts by different groups to remove tES stimulation artifacts from simultaneously recorded M/EEG signals (Helfrich et al., 2014; Neuling et al., 2015; Soekadar et al., 2013; Voss et al., 2014), a well-designed and well-evaluated pipeline for monitoring brain activity during tES is still missing. This is to some extent because previous efforts have been made without proper knowledge of the properties of stimulation artifacts. Therefore,

available artifact-removal methods are suboptimal and do not account for pitfalls of simultaneous tES and M/EEG. This dissertation contains a series of publications that provide this fundamental information for the rapidly emerging field of tES. By carefully analyzing EEG and MEG recordings during application of tES, we characterize stimulation artifacts in time and frequency domains, uncover so far unknown nonlinearities in both the amplitude and the phase of tES artifacts, and show that the projection between the artifact sources and recording sensors is time-variant. Moreover, we critically reconsider recent findings by other research groups and show that disregarding these features might have led to false positive results.

The first part of this dissertation aims to provide a brief general overview about various available invasive and non-invasive brain stimulation techniques. This includes a section focusing in more detail on tES. In the second part, we discuss benefits of monitoring brain activity during electrical stimulation, and briefly present available pipelines designed by various research groups for such an online monitoring. In the third part, we first point to the fact that all available methods are built upon untested assumptions. Next, we go through our papers and present our main findings regarding stimulation artifacts. Finally, we discuss consequences of our findings and, in their light, provide an outlook regarding possible ways to use brain-imaging techniques during tES.

2 Brain Stimulation

When we listen to a motivating TED talk, drink a cup of coffee, or take a Diazepam, we induce some changes in our brain activity. In that sense, we are all the time modulating our and others' brain activities. In neuroscience, neuromodulation, neurostimulation, and brain stimulation are similar terms referring to modulation of specific elements of either central or peripheral nervous systems, typically by electric or electromagnetic fields (Krames et al., 2009; Reti, 2015), for therapeutic, prosthetic, or investigatory purposes (Luan et al., 2014).

Application of electricity for therapeutic purposes has a long history in medicine. In the first century AD, Scribonius Largus used electric shocks generated by the torpedo fish to treat not only gout, but also headache, by applying electric shocks to the forehead (Lewis et al., 2016; Tsoucalas et al., 2014). About two thousand years later, at the end of the 18th century, discoveries by Luigi Galvani on "animal electricity", and the invention of the voltaic pile by Alessandro Volta, gave rise to a series of experiments conducted by Giovanni Aldini, which laid ground for the development of various forms of electrotherapy that were heavily used later in the 19th century (Aldini, 1803; Lewis et al., 2016; Parent, 2004). In one exciting experiment, Aldini transcranially applied electric currents of a voltaic pile to a hospitalized patient suffering from deep melancholy (Figure 1A). The treatment continued for several weeks, after which the patient was apparently completely cured and returned to live a normal life (Aldini, 1803; Parent, 2004).

Since Aldini's experiments, several findings in science, engineering and medicine have given rise to a huge neuromodulation industry with plenty of invasive and non-invasive stimulation techniques (Fregni and Pascual-Leone, 2007; Goroszeniuk and Pang, 2014; Krames et al., 2009; Lewis et al., 2016; Luan et al., 2014; Reti, 2015). Each of these techniques offers specific spatial and temporal resolutions, and requires a specific level of invasiveness (Luan et al., 2014). These properties in turn define which technique will be appropriate for a specific application. We briefly review available stimulation techniques and their applications in the following.

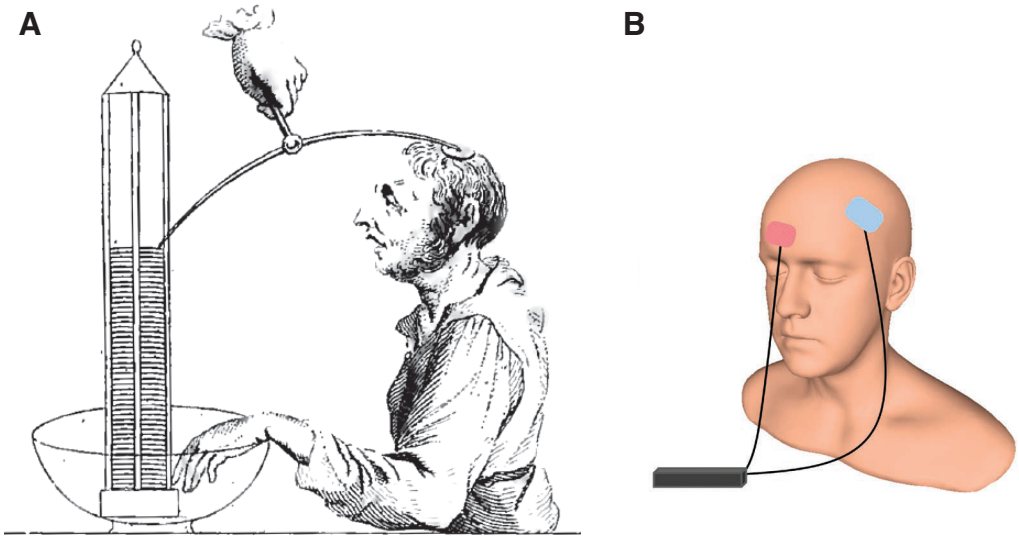

Figure 1. (A) Illustration of the electrical treatment developed by Aldini two centuries ago (Lewis et al., 2016). A patient receives strong electrical currents from a Voltaic pile that is connected to his head and hand. (B) An example of a tES electrode montage. Weak electrical currents are applied to the head through two rubber electrodes.

2.1 Invasive stimulation techniques

Invasive stimulation techniques are traditionally defined as those requiring an incision or insertion of materials into the body (Davis and Koningsbruggen, 2013). Thus, different invasive stimulation techniques require different levels of invasiveness. Examples are subcutaneous implantation of stimulation electrodes, implantation of deep brain stimulation (DBS) electrodes, or even genetic manipulation in optogenetics. Each of these techniques offers a specific level of stimulation focality and selectivity.

Among different invasive stimulation techniques, those that directly apply electrical power to the central or peripheral nervous system are the most widely used ones. By means of electrical currents, these techniques change the membrane potential of neurons, which in turn influences the function of voltage-sensitive channels of neuronal membranes (Brocker and Grill, 2013; Tehovnik, 1996). Apart from influencing neuronal cells, electrical stimulation can also modulate brain activity through its influence on glial cells, especially under conditions of high frequency stimulation (Fenoy et al., 2014).

Invasive electrical stimulation has a wide range of applications. In neuroscience, electrical microstimulation has been widely used to probe neural circuitry and function (Afraz et al., 2006; Clark et al., 2011; Fetsch et al., 2014; Salzman et al., 1990). In medicine, epidural and subdural stimulation has been used to treat chronic neuropathic pain and tinnitus (Tronnier and Rasche, 2013), and DBS is widely used to treat several disorders, including Parkinson's disease, dystonia, essential tremor and obsessive-compulsive disorder (Schwalb and Hamani, 2008; Udupa and Chen, 2015). Finally, invasive electrical stimulation of the central and peripheral nervous system has interesting applications in prosthetics (Capogrosso et al., 2016; Eapen et al., 2017), including cochlear and retina implants (Srinivasan et al., 2010; Zrenner, 2013).

Apart from electrical stimulation, many novel invasive stimulation techniques are under development, including optogenetics (Boyden et al., 2005), micromagnetic stimulation (Park et al., 2013) and thermal stimulation (Duke et al., 2013; Huang et al., 2010). Among them, optogenetics is a technique with high temporal and spatial resolution that neuroscientists widely use for investigatory purposes in animal models (Cardin et al., 2009; Fenno et al., 2011; Kim et al., 2015; Rajasethupathy et al., 2015; Wimmer et al., 2015). Each of these novel techniques faces specific challenges that have to be solved before it can be translated into clinical practice (Lewis et al., 2016; Luan et al., 2014).

2.2 Non-invasive stimulation techniques

Stimulation techniques that do not require an incision or insertion in the body are considered non-invasive brain stimulation techniques. It is noteworthy that this definition has recently been challenged (Davis and Koningsbruggen, 2013). This is due to the low spatial resolution of some techniques, which leads to unintentional stimulation of regions beyond the stimulation target (e.g., see Rossi et al., 2016). According to the traditional definition of non-invasive stimulation techniques, several techniques are available that use electricity, magnetism, or ultrasound waves to non-invasively stimulate the central or peripheral nervous system. Among them, tES and transcranial magnetic stimulation (TMS) are the most commonly used techniques. Compared to invasive stimulation methods, these techniques are applicable to both healthy and diseased subjects. However, this comes at the expense of generally lower spatial resolution and stimulation target selectivity.

Based on Faraday's law, time varying magnetic fields generate electric fields. This is the basic principle underlying TMS, in which strong but short magnetic pulses (about 1 ms long) are generated next to the subject's head. These time-varying magnetic fields induce electrical currents in the subject's brain (Barker, 1991). TMS-induced currents are strong enough to evoke neuronal spikes (Barker et al., 1985). Compared to tES, spatial resolution of TMS for cortical stimulation is quite high (Luan et al., 2014). Moreover, specific coil designs allow stimulation of deep brain structures, although with lower stimulation focality (Deng et al., 2013). However, due to safety concerns and especially in order to prevent triggering of seizures in subjects, application of TMS is restricted to short trains with limited numbers of pulses depending to the stimulation frequency (Rossi et al., 2009).

TMS has a wide range of therapeutic and investigatory applications. There are plenty of different TMS protocols (Dayan et al., 2013; Klooster et al., 2016), among which repetitive TMS (rTMS), i.e. a train of TMS pulses at a specific frequency, has been shown to be effective for the treatment of depression and migraine (Lefaucheur et al., 2014). In neuroscience, TMS has been widely used to causally study neuronal mechanisms underlying various cognitive functions (Parkin et al., 2015; Walsh and Cowey, 2000). This includes not only investigation of the functional role of cortical regions, but also the chronometry of cortical function during a specific task (Pascual-Leone et al., 2000; Sack and Linden, 2003; Veniero et al., 2016), and the role of neuronal oscillations (Romei et al., 2016a, 2011).

Apart from tES and TMS, several novel non-invasive stimulation techniques are available. Low-field magnetic stimulation (LFMS) and low-field synchronized transcranial magnetic stimulation (sTMS) are two techniques that have been used to treat major depression (Leuchter et al., 2015; Rohan et al., 2004, 2014). Both of these techniques use weak magnetic fields to stimulate the brain. In LFMS, the magnetic field is applied at 500 Hz trains that repeat every 2 seconds, while in sTMS the magnetic field is applied at an individual's alpha frequency. The other novel technique that offers very high spatial and temporal cortical stimulation resolution is low-powered transcranial focused ultrasound stimulation (tFUS). Although ultrasound was already used in 1929 to manipulate neuronal activity (Harvey, 1929), it has only recently been used as a transcranial stimulation technique to modulate brain activity in humans (Legon et al., 2014; Mueller et al., 2014). Low-powered tFUS is thought to modulate brain activity through mechanical effects on neuronal

membranes (Lewis et al., 2016). More research on tFUS is required to explore capabilities and limitations of this technique.

2.3 Transcranial Electrical Stimulation (tES)

Electrical brain stimulation has a long history in psychiatry. Since the 19th century, electroconvulsive therapy (ECT) has been widely used to treat various psychiatric disorders, including major depression and mania (Lewis et al., 2016; Reti, 2015). In this method, strong direct or alternating electrical currents are applied to the head to induce a seizure in the patient. Similar to ECT, transcranial electrical stimulation (tES) uses electrical currents to manipulate brain activity (Figure 1B). However, in contrast to ECT, electrical currents used in tES are very weak (about 1 mA) and, when kept below sensation threshold, the subject cannot distinguish between stimulation and sham (i.e. no stimulation) conditions (Ambrus et al., 2012; Gandiga et al., 2006; Wallace et al., 2016). In contrast to TMS, computational models as well as in vivo recordings in nonhuman primates and humans show that tES at usual amplitudes is unable to evoke action potentials in resting neuronal networks (Datta et al., 2009; Opitz et al., 2016; Rahman et al., 2013). Instead, tES slightly modulates neuronal resting membrane potential and cortical excitability (Huang et al., 2017; Kar et al., 2017; Veniero et al., 2016). Under specific conditions, these online modulatory effects lead to synaptic changes that last longer than the stimulation period (Fritsch et al., 2010).

In tES, electrical currents are usually injected into the head through two stimulation electrodes that are attached to the head with conductive gel (Woods et al., 2016). Electrical currents leave one stimulation electrode, go through the body, and reach the other stimulation electrode. Due to the high conductivity of the skin compared to the skull, most of the stimulation current runs through the skin. However, a small part of this current passes the skull and reaches the brain. Invasive recordings from monkeys and human studies suggest that usual tES montages, with two stimulation electrodes and stimulation amplitudes of 1 mA, generate peak stimulation strengths of about 2 V/m. It should be emphasized that the exact peak value is highly dependent on the montage of the stimulation electrodes and on details of the subject's anatomy (Huang et al., 2017; Kar et al., 2017; Opitz et al., 2016). These weak stimulation currents seem to be capable of modulating neural activity (Fritsch et al., 2010; Kar et al., 2017; Ozen et al., 2010). For example, it has

been shown that week transcranially applied electric fields are able to entrain cortical neuronal populations in rats (Ozen et al., 2010).

High conductivity of the skin compared to the skull not only weakens the current that reaches the brain, but also strongly decreases stimulation focality. This poor stimulation focality can be improved by optimizing the placement of stimulation electrodes (Dmochowski et al., 2011; Ruffini et al., 2014; Villamar et al., 2013). These optimizations are based on finite element method (FEM) computer simulations, in which the pattern of distribution of stimulation currents in the head can be predicted for each arrangement of stimulation electrodes. Consequently, one can search for the arrangement that provides the best pattern of current distribution. In fact, when details of a subject's anatomy are taken into account for optimizing electrode placement, stimulation focality can be improved by a factor of two (Dmochowski et al., 2011).

Different tES methods apply different waveforms to the brain. Transcranial direct current stimulation (tDCS), transcranial alternating current stimulation (tACS), and transcranial random noise stimulation (tRNS) are three commonly used tES methods. The most well-known tES method, tDCS, applies direct electrical currents to the head (Nitsche and Paulus, 2000). During tDCS, cortical neurons close to positive (anodal) and negative (cathodal) electrodes on average experience slight depolarization and hyperpolarization, respectively, but the details of each neuron's modulation are dependent on the exact shape of local cortical folding and the neuron's morphology (Rahman et al., 2013). tACS and tRNS use time varying stimulation currents. In tACS, the applied current has a fixed frequency, which is usually set to one of the oscillatory frequencies of the stimulated cortical region (Antal et al., 2008). In tRNS, the stimulation current is a white noise signal with a bandwidth of a couple of hundred Hertz (Terney et al., 2008). Therefore, in tACS and tRNS, neuronal membranes will not experience a constant depolarization or hyperpolarization, but a time varying modulation pattern. It is believed that these time varying modulations interact with the endogenous cortical oscillations and result in oscillatory entrainment and/or resonance (Miniussi et al., 2013; Schmidt et al., 2014).

Over the last two decades, transcranial electrical stimulation methods, especially tDCS and tACS, have been widely used to manipulate brain activity. Long lasting changes in the excitability of motor cortex following tDCS was the first reported effect of tDCS (Antal et al.,

2008; Nitsche and Paulus, 2000). This observation led to plenty of tES experiments to study and influence various aspects of brain function like memory consolidation (Lustenberger et al., 2016; Marshall et al., 2006), working memory (Violante et al., 2017), motion perception (Antal et al., 2004b), motor learning (Reis and Fritsch, 2011; Zimerman et al., 2013), decision making (Bogdanov et al., 2017; Polanía et al., 2015), disorders including Parkinson's disease (Brittain et al., 2013), depression (Fregni et al., 2006), dystonia (Furuya et al., 2014), schizophrenia (Reinhart et al., 2015), and neural mechanisms such as cortical oscillations (Polanía et al., 2012; Vossen et al., 2015; Zaehle et al., 2010). It should be noted that the wide spectrum of claimed effects, inter-subject variability, and lack of replication studies have made many researchers question the validity of some of the findings (Bestmann et al., 2015; Dubljević et al., 2014; Horvath et al., 2015; Parkin et al., 2015). Future research using tES should address these issues by standardizing stimulation protocols and optimizing tES parameters (Bestmann et al., 2015; Fertonani and Miniussi, 2016; Minarik et al., 2016; Romei et al., 2016b) before tES makes its way as a reliable therapeutic tool into the clinics (Brunoni et al., 2012).

It should be noted that to date no cases of tES induced seizure or brain damage have been reported. This is in contrast to TMS and suggests that tES is a safer method than TMS (Woods et al., 2016). In fact, tES could be used continuously for intervals of as along as 20 minutes, while TMS could be applied only discontinuously and for a restricted number of pulses. This feature, together with the high flexibility in defining stimulation currents, makes tES a potent neuromodulation technique that could not be replaced by TMS. Taken together, each of these techniques has unique features that meet requirements of specific applications. Overall, TMS fits applications that require strong and focal stimulation pulses, while tES meets requirements of applications that require slight but long and continuous excitability modulation of specific cortical regions with a specific temporal pattern.

3 Electrophysiological recordings during tES

To understand the immediate effects of tES at the network level, one needs to monitor physiological effects of tES by means of neuroimaging techniques (Miniussi et al., 2012). EEG and MEG are two widely used neuroimaging techniques that offer high temporal resolution. However, the physics behind EEG and MEG make them challenging to use during application of tES. This is because tES generates huge artifactual electrical currents that interfere with the electrical currents of interest produced by brain activity. These artifacts might even exceed the dynamic range of common recording systems. Even when recording devices provide the dynamic range to accommodate stimulation artifacts, EEG and MEG signals recorded during tES contain both brain signals and tES artifacts, which makes them hard to dissociate. Due to these technical issues, measurement of EEG and MEG in tES studies has mostly been limited to the study of tES after-effects (Miniussi et al., 2012; Thut et al., 2017).

Monitoring brain activity after application of tES has been shown to be useful for studying brain function and understanding mechanisms underlying tES effects (Antal et al., 2004a; Marshall et al., 2004; Polanía et al., 2011; Veniero et al., 2016). However, answering other specific questions requires simultaneous recordings (Miniussi et al., 2012). One example are neuronal oscillations. The causal role of the amplitude and phase of neuronal oscillations in various brain functions has been widely discussed in the last decades (Buzsáki and Draguhn, 2004; Siegel et al., 2012). One approach to study this topic is to manipulate oscillations by means of brain stimulation techniques and to probe correlated changes in behavior. In fact, several in vivo and in vitro studies suggest that electrical fields at specific frequencies are capable of entraining neuronal oscillations (Fröhlich and McCormick, 2010; Ozen et al., 2010; Schmidt et al., 2014). However, it is not clear whether weak tACS currents are able to entrain brain activity in humans. Therefore, application of tACS to study the causal role of neuronal oscillations in humans requires simultaneous monitoring of brain activity oscillations by means of EEG or MEG to check for the presence and strength of potential tACS-induced entrainments (Thut et al., 2017; Vossen et al., 2015).

Apart from purely experimental applications, simultaneous recordings make it possible to fine-tune stimulation parameters during the experiment. This might be useful not only to magnify tES effects by optimizing stimulation parameters (Romei et al., 2016b), but also give

rise to new closed-loop applications (Bergmann et al., 2016; Thut et al., 2017). For example, it has been shown that closed-loop stimulation of the motor cortex by means of tACS and phase-locked to the ongoing tremor is able to significantly suppress Parkinsonian tremor (Brittain et al., 2013). Although that study did not directly make use of brain activity during stimulation, one can think of similar experiments using EEG or MEG signals (Bergmann et al., 2016). For instance, short trains of tACS triggered by sleep spindles has been shown to enhance motor memory consolidation (Lustenberger et al., 2016).

Over the last couple of years, there have been several efforts to monitor EEG or MEG signals during tES. Each of these methods takes a different approach to remove stimulation artifacts. Next, we briefly explain them.

3.1 Available methods for simultaneous tES and M/EEG

EEG and MEG recordings during tES are contaminated by huge stimulation artifacts that have to be removed before one is able to look at brain activity (Soekadar et al., 2016). These stimulation artifacts, which look similar to the stimulation current of tES, in some sensors can be up to 1000 times bigger than normal brain signals and might exceed the dynamic range of common EEG recording devices. Therefore, expected artifact strengths should be considered before choosing an appropriate EEG device (Miniussi et al., 2012). Based on the exact features of the desired application, the required artifact-removal method might have different levels of complexity. For example, if the stimulation frequency does not overlap with the frequency band of relevant brain activity, a simple filtering might be enough for artifact-removal (Marshall et al., 2004). Here, we are interested in methods that aim to remove stimulation artifacts at the stimulation and nearby frequencies. Such methods could be used to study how brain oscillations at the stimulation frequency respond to tACS. In particular, these methods could be used to study potential entrainment of neural oscillations by means of tACS (Vossen et al., 2015). Over the last couple of years, several groups have developed methods to look into EEG and MEG recordings at tES stimulation frequency (Helfrich et al., 2014; Neuling et al., 2015; Soekadar et al., 2013; Voss et al., 2014) that we briefly explain below.

Strong magnetic fields might damage MEG sensors. This is why until recently researchers did not consider using tES inside MEG systems. In a pioneering study, Soekadar et al. (2013)

showed that, under specific conditions, tES could be combined with MEG. Further on, they suggested that beamforming might be able to remove stimulation artifacts. Beamforming is a spatial filtering technique in which signals of MEG sensors are combined in an optimal manner to estimate electrical sources of magnetic fields inside the brain (Van Veen et al., 1997). Because tES artifact sources are localized outside the brain (i.e., currents in wires and on the skin), Soekadar et al. argued that tES artifacts would not affect beamforming results. Further on, they verified this idea in a tDCS experiment on a phantom. Based on this study, Neuling et al. (2015) applied beamforming to MEG signals recorded during 10 Hz tACS to remove stimulation artifacts. They showed that the visual alpha power increase that results from eye closure could be detected in beamformed signals of both sham and tACS conditions. Neuling and colleagues took this observation as evidence in favor of the idea that source-level signals estimated by beamforming are free from artifacts.

In another study, Helfrich et al. (2014) adopted a method, which was originally designed for cleaning fMRI artifacts from EEG recordings (Niazy et al., 2005), to remove tACS artifacts from EEG. This method consists of three steps. In the first step, each channel's data is chopped into epochs that contain a desired natural number of tACS stimulation cycles. Next, for each channel, a weighted temporal average of neighboring epochs is subtracted from each epoch of EEG data. This step removes a substantial amount of artifact that neighboring epochs have in common. Finally, principle component analysis is applied to data from all sensors. After detecting artifactual components based on their spatial topography, these components are discarded (two components on average) and the rest of the components are projected back to obtain sensor-level EEG signals. Helfrich et al. evaluated the performance of this method through simulations. In their simulation, they considered each sensor's artifact to be a linearly transformed version of the stimulation current, and concluded that their method successfully removes stimulation artifacts. Using this method, Helfrich et al. (2014) claimed to observe entrainment of alpha band brain activity during 10 Hz tACS.

Finally, Voss et al. (2014) designed a two-step pipeline to remove tACS artifacts from EEG recordings during sleep. They first subtracted a template signal from an EEG channel of interest that was corrupted by artifacts. This template was constructed by scaling and phase shifting the average signal of two channels in the neighborhood of the desired channel. This

step removed most tACS artifacts. To account for residual artifacts, Voss et al. applied band-stop digital filters to the output of the first step. Similar to Soekadar et al. (2013), the authors verified this method by means of a dummy experiment. Based on behavioral results, the authors claimed that tACS applied at 40 Hz is able to induce self-awareness in dreams. Moreover, using this artifact cleaning method, they claimed that EEG signals during 40 Hz tACS show an increase in gamma band power only when subjects report experience of self-awareness in sleep. Voss et al. took these findings as evidence supporting the causal role of gamma band neural oscillations in higher-order consciousness.

4 Our results: tES artifacts in EEG and MEG

All available tES artifact-removal methods are developed based on the assumption that stimulation artifacts are linearly transformed versions of stimulation currents. This assumption manifests itself in how various groups verify their methods by means of simulations and phantom experiments. In phantom experiments, artifact-cleaning methods are applied to EEG or MEG signals recorded from a dummy during application of tES. The rational is that, if an artifact-cleaning method successfully removes tES artifacts in a dummy experiment, cleaned outputs should contain only signals from known sources positioned inside the dummy (Neuling et al., 2017; Soekadar et al., 2013; Voss et al., 2014). A similar approach is taken in verifications based on simulation. Here, the simulated signal of each sensor is set equal to a scaled version of the stimulation current (Helfrich et al., 2014). Importantly, the validity of these assumptions and verification methods has not been investigated by any of these studies (Noury et al., 2016). In other words, these methods have been designed to remove stimulation artifacts, despite the fact that properties of stimulation artifacts were not studied beforehand. Consequently, all these methods were developed based on subjective feelings about how clean processed outputs look like. This fundamental problem might lead to false positive findings driven by complex behaving residual artifacts, which could be mistaken as neural signals (Noury et al., 2016). Therefore, we set out to, for the first time, systematically characterize tACS and tDCS artifacts in EEG and MEG.

We recorded EEG and MEG signals in 4 subjects during application of 11 Hz tACS, 62 Hz tACS, and no stimulation (sham) conditions. Stimulation currents with 1 mA peak-to-peak strength were applied through Ag/AgCl EEG electrodes and 12 minutes of data per stimulation condition was recorded from each subject. Subjects were asked to fixate on a red dot at the center of the screen. To check the influence of stimulation electrodes on tES artifacts, in one control experiment we recorded EEG and MEG signals during tACS that was applied with commonly used large rubber electrodes. In another control experiment, we recorded EEG and MEG signals during tDCS to compare tDCS artifacts with tACS artifacts. In all the above experiments, EEG and MEG signals were recorded simultaneously. Therefore, in the last control experiment we recorded MEG but not EEG signals during tACS to check whether observed artifacts in MEG were dependent on the EEG device or EEG electrodes.

Importantly, in all experiments, we recorded ECG and respiratory signals of subjects in parallel to EEG and MEG signals.

4.1 First paper: amplitude of stimulation artifacts

In our first paper (Noury et al., 2016), we showed that contrary to previous assumptions tES artifacts do not simply reflect stimulation currents, but that they are amplitude-modulated versions of stimulation currents. These modulations are locked to the subject's physiological processes. In other words, we showed that although the tACS stimulation current is a sinusoidal wave with constant amplitude during the experiment, tACS artifacts in EEG and MEG signals are sinusoidal waves with time-varying amplitudes. The rhythmic part of these modulations is locked to the heartbeat and the respiratory cycle, and for most sensors, their strength is even bigger than normal EEG and MEG signals. Therefore, they cannot be discarded in the design and verification of artifact-removal methods. Moreover, we showed that these modulations happen irrespective of the stimulation frequency. Therefore, because tDCS can be seen as a special case of tACS with 0 Hz stimulation frequency, we predicted that the same modulations take place during tDCS. Indeed, this is what our tDCS experiment showed.

Most tES experiments use large rubber stimulation electrodes. Therefore, in a control experiment, we checked whether the observed nonlinear artifacts might be due to our small Ag/AgCl stimulation electrodes. We found that these modulations are not due to the size of stimulation electrodes.

From the independence of artifactual modulations from stimulation electrode type, stimulation electrode size, or stimulation waveform shape, we concluded that these modulations are results of time-varying body resistance and head position. We showed that, due to these continuous modulations, the mapping between artifact sources and recording sensors is time-variant. In other words, since the spatial pattern of tES artifacts continuously varies over time, algorithms like PCA or ICA are unable to capture tES artifacts in few components. Moreover, we showed that, in contrast to previous assumptions, tACS and tDCS artifacts are not narrow-band. This is because heartbeat and respiration-induced modulations are not sinusoidal. In fact, tACS artifacts contaminate power spectra of

recordings in a symmetric manner and are detectable at frequencies even 8 Hz beyond the stimulation frequency.

None of the currently available artifact-removal techniques has been designed to deal with either nonlinear and time-variant artifact modulations or the artifacts' dependence on the subject's physiological state. Moreover, none of the verification methods used to test the performance of these techniques is sensitive to the artifact's amplitude modulations. Therefore, in the next step we evaluated the performance of available artifact cleaning methods (Helfrich et al., 2014; Neuling et al., 2015; Soekadar et al., 2013; Voss et al., 2014). We used our findings as landmarks to track tES artifacts over different stages of artifact-removal pipelines, and to check whether the output of these pipelines is free from artifacts. In fact, we found that none of the above methods accounts for the features of tES artifacts that we described, and that their outputs are contaminated with residual artifacts. In addition, we showed that, because of the complex nature of tES artifacts and their dependence on the subject's physiological state, residual artifacts are prone to be mistaken as neural entrainment.

4.2 Second paper: phase of stimulation artifacts

In the second paper (Noury and Siegel, 2017), we extended our work by characterizing the phase of tACS stimulation artifacts in EEG and MEG recordings. It is generally assumed that sinusoidal stimulation artifacts of different channels show either zero or 180 degree phase shifts relative to the injected stimulation current. However, by carefully analyzing the phase of the recorded signals, we realized that the phase of EEG and MEG signals during tACS shows tiny, but stable, deflections from the expected zero or 180 degree phases. Moreover, we showed that the size of each channel's phase deflection is dependent on both the frequency and the strength of the stimulation artifact. Importantly, we found that these phase deflections are not due to brain activity, but that they result from a nonlinear mechanism that shifts the phase of the sinusoidal stimulation artifacts. Although these phase deflections are very small, their effective strength is often several times bigger than the brain signals. In other words, discarding them leads to residual artifacts bigger than brain signals at the sensor level. Thus, these phase deflections have to be accounted for in artifact-removal methods.

The average value of each channel's phase deflection is stable over minutes. However, the artifact's phase jitters on faster time scales. By analyzing phase variations over time, we found that the artifact's phase is modulated locked to heartbeat and respiration. Although much weaker than the average phase deflections, the effective strength of these phase modulations is comparable to normal EEG and MEG signals. These phase modulations add another dimension to the dependence of tES artifacts on the subject's physiological state.

We further discussed mechanisms underlying artifactual phase features. Especially, for the case of EEG we explained how these phase features arise from known physical properties of EEG electrodes and EEG electronics. By presenting an electrical model, we showed that these phase features happen mainly due to small capacitive effects at contact points of EEG electrodes and skin. This model explains several features of the artifact's phase, including its dependence on the stimulation frequency.

Knowledge about artifact features is not only useful for detecting artifacts, but also for simulating them. Therefore, we further summarized findings of the first and second paper in a complex-valued mathematical model. This model transforms the phase and the amplitude of the stimulation current according to the artifact features of the recorded data to simulate stimulation artifacts of various EEG or MEG sensors. These simulated artifacts can be used to evaluate the performance of artifact-removal techniques and to estimate the strength of residual artifacts in processed data. Such evaluations may be useful for interpreting electrophysiological recordings cleaned from artifacts, and for clarifying whether observed effects in artifact-cleaned signals reflect residual artifacts or changes in brain activity.

In sum, our second paper uncovers features of the heretofore disregarded phase of tACS artifacts. Together with the results of our first paper, it explains why artifact-removal methods based on PCA or beamforming fail to completely remove stimulation artifacts. This is simply because these methods assume a time-invariant and non-delayed projection from sources of artifacts to sensors. Our findings show that this assumption does not hold for EEG and MEG recordings during tES. Importantly, because tES artifacts are very strong compared to brain signals, tiny violations of this assumption lead to residual artifacts that are even bigger than usual EEG and MEG signals. Therefore, our results strongly argue for revisiting well-accepted assumptions in the design and verification of tES artifact-removal methods.

4.3 Third paper: reply and physics behind stimulation artifacts

Our third paper is to a large extent a reply to a paper by Neuling et al. (2017), which was published in response to our first paper. In their paper, Neuling et al. raised several points concerning our findings. Mainly, the authors claimed that the artifactual amplitude modulations reported by us happen due to a technical problem at the stimulator level. Despite the fact that we already explicitly addressed this issue in the first paper and showed that such a technical problem does not cause the reported effects, in our third paper we further discussed this point and showed in more detail that such a technical problem did not occur in our experiments. Briefly, we re-analyzed the electrical output current of the stimulation device, and showed that artifact features observed in EEG and MEG are not present in the stimulation current. In other words, the observed artifact features are independent from the stimulation device. To further clarify the properties of tES artifacts, using Ohm's and Biot-Savart laws, we also discussed in detail the physics behind these artifacts and showed that the artifacts' amplitude modulation is independent of the stimulator and happens due to head movement and impedance changes of the body.

5 Summary and discussion

The studies on tDCS and tACS artifacts comprised in this thesis uncover previously unknown nonlinearities, and time and physiological-state dependencies of both, the amplitude and the phase of stimulation artifacts. Our results reveal several pitfalls of investigating EEG and MEG signals recorded during tES, which might result in false positive findings. Therefore, these results should be considered in the design and evaluation of artifact-removal methods and when interpreting outputs of such methods.

Our studies suggest that the problem of removing tES stimulation artifacts from EEG and MEG recordings has been underestimated so far. This holds particularly true for the case of monitoring brain activity at frequencies close to the stimulation frequency. Currently, there is no well-evaluated pipeline available for such a purpose. So far, all efforts for designing such a pipeline have been made without considering the actual properties of the problem. In fact, future efforts should reconsider current assumptions and methodologies. Considering the revealed complexity of the problem, it is also necessary to perform cost-benefit analyses before undertaking further efforts, especially if alternative approaches are available. Next, we discuss such alternatives and also provide some ideas on how to look into brain activity by means of M/EEG during tES.

5.1 Invasive recordings

Various applications require continuous monitoring of brain activity during tES. One interesting example is related to studying the causal roles of neuronal oscillations (Buzsáki and Draguhn, 2004). It has been suggested that tACS might be able to entrain and enhance neuronal oscillations at the stimulation frequency (Fröhlich and McCormick, 2010; Zaehle et al., 2010). In that case, one could manipulate neuronal oscillations and check whether these manipulations have causal effects on brain activity and behavior (Helfrich et al., 2014; Romei et al., 2016b). However, recent evidence questions the capability of weak tACS currents to induce neuronal entrainment in the human brain (Vossen et al., 2015). Therefore, online monitoring of brain activity during tACS with high temporal resolution is necessary for understanding the true effects of tACS on human brain activity.

Such monitoring could be achieved by means of EEG or MEG. This is beneficial, especially because these non-invasive methods can be used in healthy and diseased subjects to

monitor the activity of the entire cortex. However, removing stimulation artifacts seems to be much more challenging than it was thought to be, and there is no guarantee that further efforts will result in an ideal artifact-removal method. Therefore, it might be easier to do such recordings in patients with implanted electrodes or using animal models (Huang et al., 2017; Kar et al., 2017). Through this approach, one could directly measure the effects of stimulation on the spiking of neurons without the signal being affected by technical artifacts (Kar et al., 2017; Ozen et al., 2010). However, this comes at the expense of using animals for research or strong limitations in recruiting human subjects. Moreover, this approach usually provides information about neuronal activity at few positions in the brain, which might not be enough if understanding effects of tES at the network level is required. Researchers should reconsider costs, benefits, and risks of failure of these approaches before choosing their approach in the future.

5.2 Discontinuous closed-loop approaches

The study of neuronal oscillations is not the only application that requires monitoring of brain activity during stimulation. Accumulating evidence suggests that the effect of tES on brain activity relies on the state and dynamics of cortical networks (Alekseichuk et al., 2016; Fritsch et al., 2010; Fröhlich and McCormick, 2010; Guerra et al., 2016; Romei et al., 2016b; Schmidt et al., 2014). This has motivated several closed-loop brain stimulation paradigms that make use of brain activity or behavior during stimulation to enhance memory consolidation (Lustenberger et al., 2016), control epileptic seizures (Berényi et al., 2012), or suppress Parkinsonian tremor (Brittain et al., 2013). Measurement of EEG or MEG signals during tES might be a powerful approach for such closed-loop brain stimulation paradigms (Bergmann et al., 2016). Although continuous monitoring of EEG or MEG signals at the stimulation frequency might be necessary to suppress or enhance specific neuronal dynamics in a closed-loop manner (Brittain et al., 2013; Fröhlich and McCormick, 2010), less demanding discontinuous monitoring approaches might be sufficient in some other cases. Specifically, EEG or MEG signals in absence of tES might be used to decode specific network states and trigger short stimulation trains. For example, Berényi et al. (2012) monitored electrophysiological recordings to detect epileptic seizures, and further used these events to trigger tES trains to suppress upcoming seizures. Such an approach could also be used for investigatory purposes. For instance, Lustenberger et al. (2016) took a similar approach to

study the role of brain spindles in memory consolidation. Here, spindle events triggered tES trains. In these discontinuous approaches, processing pipelines should only account for transient artifacts that result when stimulation currents are switched off (Marshall et al., 2004; Vossen et al., 2015), which is less challenging than removing artifacts in continuous approaches. In sum, when possible, problems of removing tES artifacts should be reduced by use of its less-demanding versions.

5.3 Cross-frequency approaches

In this dissertation, we focused on electrophysiological recordings at frequency bands that overlap with the stimulation frequency. However, tES at a specific frequency might also influence brain activity at frequency bands far from the stimulation frequency. In fact, many studies suggest that brain rhythms at different frequency bands interact with each other through phase coupling, amplitude coupling, or phase-amplitude coupling (Alekseichuk et al., 2016; Siegel et al., 2012). Therefore, tES at a specific frequency could be used to influence brain rhythms at other frequencies (Alekseichuk et al., 2016). For instance, in a recent example, Witkowski et al. (2016) developed a new stimulation protocol, called AM-tACS, in which tACS at a high carrier frequency (220 Hz) is used to manipulate target brain rhythms at lower frequencies. This has been done through amplitude modulation of the high carrier signal at the frequency of the target brain rhythm. Although it is not yet clear how the physiological effects of this specific stimulation approach compare to conventional tACS, stimulation artifacts of AM-tACS are significantly smaller that artifacts of tACS. In fact, in this case processing pipelines should only remove stimulation sub-harmonics from recordings. Considering their lower amplitude compared to artifacts at the stimulation frequency, removing stimulation sub-harmonics is likely to be less challenging. However, these artifacts have not been investigated so far and future research should consider characterizing them.

5.4 Accounting for residual artifacts

Although it is very challenging to completely remove stimulation artifacts at the stimulation frequency, it is possible to suppress them. In fact, all available artifact-removal methods strongly suppress tES artifacts. One possibility is to diminish the effect of residual artifacts by means of well-designed analysis pipelines. For instance, this can be done by

comparing several experimental conditions with similar levels of residual artifact. This is particularly useful when modulatory effects of tES during specific conditions, states, or at specific time points of an experiment are the matter of investigation (Marshall et al., 2016; Neuling et al., 2015; Voss et al., 2014). For example, one could ask if the amount of gamma power increase due to visual stimulation differs between sham and tES conditions. After using one of the available methods for suppressing stimulation artifacts, one could assume that the same amount of residual artifact exists prior to and after visual stimulation. Therefore, by calculating the difference between average power before and after visual stimulation, an artifact-free estimation of visual gamma power increase during tES could be obtained. Finally, this estimation could be compared with the visual gamma power increase of the sham condition (Marshall et al., 2016).

The main question regarding the aforementioned approach is how to check whether the two conditions contain the same levels of residual artifact. Our results suggest that features of stimulation artifacts depend on the subject's physiological state and, in the case of MEG, head movement. Therefore, by comparing various physiological signals and head movements between conditions, it is possible to check whether the assumption of similar residual artifact levels are justified. There are many situations in which this assumption does not hold. One recent example comes from the study by Voss et al. (2014), in which the authors compare EEG signals recorded during tACS between lucid dreaming and non-lucid dreaming conditions, despite the fact that lucid dreaming is known to influence the physiological state of subjects (LaBerge et al., 1986). Consequently, assuming similar levels of residual artifact in these two conditions is not justified. Therefore, before attributing any observed difference between signals from two conditions to a change in brain activity, the influence of a difference between residual artifacts should be investigated.

Specific measures of brain activity could also cancel out the effect of residual artifacts. In other words, while one specific measure applied to a dataset that contains residual artifacts might result in artifact-free data, another measure applied to the same dataset might result in artifactual outcomes. Here, we emphasize the prominent difference between time domain event-related analysis and frequency domain power analysis, which has been overlooked so far (Helfrich et al., 2014; Neuling et al., 2015). For the case of power analysis, residual artifacts generally lead to a positive bias in power estimates during tACS. This is

because residual artifacts are sinusoidal waves and, irrespective of their phase, their power always adds up to the power of underlying brain activity. This is not the case for time domain event-related analysis, if the stimulation current is not phase-locked to the event of interest. Under this condition, residual artifacts have random phases at each single trial. Therefore, averaging across a large number of trials generates, in a statistical sense, artifact-free event-related signals. However, it should be noted that in this case, residual artifacts effectively increase the noise level across trials. Therefore, the number of trials needed to obtain significant results might be bigger than for experiments without tES. In sum, it is important to realize that obtaining artifact-free results through one measure does not guarantee obtaining valid results through another measure of brain activity.

5.5 Computer simulations

Our findings suggest a model for stimulation artifacts that provides the nonlinear and time-variant transformations that, when applied to the stimulation current, lead to signals that resemble tES artifacts in EEG and MEG. This knowledge can be used for simulating stimulation artifacts. Such simulations could be used not only for designing new artifact-removal methods, but also to evaluate their performance and to estimate features of residual artifacts. Consequently, by comparing these estimates with results obtained from real recordings, one could argue whether the results are reflecting residual artifacts or true brain signals.

5.6 Other stimulation methods

As a final remark, we would like to mention that the last two decades have seen a strong focus on TMS and tES as two powerful non-invasive brain stimulation techniques. However, several new non-invasive brain stimulation techniques are emerging (Lewis et al., 2016). Among them, low-powered transcranial focused ultrasound stimulation (tFUS) is particularly interesting. This is not only because of the high spatial and temporal resolution of this technique, but also because it is unlikely to generate strong artifacts in EEG recordings. Recently, it has been shown that this method is able to transcranially modulate brain activity in humans (Legon et al., 2014; Mueller et al., 2014). Therefore, tFUS might be very suitable for closed-loop brain stimulation approaches that use EEG for online monitoring of brain activity. However, the capabilities of tFUS are not clear yet. For instance, although

tFUS is able to modulate neural event-related responses (Legon et al., 2014), so far its effect on neural oscillations has not been studied. More research on tFUS is required to understand its capabilities in modulating different aspects of brain function.

References

Afraz, S.-R., Kiani, R., Esteky, H., 2006. Microstimulation of inferotemporal cortex influences face categorization. Nature 442, 692–695. doi:10.1038/nature04982

Aldini, G., 1803. An account of the late improvements in galvanism : with a series of curious and interesting experiments performed before the commissioners of the French National Institute, and repeated lately in the anatomical theatres of London [WWW Document]. URL http://library.si.edu/digital-library/book/accountlateimpr00aldi (accessed 11.24.16).

Alekseichuk, I., Turi, Z., Amador de Lara, G., Antal, A., Paulus, W., 2016. Spatial Working Memory in Humans Depends on Theta and High Gamma Synchronization in the Prefrontal Cortex. Curr. Biol. 26, 1513–1521. doi:10.1016/j.cub.2016.04.035

Ambrus, G.G., Al-Moyed, H., Chaieb, L., Sarp, L., Antal, A., Paulus, W., 2012. The fade-in – Short stimulation – Fade out approach to sham tDCS – Reliable at 1 mA for naïve and experienced subjects, but not investigators. Brain Stimulat. 5, 499–504. doi:10.1016/j.brs.2011.12.001

Antal, A., Boros, K., Poreisz, C., Chaieb, L., Terney, D., Paulus, W., 2008. Comparatively weak after-effects of transcranial alternating current stimulation (tACS) on cortical excitability in humans. Brain Stimulat. 1, 97–105. doi:10.1016/j.brs.2007.10.001

Antal, A., Kincses, T.Z., Nitsche, M.A., Bartfai, O., Paulus, W., 2004a. Excitability Changes Induced in the Human Primary Visual Cortex by Transcranial Direct Current Stimulation: Direct Electrophysiological Evidence. Invest. Ophthalmol. Vis. Sci. 45, 702–707. doi:10.1167/iovs.03-0688

Antal, A., Nitsche, M.A., Kruse, W., Kincses, T.Z., Hoffmann, K.-P., Paulus, W., 2004b. Direct current stimulation over V5 enhances visuomotor coordination by improving motion perception in humans. J. Cogn. Neurosci. 16, 521–527. doi:10.1162/089892904323057263

Baillet, S., 2017. Magnetoencephalography for brain electrophysiology and imaging. Nat. Neurosci. 20, 327–339. doi:10.1038/nn.4504

Baillet, S., Mosher, J.C., Leahy, R.M., 2001. Electromagnetic brain mapping. IEEE Signal Process. Mag. 18, 14–30. doi:10.1109/79.962275

Barker, A.T., 1991. An introduction to the basic principles of magnetic nerve stimulation. J. Clin. Neurophysiol. Off. Publ. Am. Electroencephalogr. Soc. 8, 26–37.

Barker, A.T., Jalinous, R., Freeston, I.L., 1985. NON-INVASIVE MAGNETIC STIMULATION OF HUMAN MOTOR CORTEX. The Lancet, Originally published as Volume 1, Issue 8437 325, 1106–1107. doi:10.1016/S0140-6736(85)92413-4

Berényi, A., Belluscio, M., Mao, D., Buzsáki, G., 2012. Closed-Loop Control of Epilepsy by Transcranial Electrical Stimulation. Science 337, 735–737. doi:10.1126/science.1223154

Bergmann, T.O., Karabanov, A., Hartwigsen, G., Thielscher, A., Siebner, H.R., 2016. Combining non-invasive transcranial brain stimulation with neuroimaging and electrophysiology: Current approaches and future perspectives. NeuroImage 140, 4–19. doi:10.1016/j.neuroimage.2016.02.012

Bestmann, S., de Berker, A.O., Bonaiuto, J., 2015. Understanding the behavioural consequences of noninvasive brain stimulation. Trends Cogn. Sci. 19, 13–20. doi:10.1016/j.tics.2014.10.003

Bogdanov, M., Ruff, C.C., Schwabe, L., 2017. Transcranial Stimulation Over the Dorsolateral Prefrontal Cortex Increases the Impact of Past Expenses on Decision-Making. Cereb. Cortex 27, 1094–1102. doi:10.1093/cercor/bhv298

Boyden, E.S., Zhang, F., Bamberg, E., Nagel, G., Deisseroth, K., 2005. Millisecond-timescale, genetically targeted optical control of neural activity. Nat. Neurosci. 8, 1263–1268. doi:10.1038/nn1525

Brittain, J.-S., Probert-Smith, P., Aziz, T.Z., Brown, P., 2013. Tremor suppression by rhythmic transcranial current stimulation. Curr. Biol. CB 23, 436–440. doi:10.1016/j.cub.2013.01.068

Brocker, D.T., Grill, W.M., 2013. Chapter 1 - Principles of electrical stimulation of neural tissue, in: Hallett, A.M.L. and M. (Ed.), Handbook of Clinical Neurology, Brain Stimulation. Elsevier, pp. 3–18.

Brunoni, A.R., Nitsche, M.A., Bolognini, N., Bikson, M., Wagner, T., Merabet, L., Edwards, D.J., Valero-Cabre, A., Rotenberg, A., Pascual-Leone, A., Ferrucci, R., Priori, A., Boggio, P., Fregni, F., 2012. Clinical Research with Transcranial Direct Current Stimulation (tDCS): Challenges and Future Directions. Brain Stimulat. 5, 175–195. doi:10.1016/j.brs.2011.03.002

Buzsáki, G., Draguhn, A., 2004. Neuronal oscillations in cortical networks. Science 304, 1926–1929. doi:10.1126/science.1099745

Capogrosso, M., Milekovic, T., Borton, D., Wagner, F., Moraud, E.M., Mignardot, J.-B., Buse, N., Gandar, J., Barraud, Q., Xing, D., Rey, E., Duis, S., Jianzhong, Y., Ko, W.K.D., Li, Q., Detemple, P., Denison, T., Micera, S., Bezard, E., Bloch, J., Courtine, G., 2016. A brain–spine interface alleviating gait deficits after spinal cord injury in primates. Nature 539, 284–288. doi:10.1038/nature20118

Cardin, J.A., Carlén, M., Meletis, K., Knoblich, U., Zhang, F., Deisseroth, K., Tsai, L.-H., Moore, C.I., 2009. Driving fast-spiking cells induces gamma rhythm and controls sensory responses. Nature 459, 663–667. doi:10.1038/nature08002

Clark, K.L., Armstrong, K.M., Moore, T., 2011. Probing neural circuitry and function with electrical microstimulation. Proc. R. Soc. Lond. B Biol. Sci. rspb20102211. doi:10.1098/rspb.2010.2211

Datta, A., Bansal, V., Diaz, J., Patel, J., Reato, D., Bikson, M., 2009. Gyri –precise head model of transcranial DC stimulation: Improved spatial focality using a ring electrode versus conventional rectangular pad. Brain Stimulat. 2, 201–207. doi:10.1016/j.brs.2009.03.005

Davis, N.J., Koningsbruggen, M.V., 2013. “Non-invasive” brain stimulation is not non-invasive. Front. Syst. Neurosci. 7. doi:10.3389/fnsys.2013.00076

Dayan, E., Censor, N., Buch, E.R., Sandrini, M., Cohen, L.G., 2013. Noninvasive brain stimulation: from physiology to network dynamics and back. Nat. Neurosci. 16, 838–844. doi:10.1038/nn.3422

Deng, Z.-D., Lisanby, S.H., Peterchev, A.V., 2013. Electric field depth–focality tradeoff in transcranial magnetic stimulation: Simulation comparison of 50 coil designs. Brain Stimulat. 6, 1–13. doi:10.1016/j.brs.2012.02.005

Dmochowski, J.P., Datta, A., Bikson, M., Su, Y., Parra, L.C., 2011. Optimized multi-electrode stimulation increases focality and intensity at target. J. Neural Eng. 8, 046011. doi:10.1088/1741-2560/8/4/046011

Donner, T.H., Siegel, M., 2011. A framework for local cortical oscillation patterns. Trends Cogn. Sci. 15, 191–199. doi:10.1016/j.tics.2011.03.007

Dubljević, V., Saigle, V., Racine, E., 2014. The Rising Tide of tDCS in the Media and Academic Literature. Neuron 82, 731–736. doi:10.1016/j.neuron.2014.05.003

Duke, A.R., Jenkins, M.W., Lu, H., McManus, J.M., Chiel, H.J., Jansen, E.D., 2013. Transient and selective suppression of neural activity with infrared light. Sci. Rep. 3, 2600. doi:10.1038/srep02600

Eapen, B.C., Murphy, D.P., Cifu, D.X., 2017. Neuroprosthetics in amputee and brain injury rehabilitation. Exp. Neurol., Bio-electronics and prosthetics for neurological diseases 287, Part 4, 479–485. doi:10.1016/j.expneurol.2016.08.004

Fenno, L., Yizhar, O., Deisseroth, K., 2011. The development and application of optogenetics. Annu. Rev. Neurosci. 34, 389–412. doi:10.1146/annurev-neuro-061010-113817

Fenoy, A.J., Goetz, L., Chabardès, S., Xia, Y., 2014. Deep brain stimulation: Are astrocytes a key driver behind the scene? CNS Neurosci. Ther. 20, 191–201. doi:10.1111/cns.12223

Fertonani, A., Miniussi, C., 2016. Transcranial Electrical Stimulation: What We Know and Do Not Know About Mechanisms. Neurosci. Rev. J. Bringing Neurobiol. Neurol. Psychiatry. doi:10.1177/1073858416631966

Fetsch, C.R., Kiani, R., Newsome, W.T., Shadlen, M.N., 2014. Effects of cortical microstimulation on confidence in a perceptual decision. Neuron 83, 797–804. doi:10.1016/j.neuron.2014.07.011

Fregni, F., Boggio, P.S., Nitsche, M.A., Marcolin, M.A., Rigonatti, S.P., Pascual-Leone, A., 2006. Treatment of major depression with transcranial direct current stimulation. Bipolar Disord. 8, 203–204. doi:10.1111/j.1399-5618.2006.00291.x

Fregni, F., Pascual-Leone, A., 2007. Technology insight: noninvasive brain stimulation in neurology-perspectives on the therapeutic potential of rTMS and tDCS. Nat. Clin. Pract. Neurol. 3, 383–393. doi:10.1038/ncpneuro0530

Fritsch, B., Reis, J., Martinowich, K., Schambra, H.M., Ji, Y., Cohen, L.G., Lu, B., 2010. Direct Current Stimulation Promotes BDNF-Dependent Synaptic Plasticity: Potential Implications for Motor Learning. Neuron 66, 198–204. doi:10.1016/j.neuron.2010.03.035

Fröhlich, F., McCormick, D.A., 2010. Endogenous Electric Fields May Guide Neocortical Network Activity. Neuron 67, 129–143. doi:10.1016/j.neuron.2010.06.005

Furuya, S., Nitsche, M.A., Paulus, W., Altenmüller, E., 2014. Surmounting retraining limits in musicians' dystonia by transcranial stimulation. Ann. Neurol. 75, 700–707. doi:10.1002/ana.24151

Gandiga, P.C., Hummel, F.C., Cohen, L.G., 2006. Transcranial DC stimulation (tDCS): A tool for double-blind sham-controlled clinical studies in brain stimulation. Clin. Neurophysiol. 117, 845–850. doi:10.1016/j.clinph.2005.12.003

Goroszeniuk, T., Pang, D., 2014. Peripheral neuromodulation: a review. Curr. Pain Headache Rep. 18, 412. doi:10.1007/s11916-014-0412-9

Guerra, A., Pogosyan, A., Nowak, M., Tan, H., Ferreri, F., Lazzaro, V.D., Brown, P., 2016. Phase Dependency of the Human Primary Motor Cortex and Cholinergic Inhibition Cancelation During Beta tACS. Cereb. Cortex. doi:10.1093/cercor/bhw245

Harvey, E.N., 1929. The effect of high frequency sound waves on heart muscle and other irritable tissues. Am. J. Physiol.

Helfrich, R.F., Schneider, T.R., Rach, S., Trautmann-Lengsfeld, S.A., Engel, A.K., Herrmann, C.S., 2014. Entrainment of Brain Oscillations by Transcranial Alternating Current Stimulation. Curr. Biol. 24, 333–339. doi:10.1016/j.cub.2013.12.041

Horvath, J.C., Forte, J.D., Carter, O., 2015. Evidence that transcranial direct current stimulation (tDCS) generates little-to-no reliable neurophysiologic effect beyond MEP amplitude modulation in healthy human subjects: A systematic review. Neuropsychologia 66, 213–236. doi:10.1016/j.neuropsychologia.2014.11.021

Huang, H., Delikanli, S., Zeng, H., Ferkey, D.M., Pralle, A., 2010. Remote control of ion channels and neurons through magnetic-field heating of nanoparticles. Nat. Nanotechnol. 5, 602–606. doi:10.1038/nnano.2010.125

Huang, Y., Liu, A.A., Lafon, B., Friedman, D., Dayan, M., Wang, X., Bikson, M., Doyle, W.K., Devinsky, O., Parra, L.C., 2017. Measurements and models of electric fields in the in vivo human brain during transcranial electric stimulation. eLife 6, e18834. doi:10.7554/eLife.18834

Kar, K., Duijnhouwer, J., Krekelberg, B., 2017. Transcranial Alternating Current Stimulation Attenuates Neuronal Adaptation. J. Neurosci. 37, 2325–2335. doi:10.1523/JNEUROSCI.2266-16.2016

Kim, T., Thankachan, S., McKenna, J.T., McNally, J.M., Yang, C., Choi, J.H., Chen, L., Kocsis, B., Deisseroth, K., Strecker, R.E., Basheer, R., Brown, R.E., McCarley, R.W., 2015. Cortically projecting basal forebrain parvalbumin neurons regulate cortical gamma band oscillations. Proc. Natl. Acad. Sci. 112, 3535–3540. doi:10.1073/pnas.1413625112

Klooster, D.C.W., de Louw, A.J.A., Aldenkamp, A.P., Besseling, R.M.H., Mestrom, R.M.C., Carrette, S., Zinger, S., Bergmans, J.W.M., Mess, W.H., Vonck, K., Carrette, E., Breuer, L.E.M., Bernas, A., Tijhuis, A.G., Boon, P., 2016. Technical aspects of neurostimulation: Focus on equipment, electric field modeling, and stimulation protocols. Neurosci. Biobehav. Rev. 65, 113–141. doi:10.1016/j.neubiorev.2016.02.016

Krames, E.S., Peckham, P.H., Rezai, A.R. (Eds.), 2009. Neuromodulation, 1 edition. ed. Academic Press.

LaBerge, S., Levitan, L., Dement, W.C., 1986. Lucid dreaming: Physiological correlates of consciousness during REM sleep. J. Mind Behav. 7, 251–258.

Lefaucheur, J.-P., André-Obadia, N., Antal, A., Ayache, S.S., Baeken, C., Benninger, D.H., Cantello, R.M., Cincotta, M., de Carvalho, M., De Ridder, D., Devanne, H., Di Lazzaro, V., Filipović, S.R., Hummel, F.C., Jääskeläinen, S.K., Kimiskidis, V.K., Koch, G., Langguth, B., Nyffeler, T., Oliviero, A., Padberg, F., Poulet, E., Rossi, S., Rossini, P.M., Rothwell, J.C., Schönfeldt-Lecuona, C., Siebner, H.R., Slotema, C.W., Stagg, C.J., Valls-Sole, J., Ziemann, U., Paulus, W., Garcia-Larrea, L., 2014. Evidence-based guidelines on the therapeutic use of repetitive transcranial magnetic stimulation (rTMS). Clin. Neurophysiol. 125, 2150–2206. doi:10.1016/j.clinph.2014.05.021

Legon, W., Sato, T.F., Opitz, A., Mueller, J., Barbour, A., Williams, A., Tyler, W.J., 2014. Transcranial focused ultrasound modulates the activity of primary somatosensory cortex in humans. Nat. Neurosci. 17, 322–329. doi:10.1038/nn.3620

Leuchter, A.F., Cook, I.A., Feifel, D., Goethe, J.W., Husain, M., Carpenter, L.L., Thase, M.E., Krystal, A.D., Philip, N.S., Bhati, M.T., Burke, W.J., Howland, R.H., Sheline, Y.I., Aaronson, S.T., Iosifescu, D.V., O'Reardon, J.P., Gilmer, W.S., Jain, R., Burgoyne, K.S., Phillips, B., Manberg, P.J., Massaro, J., Hunter, A.M., Lisanby, S.H., George, M.S., 2015. Efficacy and Safety of Low-field Synchronized Transcranial Magnetic Stimulation (sTMS) for Treatment of Major Depression. Brain Stimulat. 8, 787–794. doi:10.1016/j.brs.2015.05.005

Lewis, P.M., Thomson, R.H., Rosenfeld, J.V., Fitzgerald, P.B., 2016. Brain Neuromodulation Techniques A Review. The Neuroscientist 1073858416646707. doi:10.1177/1073858416646707

Luan, S., Williams, I., Nikolic, K., Constandinou, T.G., 2014. Neuromodulation: present and emerging methods. Front. Neuroengineering 7. doi:10.3389/fneng.2014.00027

Lustenberger, C., Boyle, M.R., Alagapan, S., Mellin, J.M., Vaughn, B.V., Fröhlich, F., 2016. Feedback-Controlled Transcranial Alternating Current Stimulation Reveals a Functional Role of Sleep Spindles in Motor Memory Consolidation. Curr. Biol. 26, 2127–2136. doi:10.1016/j.cub.2016.06.044

Marshall, L., Helgadóttir, H., Mölle, M., Born, J., 2006. Boosting slow oscillations during sleep potentiates memory. Nature 444, 610–613. doi:10.1038/nature05278

Marshall, L., Mölle, M., Hallschmid, M., Born, J., 2004. Transcranial direct current stimulation during sleep improves declarative memory. J. Neurosci. Off. J. Soc. Neurosci. 24, 9985–9992. doi:10.1523/JNEUROSCI.2725-04.2004

Marshall, T.R., Esterer, S., Herring, J.D., Bergmann, T.O., Jensen, O., 2016. On the relationship between cortical excitability and visual oscillatory responses - A concurrent tDCS-MEG study. NeuroImage 140, 41–49. doi:10.1016/j.neuroimage.2015.09.069

Minarik, T., Berger, B., Althaus, L., Bader, V., Biebl, B., Brotzeller, F., Fusban, T., Hegemann, J., Jesteadt, L., Kalweit, L., Leitner, M., Linke, F., Nabielska, N., Reiter, T., Schmitt, D., Spraetz, A., Sauseng, P., 2016. The Importance of Sample Size for Reproducibility of tDCS Effects. Front. Hum. Neurosci. 10, 453. doi:10.3389/fnhum.2016.00453

Miniussi, C., Brignani, D., Pellicciari, M.C., 2012. Combining transcranial electrical stimulation with electroencephalography: a multimodal approach. Clin. EEG Neurosci. 43, 184–191. doi:10.1177/1550059412444976

Miniussi, C., Harris, J.A., Ruzzoli, M., 2013. Modelling non-invasive brain stimulation in cognitive neuroscience. Neurosci. Biobehav. Rev. 37, 1702–1712. doi:10.1016/j.neubiorev.2013.06.014

Mueller, J., Legon, W., Opitz, A., Sato, T.F., Tyler, W.J., 2014. Transcranial Focused Ultrasound Modulates Intrinsic and Evoked EEG Dynamics. Brain Stimulat., Special Issue: NYC Neuromodulation 2015 Conference 7, 900–908. doi:10.1016/j.brs.2014.08.008

Neuling, T., Ruhnau, P., Fuscà, M., Demarchi, G., Herrmann, C.S., Weisz, N., 2015. Friends, not foes: Magnetoencephalography as a tool to uncover brain dynamics during transcranial alternating current stimulation. NeuroImage 118, 406–413. doi:10.1016/j.neuroimage.2015.06.026

Neuling, T., Ruhnau, P., Weisz, N., Herrmann, C.S., Demarchi, G., 2017. Faith and oscillations recovered: On analyzing EEG/MEG signals during tACS. NeuroImage 147, 960–963. doi:10.1016/j.neuroimage.2016.11.022

Niazy, R.K., Beckmann, C.F., Iannetti, G.D., Brady, J.M., Smith, S.M., 2005. Removal of FMRI environment artifacts from EEG data using optimal basis sets. NeuroImage 28, 720–737. doi:10.1016/j.neuroimage.2005.06.067

Nitsche, M.A., Paulus, W., 2000. Excitability changes induced in the human motor cortex by weak transcranial direct current stimulation. J. Physiol. 527, 633–639. doi:10.1111/j.1469-7793.2000.t01-1-00633.x

Noury, N., Hipp, J.F., Siegel, M., 2016. Physiological processes non-linearly affect electrophysiological recordings during transcranial electric stimulation. NeuroImage 140, 99–109. doi:10.1016/j.neuroimage.2016.03.065

Noury, N., Siegel, M., 2017. Phase properties of transcranial electrical stimulation artifacts in electrophysiological recordings. NeuroImage 158, 406–416. doi:10.1016/j.neuroimage.2017.07.010

Opitz, A., Falchier, A., Yan, C.-G., Yeagle, E.M., Linn, G.S., Megevand, P., Thielscher, A., Deborah A., R., Milham, M.P., Mehta, A.D., Schroeder, C.E., 2016. Spatiotemporal structure of intracranial electric fields induced by transcranial electric stimulation in humans and nonhuman primates. Sci. Rep. 6, 31236. doi:10.1038/srep31236

Ozen, S., Sirota, A., Belluscio, M.A., Anastassiou, C.A., Stark, E., Koch, C., Buzsáki, G., 2010. Transcranial electric stimulation entrains cortical neuronal populations in rats. J. Neurosci. Off. J. Soc. Neurosci. 30, 11476–11485. doi:10.1523/JNEUROSCI.5252-09.2010

Parent, A., 2004. Giovanni Aldini: from animal electricity to human brain stimulation. Can. J. Neurol. Sci. J. Can. Sci. Neurol. 31, 576–584.

Park, H.-J., Bonmassar, G., Kaltenbach, J.A., Machado, A.G., Manzoor, N.F., Gale, J.T., 2013. Activation of the central nervous system induced by micro-magnetic stimulation. Nat. Commun. 4. doi:10.1038/ncomms3463

Parkin, B.L., Ekhtiari, H., Walsh, V.F., 2015. Non-invasive Human Brain Stimulation in Cognitive Neuroscience: A Primer. Neuron 87, 932–945. doi:10.1016/j.neuron.2015.07.032

Pascual-Leone, A., Walsh, V., Rothwell, J., 2000. Transcranial magnetic stimulation in cognitive neuroscience – virtual lesion, chronometry, and functional connectivity. Curr. Opin. Neurobiol. 10, 232–237. doi:10.1016/S0959-4388(00)00081-7

Polanía, R., Moisa, M., Opitz, A., Grueschow, M., Ruff, C.C., 2015. The precision of value-based choices depends causally on fronto-parietal phase coupling. Nat. Commun. 6. doi:10.1038/ncomms9090

Polanía, R., Nitsche, M.A., Korman, C., Batsikadze, G., Paulus, W., 2012. The Importance of Timing in Segregated Theta Phase-Coupling for Cognitive Performance. Curr. Biol. 22, 1314–1318. doi:10.1016/j.cub.2012.05.021

Polanía, R., Nitsche, M.A., Paulus, W., 2011. Modulating functional connectivity patterns and topological functional organization of the human brain with transcranial direct current stimulation. Hum. Brain Mapp. 32, 1236–1249. doi:10.1002/hbm.21104

Rahman, A., Reato, D., Arlotti, M., Gasca, F., Datta, A., Parra, L.C., Bikson, M., 2013. Cellular effects of acute direct current stimulation: somatic and synaptic terminal effects. J. Physiol. 591, 2563–2578. doi:10.1113/jphysiol.2012.247171

Rajasethupathy, P., Sankaran, S., Marshel, J.H., Kim, C.K., Ferenczi, E., Lee, S.Y., Berndt, A., Ramakrishnan, C., Jaffe, A., Lo, M., Liston, C., Deisseroth, K., 2015. Projections from neocortex mediate top-down control of memory retrieval. Nature 526, 653–659. doi:10.1038/nature15389

Reinhart, R.M.G., Zhu, J., Park, S., Woodman, G.F., 2015. Medial–Frontal Stimulation Enhances Learning in Schizophrenia by Restoring Prediction Error Signaling. J. Neurosci. 35, 12232–12240. doi:10.1523/JNEUROSCI.1717-15.2015

Reis, J., Fritsch, B., 2011. Modulation of motor performance and motor learning by transcranial direct current stimulation. Curr. Opin. Neurol. 24, 590–596. doi:10.1097/WCO.0b013e32834c3db0

Reti, I., 2015. Brain Stimulation: Methodologies and Interventions. John Wiley & Sons.

Rohan, M.L., Yamamoto, R.T., Ravichandran, C.T., Cayetano, K.R., Morales, O.G., Olson, D.P., Vitaliano, G., Paul, S.M., Cohen, B.M., 2014. Rapid mood-elevating effects of low

field magnetic stimulation in depression. Biol. Psychiatry 76, 186–193. doi:10.1016/j.biopsych.2013.10.024

Rohan, M., Parow, A., Stoll, A.L., Demopulos, C., Friedman, S., Dager, S., Hennen, J., Cohen, B.M., Renshaw, P.F., 2004. Low-field magnetic stimulation in bipolar depression using an MRI-based stimulator. Am. J. Psychiatry 161, 93–98. doi:10.1176/appi.ajp.161.1.93

Romei, V., Bauer, M., Brooks, J.L., Economides, M., Penny, W., Thut, G., Driver, J., Bestmann, S., 2016a. Causal evidence that intrinsic beta-frequency is relevant for enhanced signal propagation in the motor system as shown through rhythmic TMS. NeuroImage 126, 120–130. doi:10.1016/j.neuroimage.2015.11.020

Romei, V., Driver, J., Schyns, P.G., Thut, G., 2011. Rhythmic TMS over parietal cortex links distinct brain frequencies to global versus local visual processing. Curr. Biol. CB 21, 334–337. doi:10.1016/j.cub.2011.01.035

Romei, V., Thut, G., Silvanto, J., 2016b. Information-Based Approaches of Noninvasive Transcranial Brain Stimulation. Trends Neurosci. 39, 782–795. doi:10.1016/j.tins.2016.09.001

Rossi, S., Hallett, M., Rossini, P.M., Pascual-Leone, A., 2009. Safety, ethical considerations, and application guidelines for the use of transcranial magnetic stimulation in clinical practice and research. Clin. Neurophysiol. 120, 2008–2039. doi:10.1016/j.clinph.2009.08.016

Rossi, S., Santarnecchi, E., Valenza, G., Ulivelli, M., 2016. The heart side of brain neuromodulation. Phil Trans R Soc A 374, 20150187. doi:10.1098/rsta.2015.0187

Ruffini, G., Fox, M.D., Ripolles, O., Miranda, P.C., Pascual-Leone, A., 2014. Optimization of multifocal transcranial current stimulation for weighted cortical pattern targeting from realistic modeling of electric fields. NeuroImage 89, 216–225. doi:10.1016/j.neuroimage.2013.12.002

Sack, A.T., Linden, D.E.J., 2003. Combining transcranial magnetic stimulation and functional imaging in cognitive brain research: possibilities and limitations. Brain Res. Brain Res. Rev. 43, 41–56.

Salzman, C.D., Britten, K.H., Newsome, W.T., 1990. Cortical microstimulation influences perceptual judgements of motion direction. Nature 346, 174–177. doi:10.1038/346174a0

Schmidt, S.L., Iyengar, A.K., Foulser, A.A., Boyle, M.R., Fröhlich, F., 2014. Endogenous cortical oscillations constrain neuromodulation by weak electric fields. Brain Stimulat. 7, 878–889. doi:10.1016/j.brs.2014.07.033

Schwalb, J.M., Hamani, C., 2008. The history and future of deep brain stimulation. Neurotherapeutics 5, 3–13. doi:10.1016/j.nurt.2007.11.003

Siegel, M., Donner, T.H., Engel, A.K., 2012. Spectral fingerprints of large-scale neuronal interactions. Nat. Rev. Neurosci. 13, 121–134. doi:10.1038/nrn3137

Soekadar, S.R., Herring, J.D., McGonigle, D., 2016. Transcranial electric stimulation (tES) and NeuroImaging: the state-of-the-art, new insights and prospects in basic and clinical neuroscience. NeuroImage 140, 1–3. doi:10.1016/j.neuroimage.2016.08.020

Soekadar, S.R., Witkowski, M., Cossio, E.G., Birbaumer, N., Robinson, S.E., Cohen, L.G., 2013. In vivo assessment of human brain oscillations during application of transcranial electric currents. Nat. Commun. 4. doi:10.1038/ncomms3032

Srinivasan, A.G., Landsberger, D.M., Shannon, R.V., 2010. Current focusing sharpens local peaks of excitation in cochlear implant stimulation. Hear. Res. 270, 89–100. doi:10.1016/j.heares.2010.09.004

Tehovnik, E.J., 1996. Electrical stimulation of neural tissue to evoke behavioral responses. J. Neurosci. Methods 65, 1–17. doi:10.1016/0165-0270(95)00131-X

Terney, D., Chaieb, L., Moliadze, V., Antal, A., Paulus, W., 2008. Increasing Human Brain Excitability by Transcranial High-Frequency Random Noise Stimulation. J. Neurosci. 28, 14147–14155. doi:10.1523/JNEUROSCI.4248-08.2008

Thut, G., Bergmann, T.O., Fröhlich, F., Soekadar, S.R., Brittain, J.-S., Valero-Cabré, A., Sack, A.T., Miniussi, C., Antal, A., Siebner, H.R., Ziemann, U., Herrmann, C.S., 2017. Guiding transcranial brain stimulation by EEG/MEG to interact with ongoing brain activity and associated functions: A position paper. Clin. Neurophysiol. Off. J. Int. Fed. Clin. Neurophysiol. 128, 843–857. doi:10.1016/j.clinph.2017.01.003

Tronnier, V., Rasche, D., 2013. Chapter 28 - Epidural and subdural stimulation, in: Hallett, A.M.L. and M. (Ed.), Handbook of Clinical Neurology, Brain Stimulation. Elsevier, pp. 343–351.

Tsoucalas, G., Karamanou, M., Lymperi, M., Gennimata, V., Androutsos, G., 2014. The “torpedo” effect in medicine. Int. Marit. Health 65, 65–67. doi:10.5603/IMH.2014.0015

Udupa, K., Chen, R., 2015. The mechanisms of action of deep brain stimulation and ideas for the future development. Prog. Neurobiol. 133, 27–49. doi:10.1016/j.pneurobio.2015.08.001

Van Veen, B.D., van Drongelen, W., Yuchtman, M., Suzuki, A., 1997. Localization of brain electrical activity via linearly constrained minimum variance spatial filtering. IEEE Trans. Biomed. Eng. 44, 867–880. doi:10.1109/10.623056

Veniero, D., Strüber, D., Thut, G., Herrmann, C.S., 2016. Noninvasive Brain Stimulation Techniques Can Modulate Cognitive Processing. Organ. Res. Methods 1094428116658960. doi:10.1177/1094428116658960

Villamar, M.F., Volz, M.S., Bikson, M., Datta, A., DaSilva, A.F., Fregni, F., 2013. Technique and Considerations in the Use of 4x1 Ring High-definition Transcranial Direct Current Stimulation (HD-tDCS). JoVE J. Vis. Exp. e50309–e50309. doi:10.3791/50309

Violante, I.R., Li, L.M., Carmichael, D.W., Lorenz, R., Leech, R., Hampshire, A., Rothwell, J.C., Sharp, D.J., 2017. Externally induced frontoparietal synchronization modulates network dynamics and enhances working memory performance. eLife 6, e22001. doi:10.7554/eLife.22001

Vossen, A., Gross, J., Thut, G., 2015. Alpha Power Increase After Transcranial Alternating Current Stimulation at Alpha Frequency (α-tACS) Reflects Plastic Changes Rather Than Entrainment. Brain Stimulat. 8, 499–508. doi:10.1016/j.brs.2014.12.004

Voss, U., Holzmann, R., Hobson, A., Paulus, W., Koppehele-Gossel, J., Klimke, A., Nitsche, M.A., 2014. Induction of self awareness in dreams through frontal low current stimulation of gamma activity. Nat. Neurosci. advance online publication. doi:10.1038/nn.3719

Wallace, D., Cooper, N.R., Paulmann, S., Fitzgerald, P.B., Russo, R., 2016. Perceived Comfort and Blinding Efficacy in Randomised Sham-Controlled Transcranial Direct Current Stimulation (tDCS) Trials at 2 mA in Young and Older Healthy Adults. PLOS ONE 11, e0149703. doi:10.1371/journal.pone.0149703

Walsh, V., Cowey, A., 2000. Transcranial magnetic stimulation and cognitive neuroscience. Nat. Rev. Neurosci. 1, 73–80. doi:10.1038/35036239

Wimmer, R.D., Schmitt, L.I., Davidson, T.J., Nakajima, M., Deisseroth, K., Halassa, M.M., 2015. Thalamic control of sensory selection in divided attention. Nature 526, 705–709. doi:10.1038/nature15398

Woods, A.J., Antal, A., Bikson, M., Boggio, P.S., Brunoni, A.R., Celnik, P., Cohen, L.G., Fregni, F., Herrmann, C.S., Kappenman, E.S., Knotkova, H., Liebetanz, D., Miniussi, C., Miranda, P.C., Paulus, W., Priori, A., Reato, D., Stagg, C., Wenderoth, N., Nitsche, M.A., 2016. A technical guide to tDCS, and related non-invasive brain stimulation tools. Clin. Neurophysiol. 127, 1031–1048. doi:10.1016/j.clinph.2015.11.012

Zaehle, T., Rach, S., Herrmann, C.S., 2010. Transcranial Alternating Current Stimulation Enhances Individual Alpha Activity in Human EEG. PLoS ONE 5, e13766. doi:10.1371/journal.pone.0013766

Zimerman, M., Nitsch, M., Giraux, P., Gerloff, C., Cohen, L.G., Hummel, F.C., 2013. Neuroenhancement of the Aging Brain: Restoring Skill Acquisition in Old Subjects. Ann. Neurol. 73, 10–15. doi:10.1002/ana.23761

Zrenner, E., 2013. Fighting Blindness with Microelectronics. Sci. Transl. Med. 5, 210ps16–210ps16. doi:10.1126/scitranslmed.3007399

6 Manuscripts included in this thesis

6.1 Paper 1

Noury, N., Hipp, J.F., Siegel, M., 2016. Physiological processes non-linearly affect electrophysiological recordings during transcranial electric stimulation. NeuroImage 140, 99–109. doi:10.1016/j.neuroimage.2016.03.065

Statement of contributions:

Experimental design: NN, JFH and MS.

Data acquisition: NN.

Data analysis: NN.

Manuscript writing: NN and MS.

NeuroImage 140 (2016) 99–109

Contents lists available at ScienceDirect

NeuroImage

journal homepage: www.elsevier.com/locate/ynimg

Physiological processes non-linearly affect electrophysiological recordings during transcranial electric stimulation

Nima Noury [a,b,*], Joerg F. Hipp [a,c], Markus Siegel [a,*]

[a] Centre for Integrative Neuroscience & MEG Center, University of Tübingen, Germany
[b] IMPRS for Cognitive and Systems Neuroscience, Tübingen, Germany
[c] F. Hoffmann-La Roche, Pharma Research and Early Development, Basel, Switzerland

ARTICLE INFO

Article history:
Accepted 24 March 2016
Available online 1 April 2016

Keywords:
Transcranial electric stimulation (tES)
Transcranial alternating current stimulation (tACS)
Transcranial direct current stimulation (tDCS)
EEG
MEG
Neural entrainment
Stimulation artifacts

ABSTRACT

Transcranial electric stimulation (tES) is a promising tool to non-invasively manipulate neuronal activity in the human brain. Several studies have shown behavioral effects of tES, but stimulation artifacts complicate the simultaneous investigation of neural activity with EEG or MEG. Here, we first show for EEG and MEG, that contrary to previous assumptions, artifacts do not simply reflect stimulation currents, but that heartbeat and respiration non-linearly modulate stimulation artifacts. These modulations occur irrespective of the stimulation frequency, i.e. during both transcranial alternating and direct current stimulations (tACS and tDCS). Second, we show that, although at first sight previously employed artifact rejection methods may seem to remove artifacts, data are still contaminated by non-linear stimulation artifacts. Because of their complex nature and dependence on the subjects' physiological state, these artifacts are prone to be mistaken as neural entrainment. In sum, our results uncover non-linear tES artifacts, show that current techniques fail to fully remove them, and pave the way for new artifact rejection methods.

Introduction

Manipulative approaches are much needed in systems neuroscience. Take neuronal oscillations as an example. They are ubiquitous in the brain and have been implicated in various functions (Buzsáki and Draguhn, 2004; Fries, 2005; Jensen and Mazaheri, 2010; Siegel et al., 2012; Singer, 1999; Womelsdorf et al., 2014). However, supporting evidence, especially in humans, remains largely correlative and only few studies have addressed this causally (Helfrich et al., 2014; Marshall et al., 2006; Polanía et al., 2012; Romei et al., 2011, Romei et al., 2010; Voss et al., 2014). One strategy to causally assess potential roles of neural oscillations is to manipulate them and to simultaneously measure the effect on neural activity and behavior. This is technically challenging and well-defined experimental protocols as well as analysis pipelines have not been established yet.

Transcranial electric stimulation (tES) is a non-invasive brain stimulation technique, which provides the possibility to control stimulation strength, frequency and, to some extent, stimulation site (Dmochowski et al., 2011; Kanai et al., 2008; Schutter and Hortensius, 2010; Schwiedrzik, 2009). These features render tES and in particular one of its variants, transcranial alternating current stimulation (tACS), suitable for manipulating specific brain rhythms (Herrmann et al., 2013). During tACS, a sinusoidal electrical current at a specific frequency is applied to the subject through electrodes placed on the scalp. The potential of electrical stimulation to manipulate neuronal oscillations has been shown in animal models (Fröhlich and McCormick, 2010; Ozen et al., 2010). However, in humans, tACS has largely been limited to investigating effects on behavior and on neurophysiological aftereffects (Brittain et al., 2013; Herrmann et al., 2013; Marshall et al., 2011, Marshall et al., 2006; Polanía et al., 2012; Zaehle et al., 2010). A key reason for the limited number of studies directly investigating effects on neural activity during stimulation is the massive electrophysiological artifact induced by the stimulation. These artifacts are particularly problematic when attempting to investigate effects on neuronal activity within the same frequency range as the stimulation frequency (Zaehle et al., 2010).

Recently, different approaches have been proposed to remove tES artifacts from EEG and MEG for studying neuronal activity during stimulation (Helfrich et al., 2014; Neuling et al., 2015; Soekadar et al., 2013; Voss et al., 2014). Based on the assumption of linear stimulation artifacts, these methods follow approaches like template subtraction, component analysis, beamforming or temporal filtering. However, a thorough characterization of stimulation artifacts, which is needed for assessing artifact cleaning procedures, is missing. Here we provide this characterization.

* Corresponding authors at: Centre for Integrative Neuroscience, University of Tübingen, Otfried-Müller-Str. 25, 72076 Tübingen, Germany.
E-mail addresses: nima.noury@cin.uni-tuebingen.de (N. Noury), markus.siegel@uni-tuebingen.de (M. Siegel).

http://dx.doi.org/10.1016/j.neuroimage.2016.03.065
1053-8119/

Materials and methods

Methods outline

We measured EEG and MEG during several different tES conditions. First, we tested if a pure sinusoidal model can explain tES artifacts. Next, we investigated in the time and frequency domain whether heartbeat and respiration modulate tES artifacts. Finally, we used temporal and spectral features of tES artifacts to track them through different stages of available artifact rejection pipelines. The rationale behind each analysis is explained in the Results section.

Participants and experimental protocol

All experiments were conducted in 5 healthy male participants. All subjects gave written informed consent before participating. All experiments were conducted in accordance with the Declaration of Helsinki and approved by the local ethics committee. The main tACS experiment with small stimulation electrodes was conducted in 4 subjects that each participated in 6 experimental runs. Each run consisted of the following sequential conditions: sham, tACSa, tACSb, sham, tACSb, and tACSa. Each condition lasted 66 s. For each run, 11 Hz tACS and 62 Hz tACS were randomly assigned to tACSa and tACSb conditions to avoid any potential sequence effects. During the first 5 runs, subjects fixated a central fixation spot at the center of a blank monitor (60 Hz refresh rate). In the last run subjects kept their eyes closed. Before start of the experiment, subjects were habituated to transcranial electric stimulation. In one of the four subjects, we performed a control experiment with large rubber electrodes. In this control experiment runs 3 and 6 were measured with eyes closed. We performed two more control experiments on a fifth subject with the same electrode layout as in the main tACS experiment. In both experiments, the subject fixated a central fixation spot. In the first control experiment, we checked for the potential influence of the EEG ground electrode placement on the stimulation artifact during 62 Hz tACS. We recorded 10 min of EEG with ground on the right forearm and 10 min with ground on the forehead (Fpz of 10–10 system). In the second control experiment, we recorded MEG and EEG during cathodal tDCS, anodal tDCS and sham conditions (10 min per condition). Cathodal and anodal are defined based on the polarity of the parietal stimulation electrode.

Transcranial electric stimulation

Stimulation current was applied with an IZ2h stimulator (Tucker Davis Technologies Inc.). Stimulation amplitude was 0.5 mA (i.e., 1 mA peak-to-peak for tACS). Stimulation did not induce flicker percepts. For the main experiment, stimulation was applied through two standard Ag/AgCl EEG electrodes over right occipital and right parietal areas (electrodes O10 and CP4 of the 10–10 electrode system). For the control experiment with large electrodes, 35 cm^2 MR-compatible rubber electrodes (neuroConn GmbH) were placed over occipital and frontal lobes underneath the EEG cap. For all experiments, stimulation electrodes were attached using Ten20 conductive paste (Weaver and Company) and their impedance was kept below 2.5 kΩ. To minimize magnetic artifacts produced by the stimulation current, we carefully twisted all stimulation cables.

Data acquisition and preprocessing

We simultaneously recorded 72-channel EEG (NeurOne system, Mega Electronics Ltd) and 272-channel MEG (Omega 2000, CTF Systems) throughout all experiments at 10,000 Hz and 2343.8 Hz sampling rate, respectively. EEG electrodes were positioned based on the 10–10 electrode system using an EEG cap (EC80, EASYCAP). All signals were in the dynamic range of recording systems and no clipping was observed for either EEG or MEG signals. Due to the interference between stimulation currents and electrical currents of the head-positioning circuits of the MEG system, we could not monitor head movement continuously during the experiment. Instead we measured head positions at the beginning and at the end of each run.

EEG electrodes were attached using Abratyl 2000 conductive gel and impedances were kept below 2.5 kΩ for most electrodes. We referenced EEG electrodes to FCz and, except for one control experiment, positioned a ground electrode on the right forearm. EEG signals were re-referenced to average reference offline. Along with EEG and MEG, we recorded the injected current, the ECG and respiratory movements using bipolar channels of the EEG system. The injected current was indirectly measured by recording the voltage drop across a 200 Ω resistor positioned in series to the head. The ECG was recorded through 2 electrodes placed below the right clavicle and below the left pectoral muscle. Respiration was continuously recorded with a piezo respiratory belt transducer (Vermed-Medizintechnik).

Sinusoidal model subtraction

To remove an optimal sinusoidal model from artifactual signals, we fitted the amplitude, frequency and phase of a sinusoid to the MEG and EEG data and subtracted it from the data. For this, it is important to estimate the stimulation frequency with μHz accuracy. This is because, if the internal clocks of the stimulation and recording systems are not synchronized, as in the present case, even small errors of the estimated stimulation frequency lead to strong residual artifacts around the main peak. To this end, we first chose 20 MEG channels with strongest tACS artifacts and split their data into 33 s long segments on which we fitted amplitude, frequency and phase of a sinusoidal model separately for each channel. We estimated the stimulation frequency as the median across all segments and channels (standard deviation of 8.50 and 4.85 μHz, for 11 Hz and 62 Hz tACS, respectively). Next, we defined a new sinusoidal model fixing its frequency at the estimated stimulation frequency. We then separately fitted amplitude and phase of this new model to each segment and channel and removed it from the data.

We followed a similar strategy for EEG. As we also recorded the injected current with the EEG system, this allowed for estimating the stimulation frequency based on the injected current. This is more accurate than estimation based on the EEG signal, because the injected current does not include any brain signals. As for the MEG, we split the injected current into 33 s long segments and estimated the stimulation frequency for each piece. We estimated the stimulation frequency as the median across all segments (standard deviation of 0.10 and 0.66 μHz, for 11 Hz and 62 Hz tACS, respectively).

Spectral analyses

To estimate the power spectral density (PSD) in tACS experiments, we first split the data into either 4 s or 33 s long segments, according to the desired spectral resolution. Then, we applied a Hanning window to each segment and computed its Fourier transform. Finally, we calculated the average power across all segments and scaled the results to PSD (μV^2/Hz and fT^2/Hz for EEG and MEG, respectively). For the case of tDCS and to reveal the spectral structure of artifacts in face of strong low frequency activity of EEG and MEG, we estimated spectra with higher resolution. We split the data into 120 s segments, estimated the Thomson's multitaper PSD of each segment (Slepian tapers with 0.05 Hz bandwidth, NW = 6) and calculated the average power across all segments.

Heartbeat and respiration frequencies

For each subject, heartbeat and respiration rates were defined as the inverse of the median of the temporal intervals between successive ECG R-peaks and respiration ends, respectively.

Temporal analyses

For all analyses of tACS artifact envelopes, we first band-pass filtered the recorded signals using a 6th-order zero-phase Butterworth filter centered at the stimulation frequency of interest with a pass-band of ±5 Hz. For all comparisons between sham and tACS conditions, we filtered the sham data with the same filter that we applied to the corresponding tACS data. After band-pass filtering, we down-sampled EEG and MEG signals to 1000 Hz and 781.25 Hz, respectively, and applied the Hilbert transform to obtain signal envelopes. To investigate heartbeat and respiration locked modulations, we extracted 4 s or 8 s long envelope segments centered on all ECG R-peaks or inspiration ends, respectively. We subtracted the temporal mean from each segment and tested a significant modulation at each time point using permutation statistics: We compared the average envelope across all segments against the distribution of average envelopes from 1000 random placements of segments on the data. We converted the resulting p-values to z-scores for displaying modulation envelopes. We Bonferroni-corrected p-values for the number of time points to assess the significance of modulation for each channel.

For testing the effect of heartbeat and respiration on the tDCS artifact, we band-pass filtered the recorded signals using a 6th-order zero-phase Butterworth filter between 0.05 and 5 Hz, extracted 4 s long heartbeat-locked and 8 s long respiration-locked segments, removed the mean of each segment, and applied the same permutation statistics as for tACS.

We performed an adapted PCA on the average heartbeat and respiration locked envelopes to test the temporal stability of spatial artifact patterns. For each sensor, we calculated the average of all envelope segments without removing their mean. These average envelopes contain the amplitude of the constant sinusoidal artifacts (the temporal mean of the envelopes) together with their heartbeat locked modulation. We derived the temporal mean of the envelopes of all channels as the first PC. We then removed this first PC from the average envelopes and applied PCA on the resulting zero-mean envelopes to derive the remaining PCs.

AM-transformation of modulation kernel

For each channel and each subject, we refer to the mean-removed average of all heartbeat-locked modulations as the heartbeat kernel. To calculate the AM-transformed heartbeat kernel (Fig. 5), we applied the AM model and simply multiplied the kernel with a 62 Hz sinusoidal wave.

Template subtraction and PCA based artifact removal

We applied the procedure used by Helfrich et al. (2014) on the EEG data recorded during 11 Hz tACS with small stimulation electrodes of one subject. We first band-pass filtered the data between 1 Hz and 35 Hz using a 4th-order zero-phase Butterworth filter and up-sampled the data to 30 kHz. Next, we split one channel's signal into 3 s long segments and adjusted the temporal position of each segment to maximize its correlation with the first segment. We segmented all remaining channels according to these adjusted alignments. Next, for each segment and channel, we calculated an artifact template by averaging the ten adjacent segments. To construct the template-subtracted signal, each segments' template was regressed out from the corresponding segment.

In a second step, we applied PCA on the template-subtracted data. For investigating heartbeat-related modulations of the resultant PCs, we first extracted heartbeat-locked segments from 0.7 s prior to 1 s after ECG R-peaks. As the method applied by Helfrich et al. (2014) cuts the data into 3-s segments, we restricted the analysis on heartbeats for which the entire 1.7 s interval fell in one segment (about one third of heartbeats). For each heartbeat-locked segment, we computed the envelope of 11 Hz power using a sliding window Fourier-analysis (0.5 s Hanning window, 0.1 s step size). Because the first template-subtraction step destroyed the consistent heartbeat-locked envelope modulation, it became more difficult to track the non-linear artifact during the second step (PCA). Notably, the difficulty to track the artifact does not imply that it is gone. To overcome this problem, we devised a 3-step procedure. PC1 strongly captured the stimulation artifact (Fig. 8c): The topography reflected the position of stimulation electrodes, the power spectrum showed symmetric peaks around the stimulation frequency, and 11 Hz power was significantly modulated by each heartbeat ($P < 0.05$; permutation test). We used these features of PC1, to identify additional artifactual PCs. First, we tested which PCs show heartbeat-locked modulations of 11 Hz power significantly correlated to the heartbeat-locked modulation of PC1. 9 PCs showed this artifactual feature, even though their topographies seemed physiological ($P < 0.05$ uncorrected). Second, we employed a similar analysis to also account for non-linear artifacts not locked to heartbeats. We tested which PCs showed a significant correlation of modulations of 11 Hz power to modulations of PC1 across all 3-s segments. We found 8 PCs out of the remaining 62 PCs that showed significantly correlated modulations ($P < 0.05$ uncorrected). Third, as a simple spectral heuristic for additional potentially artifactual PCs, we checked which PCs showed symmetric peaks around the stimulation frequency in their spectrums. We found that among 54 remaining PCs, 18 showed this symmetricity of their power spectrum.

Beamforming

We applied adaptive linear spatial filtering (beamforming) (Van Veen et al., 1997) to the MEG data of the final two runs of tACS stimulation with small stimulation electrodes, which includes one run with eyes open and one run with eyes closed. We first band-passed the data using a 6th-order zero-phase Butterworth high-pass filter at 2 Hz and a low-pass filter at 90 Hz. Afterwards we notch filtered the line noise by means of a 6th-order zero-phase Butterworth band-stop filter from 49.8 Hz to 50.2 Hz band. We down sampled the data to 585.94 Hz and calculated the covariance matrix based on the concatenated data of the 11 Hz tACS and sham conditions of both runs. For tACS recordings, the high signal power caused by the stimulation artifact makes it difficult to determine the cutoff between brain signals and sensor noise. Thus, we set the regularization factor (λ), which is an estimate of measurement noise, based on sham recordings only. To this end, we applied PCA on the covariance matrix of sham recordings, and set the regularization factor equal to Eigenvalue of PC at which the cumulative explained variance reached 99% of the total variance. Finally, based on the covariance matrix and regularization factor, for each source location, we calculated three orthogonal filters (one for each spatial dimension) and linearly combined them to a single filter in the direction of maximum variance.

Source locations and physical forward model

We performed the beamforming analysis on a regular three-dimensional grid that covered the whole brain with 1-cm spacing in MNI space (2982 source locations). We nonlinearly transformed source locations into individual head space using the participants' individual T1-weighted structural MRI. The MEG sensors were aligned to the head geometry on the basis of three fiducial points (nasion, left ear, right ear) that were registered before and after the MEG acquisition by three head localization coils. To derive the physical relation between sources and sensors (leadfield), we employed a single-shell head model (Nolte, 2003).

Source-space analysis

We computed the ratio of source-level alpha power (8–14 Hz) between eyes open and eyes closed conditions, to test if beamforming during tACS was able to reveal physiological activity. To this end, we band-pass filtered the source-level time-courses from 8 to 14 Hz using

a 4^{th} order zero-phase Butterworth filter and divided the variance of eyes closed time-courses by the variance of eyes open time-courses. To assess the significance of alpha-power modulation we compare the log power of 2 s segments between eyes open and eyes closed conditions (120 segments each) using t-statistics. To test if source-level activity was contaminated by the non-linear stimulation artifact, we estimated the power spectrum at each source position with 0.05 Hz resolution (20 s segments, Hanning window). We then computed the linear correlation (Pearson's r) between the brain-wide distribution of 11 Hz power and the distribution of power at all other frequencies. We tested if this correlation peaked specifically at the stimulation frequency ± the heart rate.

Analysis software

All data analyses were performed in Matlab (MathWorks) using custom scripts and the open source toolbox Fieldtrip (Oostenveld et al., 2011).

Results

tACS artifacts in EEG and MEG

We recorded EEG and MEG during 11 Hz tACS, 62 Hz tACS, and sham stimulation in 4 subjects. Stimulation currents were injected through two Ag/AgCl electrodes with 1 mA peak-to-peak strength (Fig. 1a). EEG was recorded through the 72 remaining electrodes of the 10–10 electrode system, along with 272 MEG channels. Throughout the experiment, we also recorded the electrocardiogram (ECG) and respiration of subjects. For both, EEG and MEG, during stimulation, signals showed strong artifacts at tACS frequencies (Fig. 1b–g). These stimulation artifacts were observed at almost all electrodes with a spatial distribution that reflected the location of stimulation electrodes. At electrodes near the stimulation site, artifacts were more than 1000 times bigger than neural signals. In the frequency domain, artifacts manifested as a main peak at the stimulation frequency together with its harmonics. This reflected the spectral peaks of the stimulation current (Supplementary Figure 1a, b).

Nonlinear effect of heartbeat and respiration

To characterize the tACS artifact in more detail, we first evaluated the performance of the stimulation system and tested if, as intended, the main peak of the stimulation current resembled a pure sinusoid. This is critical, because any imperfection of the stimulation current would be reflected in the stimulation artifact. Subtracting an optimum sinusoidal model from the injected current almost perfectly removed the main peak (more than 100 dB suppression; Fig. 2a, b; Materials and methods). Thus, the main stimulation peak of the injected current well resembled a pure sinusoid.

Next, we characterized stimulation artifacts on EEG and MEG. A key question about the nature of these artifacts is if they reflect a simple sinusoid as the injected current, or if they show more complex characteristics. To test this, we performed the same analysis as for the stimulation current and removed a sinusoidal artifact model from the EEG and MEG during tACS (Fig. 2c–f). This indeed removed the main stimulation peak for 11 Hz and 62 Hz tACS. However, high-resolution spectra revealed that, in contrast to the stimulation current, many EEG and MEG channels showed prominent side peaks up to several Hertz around the stimulation frequency. These side peaks remained after removing the sinusoidal model (see Supplementary Figure 2 for a larger frequency range). Thus, stimulation effects on EEG and MEG were not purely sinusoidal as the stimulation current. Does this reflect neural entrainment?

Notably, side peaks in EEG and MEG were symmetric around the stimulation frequency and very similar for 11 Hz and 62 Hz tACS. These characteristics suggested that side peaks reflected a non-linear process underlying artifact generation, rather than neural entrainment. Symmetric side-peaks around a central frequency are reminiscent of the amplitude modulation (AM) technique that is used in electronic communication. In this technique, the amplitude of a high-frequency sinusoidal carrier is modulated by a low frequency signal. This results in a spectrum with symmetric side-peaks, which reflect the low-frequency signals' spectrum around the carrier frequency peak (Fig. 2g–i). The fact that we found side peaks positioned symmetrically around the stimulation frequency (Fig. 2) suggested that AM modulation may be involved in the non-linear stimulation artifact. Which processes may modulate the stimulation artifact? We hypothesized that this may be the subjects' heartbeat and respiration. If that was true, spectra should show side peaks at the stimulation frequency ± individual heartbeat and respiration frequencies. Indeed, for each subject, we found four side peaks at exactly the predicted frequencies (Fig. 2c–f).

To directly test our hypothesis in the time domain, we performed a time-locked analysis in which we averaged the M/EEG signals' envelope at the stimulation frequency temporally aligned on heartbeats (Fig. 3a–d). Indeed, in all subjects we consistently found that the heartbeat strongly modulated the main stimulation artifact. This modulation happened for both EEG and MEG, and irrespective of the

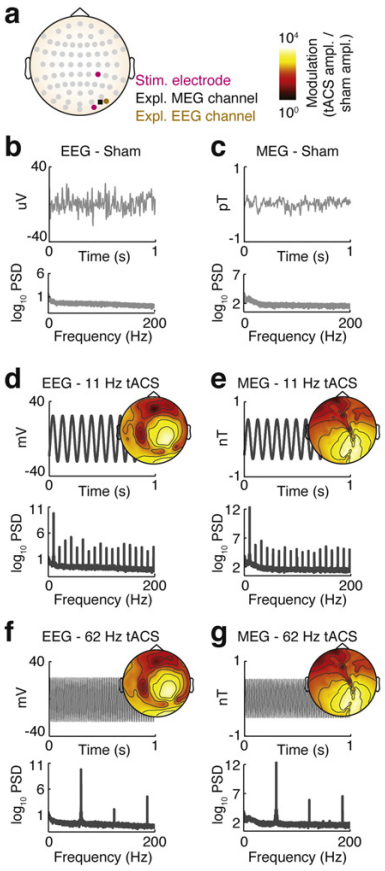

Fig. 1. Simultaneous tACS, EEG, and MEG. (*a*) EEG and tACS were performed with 74 Ag/AgCl electrodes placed according to the 10–10 system. Purple circles indicate the position of the stimulation electrodes. The brown circle and black square indicate the position of channels used for demonstrating EEG (PO10) and MEG (MRT57) results, respectively. (*b*) Typical EEG signal and average EEG power spectral density during sham. (*c*) Typical MEG signal and average MEG power spectral density during sham. (*d*) EEG and (*e*) MEG signals and spectra during 11 Hz tACS. (*f*) EEG and (*g*) MEG signals and spectra during 62 Hz tACS. Topographies show the strength of artifacts, quantified as decadic logarithm of the standard deviation of signals during tACS divided by standard deviation of signals during sham. This figure shows data from subject S1, during one experimental run with eyes open.

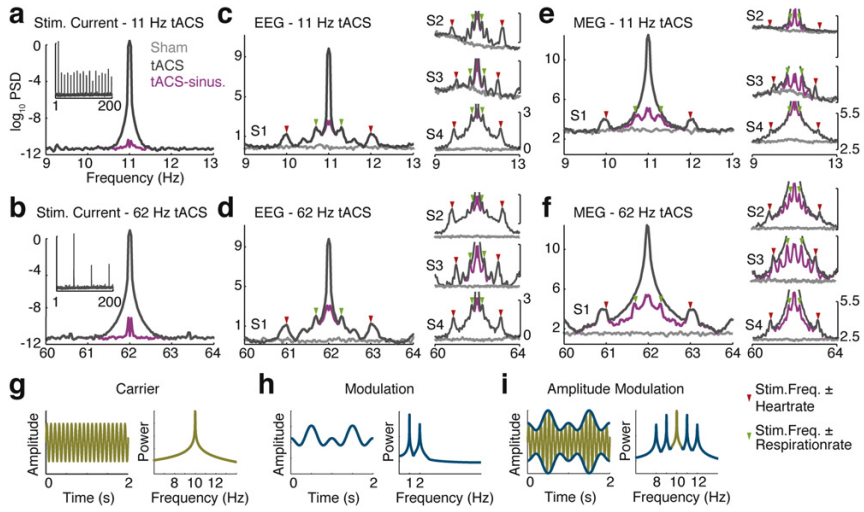

Fig. 2. Stimulation artifacts in the frequency domain. (*a*, *b*) Power spectral density of the stimulation current around the stimulation frequency for 11 Hz and 62 Hz tACS. Subtracting a sinusoidal model from the stimulation current (magenta) removed almost all power. (*c*) EEG power spectral density around the stimulation frequency during sham and 11 Hz tACS, with and without removal of a sinusoidal artifact model. The large spectrum shows data from subject S1. Smaller spectra show all other subjects. Red and green arrows mark the stimulation frequency ± individual average heartbeat and respiration frequencies, respectively. (*d*) EEG spectra for 62 Hz tACS. (*e*) MEG spectra for 11 Hz tACS. (*f*) MEG spectra for 62 Hz tACS. Subtracting the sinusoidal artifact model reveals the symmetric spectral peaks. See Supplementary Figure 2 for a wider frequency range. EEG and MEG data show channels PO10 and MRT57, respectively. (*g*, *h*, and *i*) Schematic illustration of amplitude modulation (AM) in time and frequency domains. The amplitude of a carrier signal (*g*) is modulated by a slower modulation signal (*h*), which results in the amplitude-modulated signal (*i*). In the frequency domain, this corresponds convolution of modulation and carrier spectra, which results in a symmetric spectrum, where the spectrum of the modulation signal is symmetric around the peak of the carrier frequency.

stimulation frequency. Almost all M/EEG channels showed a significant modulation by heartbeat ($p < 0.05$ corrected, permutation test) with strongest effects close to the stimulation site. Effects were clearer for 62 Hz stimulation frequency likely reflecting weaker electrophysiological signals at that frequency (see also Supplementary Figure 2). Importantly, for many channels the strength of non-linear modulation was even bigger than strength of neural signals recorded during the sham condition (Fig. 3 topographies).

Control analyses

Any change in the injected current influences the stimulation artifact. Thus, we performed a control analysis and tested if the injected current showed heartbeat-locked modulations. We did not find any side-peaks around the stimulation frequency and no heartbeat-locked modulations of the injected current (Fig. 2a, b and Supplementary Figures 1c, d). This rules out that the heartbeat-locked modulations of artifacts were driven by variations of the injected current.

In another control analysis, we investigated if the non-linear stimulation artifact reflected the well-known electro- and magnetocardiogram (E/MCG; Supplementary Figure 3). To this end, we removed the average E/MCG around each heartbeat. This had no effect on the heartbeat-locked envelope modulation during tACS. In sum, we concluded that the non-linear stimulation artifact neither was driven by modulation of the stimulation current nor merely reflected the E/MCG.

Spatial stability of heartbeat-locked non-linear artifact

We next investigated if the heartbeat-locked non-linear artifact had a constant spatial pattern over time similar to the spatial pattern of the main stimulation peak. This is particularly important for potential artifact cleaning algorithms that employ linear decomposition or spatial filtering, such as e.g. PCA, ICA or beamforming. To this end, we employed an adapted PCA and tested if the stimulation artifact's envelope was captured in one component (Fig. 3e–f; see Materials and methods). The first principal component captured the average stimulation artifact together with part of its modulation over time. However, in addition to the first components, 6 additional components for EEG and 3 additional components for MEG also showed clear rhythmic modulations (Fig. 3e–f). Accordingly, the relation between rhythmically modulated components was not constant over time. Thus, the spatial pattern of the stimulation artifact was not constant over time, but was modulated by heartbeats, for both EEG and MEG.

Respiration-locked modulation

We repeated the time-locked analysis using the respiration signal (Fig. 4a–d). Irrespective of stimulation frequency, artifact envelopes of most EEG and MEG channels were strongly modulated by respiration ($p < 0.05$ corrected, permutation test). Similar to heartbeat-locked modulations, for many channels, respiration-related modulations were stronger than neural activity and were easier observable for 62 Hz than for 11 Hz tACS. We performed a control analysis of the injected current and ruled out any influence of the injected current on the observed respiration-locked artifact (Supplementary Figures 1e–f). Again, we performed an adapted PCA on the average respiration locked envelopes, to check if respiration-locked modulations showed a stable spatial pattern over time (Fig. 4e–f). Similar as for the heartbeat-locked effect, we found that PCA did not capture the artifact in one principal component. Thus, we concluded that, alike heartbeats, respiration non-linearly modulated the strength and spatial pattern of the stimulation artifact over time.

Ground electrode

We checked whether the stimulation artifacts observed in EEG may be related to the position of the EEG ground electrode. Thus, in one subject we recorded two sessions of EEG signals during 62 Hz tACS with the ground electrode positioned on either the forearm or forehead. We observed very similar stimulation artifacts for both ground positions (Supplementary Figure 4). Thus, we concluded that heartbeat-locked and

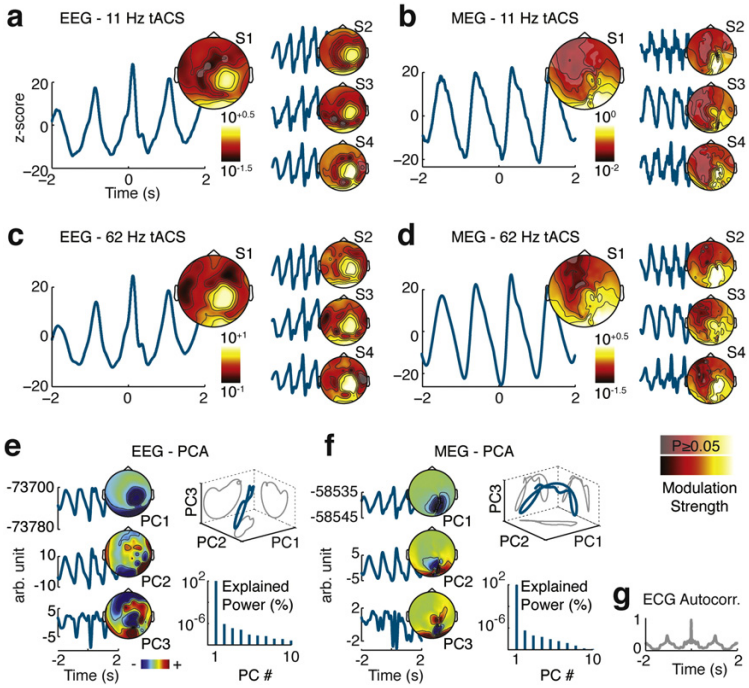

Fig. 3. Heartbeat locked artifacts. (*a*) Time-courses depict the modulation of the EEG envelope around the time of heartbeats during 11 Hz tACS quantified as the statistical z-score against a null-hypothesis of no modulation. The topography shows the strength of modulation relative to the neural signal of interest quantified as the decadic logarithm of the standard deviation of heartbeat-locked modulation divided by standard deviation of the sham signal at the stimulation frequency (non-significant modulations are masked at P = 0.05 corrected). The large panel shows data from subject S1. Smaller panels show all other subjects. (*b*) Heartbeat locked modulation of MEG envelope during 11 Hz tACS. (*c*) Heartbeat locked modulation of EEG envelope during 62 Hz tACS. (*d*) Heartbeat locked modulation of MEG envelope during 62 Hz tACS. EEG and MEG data show channels PO10 and MRT57, respectively. (*e*) PCA of average heartbeat-locked EEG envelope modulations during 62 Hz tACS. Shown are the first 3 PCs in the time domain together with their sensor topographies (eigenvectors). PCs are sorted by explained power as indicated in the lower right panel. The top right panel shows the average heartbeat-locked modulation time-course projected on the first three PCs. (*f*) PCA of average heartbeat-locked MEG envelope modulations during 62 Hz tACS. (*g*) Autocorrelation of the ECG.

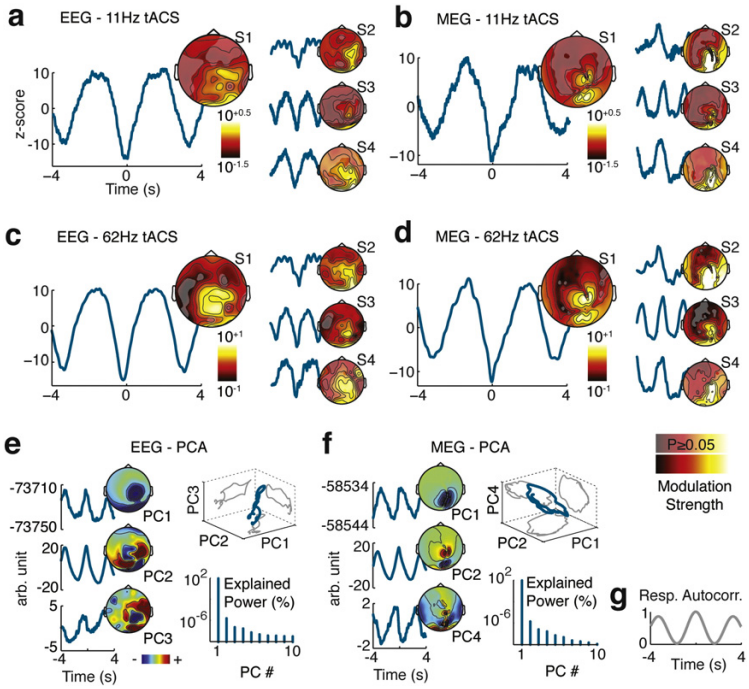

Fig. 4. Respiration locked artifacts. Modulation of (*a*) EEG and (*b*) MEG envelope by respiration during 11 Hz tACS. Modulation of (*c*) EEG and (*d*) MEG envelope by respiration during 62 Hz tACS. PCA of average heartbeat-locked (*e*) EEG and (*f*) MEG envelope modulations during 62 Hz tACS. (*g*) Autocorrelation of the respiration signal. All other conventions as in Fig. 3.

respiration-locked stimulation artifacts are not related to the position of the ground electrode.

Bandwidth of non-linear stimulation artifact

We next assessed the spectral extent of the non-linear stimulation artifact (Fig. 5). Heartbeat and respiration modulations are not purely sinusoidal (Figs. 3 and 4) and may thus affect M/EEG signals during tACS beyond the side peaks directly related to heart and respiration rate. Because heart rate is high compared to respiration rate, in particular harmonics of heart rate may contaminate electrophysiological signals in a wide frequency band. To investigate this, similar to the AM model, we multiplied the average heartbeat-locked envelope artifact, which in the following we term the heartbeat kernel, with a sinusoid at the stimulation frequency and compared the resultant power spectrum to the measured spectrum. Indeed, in all subjects, all peaks of the transformed heartbeat kernels well matched the symmetric peaks of M/EEG spectra during tACS. Importantly, these peaks reached ± 10 Hz beyond the stimulation frequency. Furthermore, because subjects showed different modulation patterns, the artifact bandwidth and spectral pattern was unique for each subject. We concluded that the non-linear stimulation artifact affected M/EEG signals during tACS up to 10 Hz around the stimulation frequency.

Electrode size

In contrast to the small stimulation electrodes used here, many tACS studies use big rubber electrodes for stimulation. Thus, we repeated the experiments with big rubber electrodes in one subject, to test if our results may depend on the size of stimulation electrodes (Fig. 6). We found the same results for big rubber electrodes indicating that the observed artifacts are not related to electrode size.

In sum, our results demonstrate non-linear tACS artifacts related to physiological processes (heartbeat, respiration) that have a variable topography, are on the order of concurrent electrophysiological signals of interest, and are consistently found in all tested subjects. These artifacts pose a substantial problem for assessing neuronal activity during tACS.

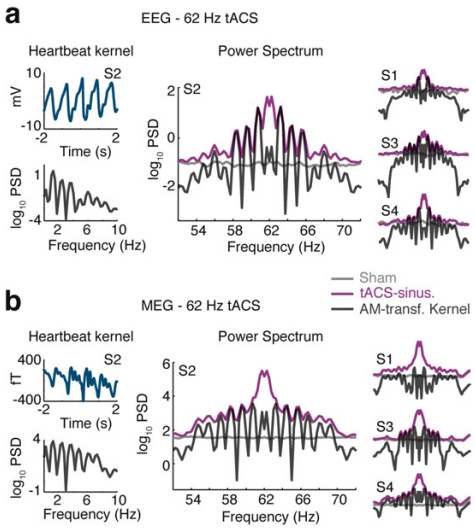

Fig. 5. AM transformation of heartbeat kernel. (*a*) Left panels depict the average heartbeat-locked EEG envelope modulation (heartbeat kernel) in time (top) and frequency (bottom) domains for subject S2 (channel PO10). The central panel shows EEG power spectral density for 62 Hz tACS, sham, and the AM-transformed heartbeat kernel. Smaller panels on the right show all other subjects. For tACS spectra, the main stimulation artifact was removed by subtracting a sinusoidal artifact model. (*b*) AM transformation of heartbeat kernel for MEG during 62 Hz tACS. EEG and MEG data show channels PO10 and MRT57, respectively.

tDCS artifact

The observed heartbeat-locked and respiration-locked tACS artifacts occur irrespective of the stimulation frequency. Thus, we hypothesized that the same artifacts also interfere with EEG and MEG during transcranial direct current stimulation (tDCS), which can be interpreted as tACS at 0 Hz. To test this, we performed a control experiment, in which we recorded EEG and MEG during cathodal and anodal tDCS. Indeed, the recorded EEG and MEG signals showed heartbeat and respiration related artifacts similar to tACS artifacts in both, frequency and time domains (Fig. 7). High-resolution spectra of EEG and MEG signals showed clear peaks at the individual's heart rate and its harmonic during both cathodal and anodal tDCS (filled and open red triangles in Fig. 7). Concerning respiration, strong signals below 1 Hz masked potential peaks at the individual's respiration rate (filled green triangles in Fig. 7), but peaks at the first harmonic of the respiration rate were clearly visible in the power spectrum (open green triangles in Fig. 7). Next, we applied heartbeat-locked and respiration-locked analyses in the time domain. Similar to tACS, recordings during tDCS showed strong rhythmic modulations locked to heartbeat and respiration (Fig. 7). The opposite polarity of these artifacts for cathodal and anodal stimulation as well as the artifact topography show that these modulations do not merely reflect the well-known electro- and magnetocardiogram (E/MCG) or respiration artifacts that are also observable during the sham condition. In sum, we concluded that EEG and MEG recordings during tDCS show artifacts similar to tACS artifacts.

Available artifact rejection methods

Recently, different approaches have been proposed to clean EEG and MEG signals from tES artifacts (Helfrich et al., 2014; Neuling et al., 2015; Soekadar et al., 2013; Voss et al., 2014). As our above findings provide new insights into the extent and characteristics of stimulation artifacts, we tested if existing methods account for them (Fig. 8; see also Materials and methods).

A recent combined EEG and tACS study (Helfrich et al., 2014) adopted a method used in simultaneous EEG-fMRI studies (Niazy et al., 2005) for cleaning of tACS artifacts: First, an adaptive artifact template is subtracted from each channel followed by PCA to remove artifactual components. We applied this approach on the EEG of one subject during 11 Hz tACS and investigated how well heartbeat-related non-linear artifacts were accounted for. We hypothesized that this approach was not able to completely remove the non-linear stimulation artifact, first, because the artifact template subtracted in the first step is temporally not aligned to heartbeat locked modulations, and second, because the variable spatial pattern of non-linear artifacts prevents fully capturing them in few components (Figs. 3 and 4). Indeed, we found that template subtraction did only reduce the main stimulation peak, but did not remove the side-peaks related to non-linear artifacts (Fig. 8a). Furthermore, because heartbeats are randomly positioned relative to stimulation phase, template subtraction destroyed the consistent heartbeat-locked modulation and replaced it with a variable modulation (Fig. 8b). This does not only fail to remove non-linear artifacts, but also complicates tracking them. As hypothesized, the second PCA step did not capture the non-linear artifacts in few components (Fig. 8c). We developed a pipeline based on three different criteria to identify components potentially affected by non-linear stimulation artifacts (Materials and methods). With this, we found about half of the components (36 of 72) as potentially affected. In sum, we concluded that the template subtraction step did not remove non-linear artifacts, but rather complicated tracking them, and that removing few principal components, did reduce, but not entirely remove non-linear artifacts.

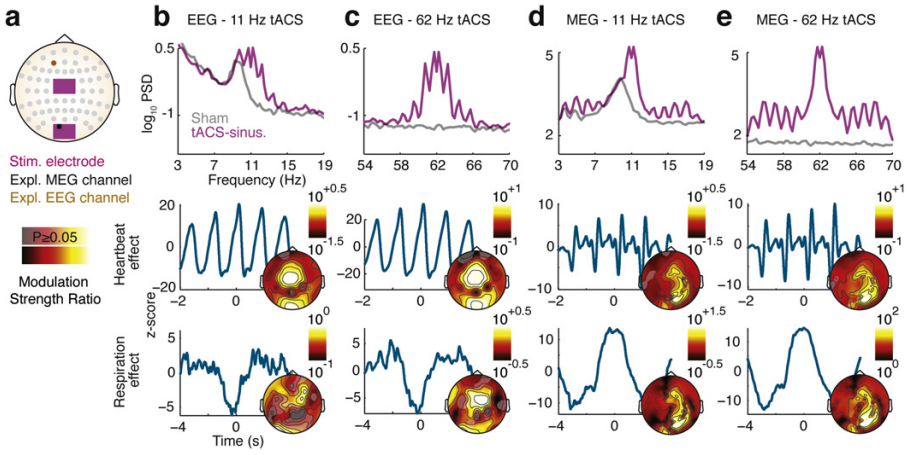

Fig. 6. tACS artifacts for large stimulation electrodes. (*a*) Two large rubber stimulation electrodes were positioned between 62 EEG electrodes placed according to the 10–10 system. The brown circle and black square indicate the position of channels used for demonstrating EEG (AF3) and MEG (MLO31) results, respectively. (*b*) The top panel shows the EEG power spectral density around the stimulation frequency during 11 Hz tACS and sham. The middle and bottom panels show heartbeat- and respiration-locked modulations of EEG envelope, respectively. Topographies show the strength of modulation relative to the neural signal of interest quantified as the decadic logarithm of the standard deviation of heartbeat-locked modulation divided by standard deviation of the sham signal at the stimulation frequency (non-significant modulations are masked at P = 0.05 corrected). (*c*) EEG artifacts for 62 Hz tACS. (*d*) MEG artifacts for 11 Hz tACS. (*e*) MEG artifacts for 62 Hz tACS.

Other recent combined MEG and tES studies (Neuling et al., 2015; Soekadar et al., 2013) suggested that adaptive linear spatial filtering (beamforming) (Van Veen et al., 1997) may not only map sensor signals to source space, but also remove stimulation artifacts. To test this for tACS and similar to another recent study (Neuling et al., 2015), we employed beamforming on our MEG recordings during 11 Hz tACS (Fig. 8d–e). At first sight, beamforming results looked promising. Comparing eyes open and eyes closed conditions revealed similar occipital alpha power increases for closed eyes during sham and tACS (Fig. 8d). However, source-level activity during tACS may be confounded by

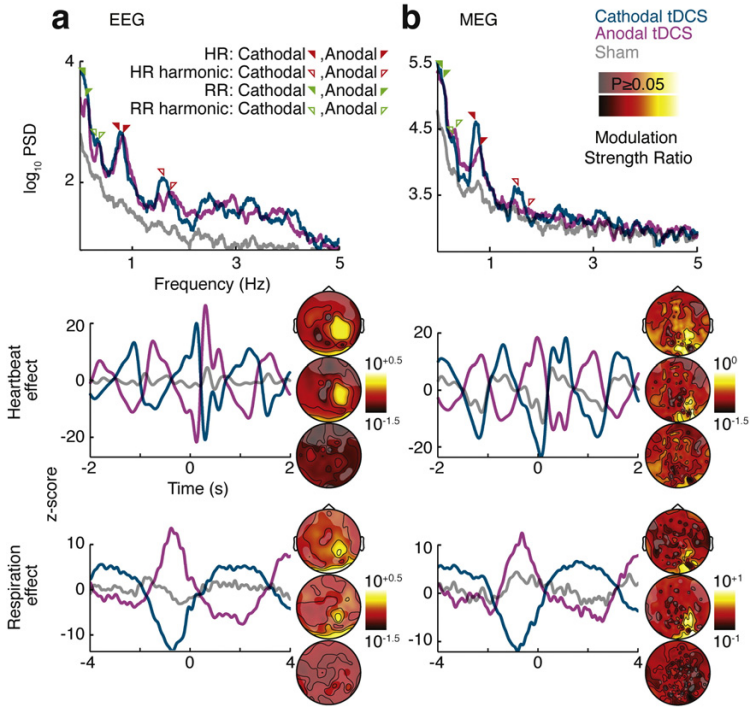

Fig. 7. tDCS artifacts. (*a*) Top panel shows the power spectral density of EEG signals during cathodal (blue) and anodal (magenta) tDCS compared to sham (gray). Power spectra show peaks at heart rate (HR) and respiration rate (RR) related frequencies. Harmonic of each rhythm refers to twice its rate. Middle and bottom panels depict z-score of heartbeat-locked and respiration-locked modulations of EEG during cathodal and anodal tDCS. Polarity of modulations depends on stimulation polarity. The three topographies in each panel show the strength of the artifact for cathodal (top), anodal (middle) and sham (bottom) recordings. Artifact strength is quantified as the decadic logarithm of the standard deviation of heartbeat or respiration-locked modulations divided by standard deviation of the sham signal (non-significant modulations are masked at P = 0.05 corrected). (*b*) Heartbeat and respiration artifacts in MEG signals recorded during tDCS. All conventions as in (*a*). MEG artifacts during sham might be enhanced due to the stimulation and EEG setup. EEG and MEG data show channels PO10 and MZO2, respectively.

stimulation artifacts, which subtracted out when comparing eyes open and eyes closed conditions. To test this, we exploited our finding that spectra of non-linear artifacts peaked at the stimulation frequency ± heartbeat and respiration frequencies. We hypothesized that, if stimulation artifacts confounded source-level activity, we should observe a spectrally specific correlation between the spatial patterns of source activities at 11 Hz (i.e. the stimulation frequency) and 11 Hz ± heartbeat and respiration frequencies. This is exactly what we found (Fig. 8e). We concluded that beamforming did not remove non-linear stimulation artifacts, but that they were still detectable at the source-level.

In summary, although current artifact-cleaning approaches reduced non-linear artifacts, they did not entirely remove them. Consequently, even after applying these approaches, power enhancements during stimulation may reflect remaining stimulation artifacts rather than neural entrainment.

Discussion

Here, we provide, to the best of our knowledge, the first systematic characterization of transcranial electric stimulation artifacts on EEG and MEG. We uncovered so far unknown non-linear stimulation artifacts, which reflect the modulation of stimulation artifacts by heartbeat and respiration.

Artifact mechanism

Non-linear stimulation artifacts were not caused by modulations of injected currents. Thus, following Ohm's law, we conclude that modulations observed in EEG are due to rhythmic changes of the body's impedance. Indeed, variations of blood volume in vessels caused by heartbeat and respiration, rhythmically modulate body impedance, a phenomenon that is used in impedance plethysmography to monitor cardiodynamic parameters (Dornhorst et al., 1952; Kristiansen et al., 2005; Michard, 2005; Nyboer et al., 1950).

For MEG, heartbeat and respiration can modulate the artifact through two different mechanisms. First, changes of body impedance slightly change the distribution of stimulation current on the head, which in turn influences the measured magnetic fields. A second mechanism, that may even contribute more strongly, is the movement of head and body due to respiratory efforts and heartbeats, a phenomenon used in ballistocardiography (Pinheiro et al., 2010). Rhythmic body movements change the distance between stimulation current, both on wires and on the head, and MEG sensors, which in turn leads to rhythmic modulations of the measured magnetic fields.

An important consequence of these mechanisms it that not only heartbeat and respiration, but also other factors that modulate body impedance, such as e.g. sweating or blood pressure, will non-linearly affect stimulation artifacts in EEG. In analogy, also other factors that cause body movement will non-linearly contribute to artifacts in MEG. Beyond the heartbeat and respiration related side-peaks, such slow changes of body impedance and head position may contribute to the width of the artifact peak in the power spectrum (Fig. 2).

Artifact characteristics

The strength of the demonstrated non-linear artifacts renders them highly relevant for the investigation of neural activity. For stimulation currents with 0.5 mA amplitude, which are commonly applied in the field, artifacts for many channels were stronger than the brain signals of interest. In the frequency domain, non-linear artifacts manifest as symmetric contamination of the neighborhood of the stimulation frequency, which corresponds to a spreading of artifacts well up to 10 Hz beyond the stimulation frequency. The extent and strength of this contamination depends on the exact strength and shape of variations in body impedance (EEG) and movements (MEG). Thus, the bandwidth and strength of the non-linear artifact differs between subjects. Furthermore, non-linear artifacts are more easily observed for higher stimulation frequencies where neural activity is weaker.

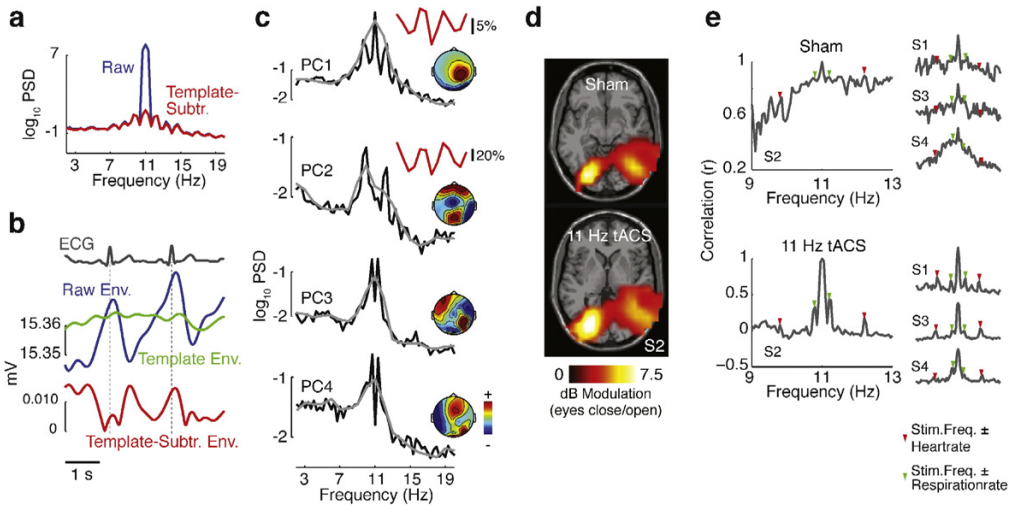

Fig. 8. Evaluation of existing artifact rejection approaches. (*a*–*c*) Method proposed by Helfrich et al. (2014). (*a*) Power spectral density before and after template subtraction. (*b*) Effect of template subtraction on heartbeat-locked modulations. Envelopes of raw signal, constructed template, and template-subtracted signal during 2 consecutive heartbeats for one EEG channel (O9, 11 Hz tACS). The raw envelope is consistently modulated with the ECG. Template subtraction yields inconsistent modulations reflecting the variable mismatch between raw signal and template (*c*) 4 example PCs. The power spectrum of each PC is shown with high (0.3 Hz, black) and low (1 Hz, gray) resolutions. PC1 has a symmetric power spectrum, an artifactual topography, and its 11 Hz power modulates significantly locked to heartbeats ($P < 0.05$). The small red inset shows %-modulation of 11 Hz power relative to the PC's average power before the R-peak. PC2 is an example PC with heartbeat-locked modulation of 11 Hz power significantly correlated to PC1's heartbeat-locked modulation ($P < 0.05$). PC3 is an example PC with non heartbeat-locked modulations of 11 Hz power significantly correlated to modulations of PC1 ($P < 0.05$). PC4 is an example PC with symmetric spectral peaks around the stimulation frequency. Notably, symmetric spectral peaks are detectable only with high-resolution spectra. (*d*, *e*) Evaluation of beamforming. (*d*) Source-level contrast between alpha power for eyes closed and eyes open conditions during sham and 11 Hz tACS (masked for $P < 10^{-7}$; subject S2). (*e*) Correlation between the source distribution of 11 Hz power and the power distribution at other frequencies for sham and 11 Hz tACS. Red and green arrows mark the stimulation frequency ± individual average heartbeat and respiration frequencies, respectively.

Importantly, respiration, heart rate, and other physiological parameters such as skin conductance and blood pressure do not only vary between subjects, but also between cognitive states. Thus, when comparing different cognitive states, potential changes in physiological parameters, and thus stimulation artifacts, need to be ruled out or accounted for. For example, a recent tACS study compared lucid and non-lucid dreaming (Voss et al., 2014). Heart and respiration rates change during lucid dreaming (LaBerge et al., 1986). Thus, confounding factors due to such physiological changes should be ruled out when attributing power changes to neural entrainment.

The nature of the non-linear artifact implies that it is independent of the stimulation frequency. This has several important consequences: First, not only the main stimulation frequency, but also all harmonics in the injected current are contaminated by non-linear artifacts. Thus, in particular for low stimulation frequencies like 10 Hz with many nearby harmonics most of the spectrum is contaminated. Second, the spectral bandwidth of non-linear artifacts will be identical for different stimulation frequencies. Thus when comparing different simulation frequencies, potential filtering in the frequency domain should be identical for all frequencies. In contrast, a recent study applied different filters for different stimulation frequencies (Voss et al., 2014). This may be problematic, because different remaining artifacts may in principle induce spurious differences between stimulation frequencies. Third, as our data and other recent results (Marshall et al., 2016) show, non-linear artifacts also affect electrophysiological recordings during tDCS, which is effectively tACS at 0 Hz. Modulations contaminate electrophysiological signals well up to the theta range, while higher frequencies may be clean due to the lack of harmonics (Marshall et al., 2016; Soekadar et al., 2013). It should be noted that artifactual modulations during tDCS have opposite polarities in cathodal and anodal conditions. Thus, their combination with normal E/MCG and, respiration artifacts that are independent of tDCS polarity, may lead to spurious differences of recorded low-frequency power between anodal and cathodal stimulation. This difference between cathodal and anodal stimulation also has to be accounted for in ERP/ERF analyses, when the events of interest interfere with heart and respiration rhythms.

We found that heartbeats and respiration do not only modulate the amplitude of the stimulation artifact, but also its spatial pattern (Figs. 3 and 4). In other words, the stimulation artifact is not projected onto sensors with a constant weight vector, but with a rhythmically varying vector. In turn, this implies that there is no single linear combination of sensor signals that fully captures the artifact. This property is problematic for potential cleaning procedures that are based on linear decompositions or linear filtering such as e.g. PCA, ICA, or beamforming. These methods rely on a constant spatial relationship between sources of interest and sensors. Indeed, our results indicate that removal of few principal components or beamforming does not completely remove non-linear artifacts. Our results accord well with recent findings that beamforming does not eliminate heartbeat-locked tDCS artifacts in MEG (Marshall et al., 2016).

Artifact rejection

Our findings allow for assessing existing artifact rejection approaches and provide critical constraints for developing new model-based rejection methods.

One application of our work is to track and quantify stimulation artifacts through steps of cleaning pipelines to evaluate their performance. We have shown how different characteristics of stimulation artifacts can be used as landmarks to detect stimulation artifacts (Fig. 8). Importantly, the employed approach needs to be adapted to the specific artifact rejection method at hand. For example, as we have shown, certain processing steps may destroy the consistent pattern of heartbeat-locked modulations and therefore a simple heartbeat-locked analysis of envelopes would not be able to track artifacts.

Although the discussed artifact-cleaning methods were not able to fully reject the stimulation artifact, they substantially suppressed it. While this suppression may allow for studying physiological responses (Helfrich et al., 2014; Neuling et al., 2015; Soekadar et al., 2013), spectral changes due to stimulation may still reflect remaining artifacts rather than stimulation induced neuronal entrainment. The same holds for observed changes of spectral modulations by cognitive state (Voss et al., 2014). In this situation, a feasible strategy may be to estimate the strength of residual artifacts as a necessary lower bound for potential entrainment of neural activity. Our work provides the basis for this approach.

Finally, our results pave the way for new artifact-suppressing methods. For example, one may regress out an amplitude-modulation model of the stimulation artifact from the data. This model may be constructed by combining the average kernel of heartbeat and respiration induced modulations with ECG and respiration peaks (Fig. 5). Another option would be to use the output voltage of the stimulation system for cleaning artifacts from EEG, because the output voltage at least partly reflects the underlying changes in body impedance. Similarly, for MEG it may be useful to track head-movements during stimulation and measurements. However, an important caveat for all these approaches is that any error in estimating the artifact amplitude, no matter whether over- or underestimating it, leads to an artifactual increase in signal power at the stimulation frequency, which might be mistaken as neural entrainment.

Apart from artifact suppression methods, also new stimulation approaches may allow for reducing stimulation artifacts. E.g., amplitude-modulated tACS may allow for effectively avoiding stimulation artifacts at the frequency band of interest (Witkowski et al., 2016). It remains to be determined how the physiological effects of this stimulation approach compare to conventional tACS.

Conclusion

In sum, we have uncovered and characterized non-linear stimulation artifacts in EEG and MEG during transcranial electric stimulation. These artifacts depend on the subjects' physiological state and are not fully accounted for by current artifact rejection methods. Our work shows how to track these artifacts and paves the way for new artifact rejection approaches.

Funding

This work was supported by the Centre for Integrative Neuroscience (Deutsche Forschungsgemeinschaft, EXC 307).

Notes

All authors designed the research; N.N. performed the experiments and analyzed the data; N.N. and M.S. wrote the manuscript.

Appendix A. Supplementary data

Supplementary data to this article can be found online at http://dx.doi.org/10.1016/j.neuroimage.2016.03.065.

References

Brittain, J.-S., Probert-Smith, P., Aziz, T.Z., Brown, P., 2013. Tremor suppression by rhythmic transcranial current stimulation. Curr. Biol. 23, 436–440. http://dx.doi.org/10.1016/j.cub.2013.01.068.

Buzsáki, G., Draguhn, A., 2004. Neuronal oscillations in cortical networks. Science 304, 1926–1929. http://dx.doi.org/10.1126/science.1099745.

Dmochowski, J.P., Datta, A., Bikson, M., Su, Y., Parra, L.C., 2011. Optimized multi-electrode stimulation increases focality and intensity at target. J. Neural Eng. 8, 046011. http://dx.doi.org/10.1088/1741-2560/8/4/046011.

Dornhorst, A.C., Howard, P., Leathart, G.L., 1952. Respiratory variations in blood pressure. Circulation 6, 553–558. http://dx.doi.org/10.1161/01.CIR.6.4.553.

Fries, P., 2005. A mechanism for cognitive dynamics: neuronal communication through neuronal coherence. Trends Cogn. Sci. 9, 474–480. http://dx.doi.org/10.1016/j.tics.2005.08.011.
Fröhlich, F., McCormick, D.A., 2010. Endogenous electric fields may guide neocortical network activity. Neuron 67, 129–143. http://dx.doi.org/10.1016/j.neuron.2010.06.005.
Helfrich, R.F., Schneider, T.R., Rach, S., Trautmann-Lengsfeld, S.A., Engel, A.K., Herrmann, C.S., 2014. Entrainment of brain oscillations by transcranial alternating current stimulation. Curr. Biol. 24, 333–339. http://dx.doi.org/10.1016/j.cub.2013.12.041.
Herrmann, C.S., Rach, S., Neuling, T., Strüber, D., 2013. Transcranial alternating current stimulation: a review of the underlying mechanisms and modulation of cognitive processes. Front. Hum. Neurosci. 7, 279. http://dx.doi.org/10.3389/fnhum.2013.00279.
Jensen, O., Mazaheri, A., 2010. Shaping functional architecture by oscillatory alpha activity: gating by inhibition. Front. Hum. Neurosci. 4, 186. http://dx.doi.org/10.3389/fnhum.2010.00186.
Kanai, R., Chaieb, L., Antal, A., Walsh, V., Paulus, W., 2008. Frequency-dependent electrical stimulation of the visual cortex. Curr. Biol. 18, 1839–1843. http://dx.doi.org/10.1016/j.cub.2008.10.027.
Kristiansen, N.K., Fleischer, J., Jensen, M.S., Andersen, K.S., Nygaard, H., 2005. Design and evaluation of a handheld impedance plethysmograph for measuring heart rate variability. Med. Biol. Eng. Comput. 43, 516–521.
LaBerge, S., Levitan, L., Dement, W.C., 1986. Lucid dreaming: physiological correlates of consciousness during REM sleep. J. Mind Behav. 7, 251–258.
Marshall, L., Helgadóttir, H., Mölle, M., Born, J., 2006. Boosting slow oscillations during sleep potentiates memory. Nature 444, 610–613. http://dx.doi.org/10.1038/nature05278.
Marshall, L., Kirov, R., Brade, J., Mölle, M., Born, J., 2011. Transcranial electrical currents to probe EEG brain rhythms and memory consolidation during sleep in humans. PLoS One 6, e16905. http://dx.doi.org/10.1371/journal.pone.0016905.
Marshall, T.R., Esterer, S., Herring, J.D., Bergmann, T.O., Jensen, O., 2016. On the relationship between cortical excitability and visual oscillatory responses—a concurrent tDCS-MEG study. NeuroImage 104, 41–49.
Michard, F., 2005. Changes in arterial pressure during mechanical ventilation. Anesthesiology 103, 419–428 quiz 449–445.
Neuling, T., Ruhnau, P., Fuscà, M., Demarchi, G., Herrmann, C.S., Weisz, N., 2015. Friends, not foes: magnetoencephalography as a tool to uncover brain dynamics during transcranial alternating current stimulation. NeuroImage 118, 406–413. http://dx.doi.org/10.1016/j.neuroimage.2015.06.026.
Niazy, R.K., Beckmann, C.F., Iannetti, G.D., Brady, J.M., Smith, S.M., 2005. Removal of FMRI environment artifacts from EEG data using optimal basis sets. NeuroImage 28, 720–737. http://dx.doi.org/10.1016/j.neuroimage.2005.06.067.
Nolte, G., 2003. The magnetic lead field theorem in the quasi-static approximation and its use for magnetoencephalography forward calculation in realistic volume conductors. Phys. Med. Biol. 48, 3637. http://dx.doi.org/10.1088/0031-9155/48/22/002.
Nyboer, J., Kreider, M.M., Hannapel, L., 1950. Electrical impedance plethysmography a physical and physiologic approach to peripheral vascular study. Circulation 2, 811–821. http://dx.doi.org/10.1161/01.CIR.2.6.811.
Oostenveld, R., Fries, P., Maris, E., Schoffelen, J.-M., 2011. FieldTrip: open source software for advanced analysis of MEG, EEG, and invasive electrophysiological data. Comput. Intell. Neurosci. 2011, 156869. http://dx.doi.org/10.1155/2011/156869.
Ozen, S., Sirota, A., Belluscio, M.A., Anastassiou, C.A., Stark, E., Koch, C., Buzsáki, G., 2010. Transcranial electric stimulation entrains cortical neuronal populations in rats. J. Neurosci. 30, 11476–11485. http://dx.doi.org/10.1523/JNEUROSCI.5252-09.2010.
Pinheiro, E., Postolache, O., Girão, P., 2010. Theory and developments in an unobtrusive cardiovascular system representation: ballistocardiography. Open Biomed. Eng. J. 4, 201–216. http://dx.doi.org/10.2174/1874120701004010201.
Polanía, R., Nitsche, M.A., Korman, C., Batsikadze, G., Paulus, W., 2012. The importance of timing in segregated theta phase-coupling for cognitive performance. Curr. Biol. 22, 1314–1318. http://dx.doi.org/10.1016/j.cub.2012.05.021.
Romei, V., Gross, J., Thut, G., 2010. On the role of prestimulus alpha rhythms over occipito-parietal areas in visual input regulation: correlation or causation? J. Neurosci. 30, 8692–8697. http://dx.doi.org/10.1523/JNEUROSCI.0160-10.2010.
Romei, V., Driver, J., Schyns, P.G., Thut, G., 2011. Rhythmic TMS over parietal cortex links distinct brain frequencies to global versus local visual processing. Curr. Biol. 21, 334–337. http://dx.doi.org/10.1016/j.cub.2011.01.035.
Schutter, D.J.L.G., Hortensius, R., 2010. Retinal origin of phosphenes to transcranial alternating current stimulation. Clin. Neurophysiol. 121, 1080–1084. http://dx.doi.org/10.1016/j.clinph.2009.10.038.
Schwiedrzik, C.M., 2009. Retina or visual cortex? The site of phosphene induction by transcranial alternating current stimulation. Front. Integr. Neurosci. 3. http://dx.doi.org/10.3389/neuro.07.006.2009.
Siegel, M., Donner, T.H., Engel, A.K., 2012. Spectral fingerprints of large-scale neuronal interactions. Nat. Rev. Neurosci. 13, 121–134. http://dx.doi.org/10.1038/nrn3137.
Singer, W., 1999. Neuronal synchrony: a versatile code for the definition of relations? Neuron 24 (49–65), 111–125.
Soekadar, S.R., Witkowski, M., Cossio, E.G., Birbaumer, N., Robinson, S.E., Cohen, L.G., 2013. In vivo assessment of human brain oscillations during application of transcranial electric currents. Nat. Commun. 4. http://dx.doi.org/10.1038/ncomms3032.
Van Veen, B.D., van Drongelen, W., Yuchtman, M., Suzuki, A., 1997. Localization of brain electrical activity via linearly constrained minimum variance spatial filtering. IEEE Trans. Biomed. Eng. 44, 867–880. http://dx.doi.org/10.1109/10.623056.
Voss, U., Holzmann, R., Hobson, A., Paulus, W., Koppehele-Gossel, J., Klimke, A., Nitsche, M.A., 2014. Induction of self awareness in dreams through frontal low current stimulation of gamma activity. Nat. Neurosci. http://dx.doi.org/10.1038/nn.3719 (advance online publication).
Witkowski, M., Cossio, E.G., Chander, B.S., Braun, C., Birbaumer, N., Robinson, S.E., Soekadar, S.R., 2016. Mapping entrained brain oscillations during transcranial alternating current stimulation (tACS). NeuroImage 104, 89–98.
Womelsdorf, T., Valiante, T.A., Sahin, N.T., Miller, K.J., Tiesinga, P., 2014. Dynamic circuit motifs underlying rhythmic gain control, gating and integration. Nat. Neurosci. 17, 1031–1039. http://dx.doi.org/10.1038/nn.3764.
Zaehle, T., Rach, S., Herrmann, C.S., 2010. Transcranial alternating current stimulation enhances individual alpha activity in human EEG. PLoS One 5, e13766. http://dx.doi.org/10.1371/journal.pone.0013766.

Supplementary Information

Physiological processes non-linearly affect electrophysiological recordings during transcranial current stimulation

Nima Noury[1, 2], Joerg F. Hipp[1, 3] and Markus Siegel[1]

[1] Centre for Integrative Neuroscience & MEG Center, University of Tübingen, Germany

[2] IMPRS for Cognitive and Systems Neuroscience, Tübingen, Germany

[3] F. Hoffmann-La Roche, Pharma Research and Early Development, Basel, Switzerland

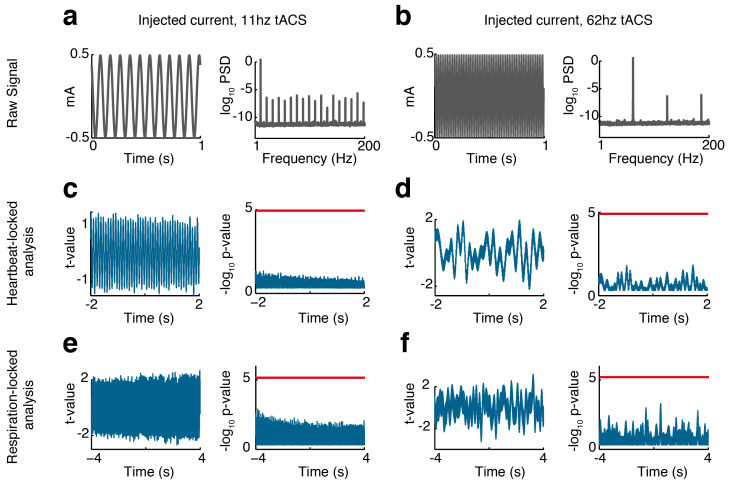

Supplementary Figure 1. Stimulation current. (*a*) Raw stimulation current in the time-domain (left) and broad-band power spectral density (right) of the 11 Hz tACS stimulation current. (*b*) Stimulation current for 62 Hz tACS. (*c*) The left panel shows the average heartbeat-locked envelope of the stimulation current for 11 Hz tACS quantified as t-scores against the null-hypothesis of no modulation. The right panel shows the corresponding p-values. The red line shows the significance threshold at P=0.05 corrected for the number of time points. (*d*) Heartbeat-locked envelope of 62 Hz tACS stimulation current. (*e*) Respiration-locked envelope of 11 Hz tACS stimulation current. (*f*) Respiration-locked envelope of 62 Hz tACS stimulation current.

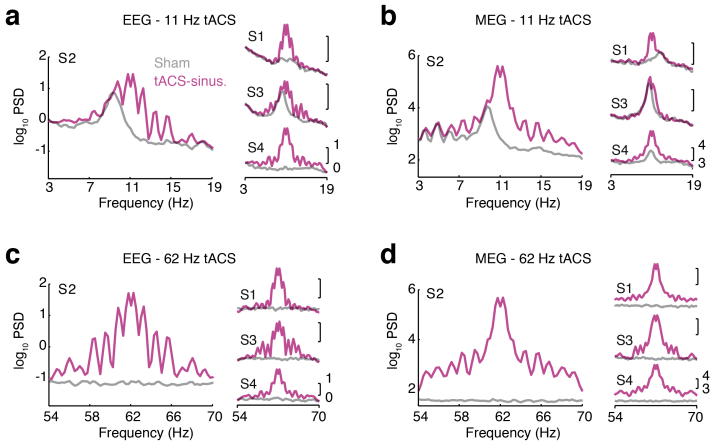

Supplementary Figure 2. Broad-band tACS artifacts. (*a*) EEG power spectral density around the stimulation frequency during sham and 11 Hz tACS (0.25 Hz resolution). For the tACS condition, a sinusoidal artifact model was removed from the data. The large spectrum shows data from subject S2. Smaller spectra show all other subjects. (*b*) MEG spectra for 11 Hz tACS. (*c*) EEG spectra for 62 Hz tACS. (*d*) MEG spectra for 62 Hz tACS. EEG and MEG data show channels PO10 and MRT57, respectively.

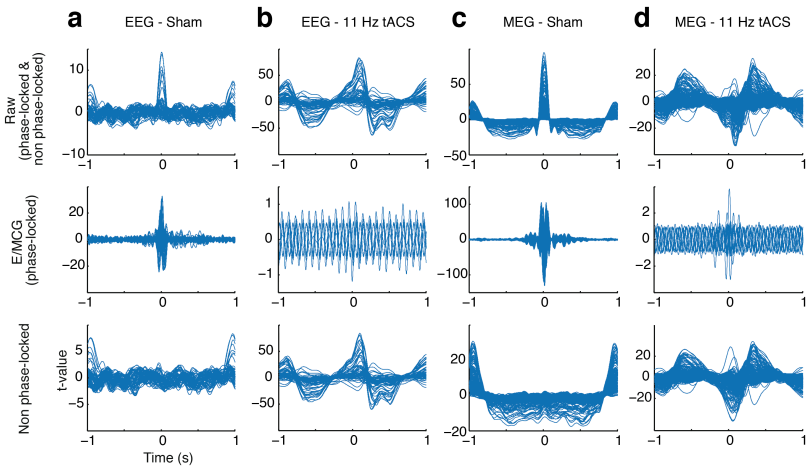

Supplementary Figure 3. tACS artifacts and E/MCG. To test if heartbeat-locked modulations of envelopes merely reflected the E/MCG, we computed the E/MEG signal phase-locked to heartbeats, i.e. the E/MCG, by heartbeat-locked averaging. Non-phase locked signals were computed by subtracting the E/MCG aligned to heartbeats from the raw signals (*a*) Top panel: Heartbeat-locked envelope modulation at 11 Hz during sham for the raw EEG. Middle panel: ECG (EEG phase-locked to heartbeats). Bottom panel: Heartbeat-locked modulation of 11 Hz envelope for the EEG non phase-locked to heartbeats, i.e. after removing the ECG. During sham, the ECG contributes to a significant envelope modulation at 11 Hz. (*b*) 11 Hz envelope modulations during 11 Hz tACS. Removing the phase-locked components, i.e. removing the ECG, does not affect the large heartbeat-locked envelope modulations. Thus these modulations do not merely reflect the ECG (*c*) MEG sham and (*d*) MEG 11 Hz tACS show the same results. All signals are quantified as t-scores against the null-hypothesis of no modulation. All EEG and MEG channels are depicted.

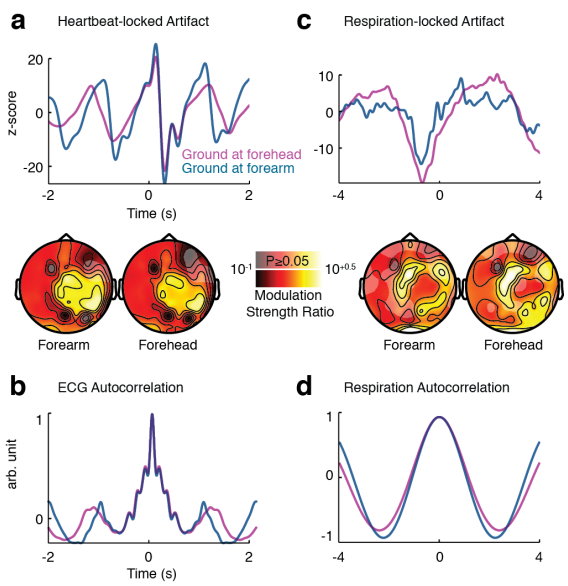

Supplementary Figure 4. Effect of the ground electrode. (*a*) Top panel shows the heartbeat-locked envelope artifact during 62 Hz tACS in EEG recordings (channel PO10) with ground electrode placed either on forearm (blue) or forehead (purple). The topographies in the bottom panel show the strength of modulation relative to the neural signal quantified as the decadic logarithm of the standard deviation of heartbeat-locked modulation divided by standard deviation of the sham signal at the stimulation frequency in recordings with ground electrode placed on either forearm (left) or forehead (right). non-significant modulations are masked at P = 0.05 corrected. (*b*) Autocorrelation of the ECG signal in the two EEG recordings. The difference in the average heart rate of the two recordings is evident in both ECG autocorrelation (*b*) and the rhythmic envelope modulations (*a*). (*c,d*) Respiration-locked envelope artifact (*c*) and autocorrelation of recorded respiratory effort (*d*). All conventions as in (*a*) and (*b*).

6.2 Paper 2

Noury, N., Siegel, M., Phase properties of transcranial electrical stimulation artifacts in electrophysiological recordings. NeuroImage 158, 406–416. doi:10.1016/j.neuroimage.2017.07.010

Statement of contributions:

Experimental design: NN and MS.

Data acquisition: NN.

Data analysis: NN.

Manuscript writing: NN and MS.

NeuroImage 158 (2017) 406–416

Contents lists available at ScienceDirect

NeuroImage

journal homepage: www.elsevier.com/locate/neuroimage

Phase properties of transcranial electrical stimulation artifacts in electrophysiological recordings

Nima Noury [a,b,*], Markus Siegel [a,*]

[a] Centre for Integrative Neuroscience & MEG Center, University of Tübingen, Germany
[b] IMPRS for Cognitive and Systems Neuroscience, Tübingen, Germany

ARTICLE INFO

Keywords:
Transcranial electric stimulation (tES)
Transcranial alternating current stimulation (tACS)
Transcranial direct current stimulation (tDCS)
EEG
MEG
Neural entrainment
Stimulation artifacts

ABSTRACT

Monitoring brain activity during transcranial electric stimulation (tES) is an attractive approach for causally studying healthy and diseased brain activity. Yet, stimulation artifacts complicate electrophysiological recordings during tES. Design and evaluation of artifact removal methods require a through characterization of artifact features, i.e. characterization of the transfer function that defines the relationship between the tES stimulation current and tES artifacts. Here we characterize the phase relationship between stimulation current and tES artifacts in EEG and MEG. We show that stimulation artifacts are not pure in-phase or anti-phase signals, but that non-linear mechanisms induce steady phase deflections relative to the stimulation current. Furthermore, phase deflections of stimulation artifacts are slightly modulated by each heartbeat and respiration. For commonly used stimulation amplitudes, artifact phase deflections correspond to signals several times bigger than normal brain signal. Moreover, the strength of phase deflections varies with stimulation frequency. These phase effects should be accounted for during artifact removal and when comparing recordings with different stimulation frequencies. We summarize our findings in a mathematical model of tES artifacts and discuss how this model can be used in simulations to design and evaluate artifact rejection techniques. To facilitate this research, all raw data of this study is made freely available.

1. Introduction

Current neuroscience in humans largely relies on correlative approaches. Thus, manipulative techniques to precisely interfere with human brain function are much needed. Transcranial Electric Stimulation (tES) is a non-invasive brain stimulation technique, applicable to both healthy and diseased subjects, in which a weak electrical current is applied to the subject's head (Fertonani and Miniussi, 2016; Nitsche and Paulus, 2000). Despite promising behavioral effects of tES, its use in both forms of direct and alternating current stimulation (tDCS and tACS, respectively) has been mainly restricted to behavioral and after effect studies (Kuo and Nitsche, 2012; Soekadar et al., 2016; Thut et al., 2017). This is because strong stimulation artifacts interfere with simultaneous electrophysiological recordings (Noury et al., 2016).

Recently, several approaches to monitor brain activity during tES by means of EEG and MEG have been proposed (Helfrich et al., 2014; Neuling et al., 2015; Soekadar et al., 2013; Voss et al., 2014; Witkowski et al., 2016). Several of these efforts are based on artifact removal techniques that aim to dissociate brain signals from stimulation artifacts. These techniques, as well as computer simulations and phantom experiments employed to design and evaluate these techniques, are based on critical assumptions about stimulation artifacts. If these assumptions are wrong, this may lead to misleading results and wrong interpretations when trying to dissociate human brain signals and tES artifacts from EEG and MEG (Noury et al., 2016). Thus, a thorough understanding of stimulation artifacts is needed to prevent pitfalls of simultaneous tES-M/EEG research and to pave the way for new artifact removal methods. Importantly, this understanding of stimulation artifacts is also needed to verify artifact removal methods by means of phantoms or computer simulations.

Recently, we characterized the amplitude of tES artifacts and showed that, contrary to previous assumptions, for both EEG and MEG, tES artifacts do not simply reflect stimulation currents, but that heartbeat and respiration strongly modulate the strength of stimulation artifacts in a non-linear fashion and cause a time-varying mapping between stimulation current and tES artifacts (Noury et al., 2016). Here, we extend our previous work by characterizing the phase properties of tACS stimulation artifacts.

* Corresponding authors. Centre for Integrative Neuroscience, University of Tübingen, Otfried-Müller-Str. 25, 72076 Tübingen, Germany.
E-mail addresses: nima.noury@cin.uni-tuebingen.de (N. Noury), markus.siegel@uni-tuebingen.de (M. Siegel).

http://dx.doi.org/10.1016/j.neuroimage.2017.07.010
Received 23 February 2017; Received in revised form 14 June 2017; Accepted 9 July 2017
Available online 12 July 2017

2. Materials and Methods

2.1. Participants and experimental protocol

All experiments were conducted in 5 healthy male participants, were carried out in accordance with the Declaration of Helsinki, and were approved by the local ethics committee. All subjects gave written informed consent before participating. 4 subjects participated in 6 experimental runs of the main tACS experiment with small stimulation electrodes. EEG and MEG signals were recorded during the entire experiment. Each run consisted of the following sequential conditions: sham, tACSa, tACSb, sham, tACSb, tACSa. Each condition was 66 s, and tACSa and tACSb were randomly assigned to 11 Hz and 62 Hz tACS. In the first 5 runs, subjects were fixating at a central fixation spot (60 Hz monitor refresh rate) and in the last run they were asked to close their eyes.

To check the influence of stimulation electrode size on the artifact's phase, we performed a control experiment with large rubber electrodes in one subject (6 experimental runs similar to the main experiment, subject 2). In another control experiment in the same subject, we recorded one experimental run with only MEG signals recorded during application of tACS with large rubber electrodes (no EEG cap attached to the subject, eyes open). The aim of this control experiment was to check for potential noise effects of the EEG device on the MEG system. We performed one more control experiment on another single subject (subject 5) to check for the potential influence of the EEG ground electrode placement on the stimulation artifact. The recording and stimulating electrode layout was the same as the layout in the main tACS experiment. In this control experiment, we applied 62 Hz tACS and continuously and recorded 10 min of EEG with ground on the right forearm and 10 min of EEG with ground on the forehead (Fpz of 10-10 system), while the subject fixated a central fixation spot.

2.2. Transcranial electric stimulation

Stimulation current was applied with an IZ2h stimulator (Tucker Davis Technologies Inc.) with 0.5 mA amplitude (i.e., 1 mA peak-to-peak for tACS). None of the subjects reported any flicker percept. For the main experiment, stimulation was applied through two standard Ag/AgCl EEG electrodes over right occipital and right parietal areas (electrodes O10 and CP4 of the 10-10 electrode system). For the control experiment with large electrodes, 35 cm^2 MR-compatible rubber electrodes (neuroConn GmbH) were placed over occipital and frontal lobes underneath the EEG cap. For all experiments, stimulation electrodes were attached using Ten20 conductive paste (Weaver and Company) and their impedance was kept below 2.5 kΩ. To minimize magnetic artifacts produced by the stimulation current, we carefully twisted all stimulation cables.

2.3. Data acquisition and preprocessing

We simultaneously recorded 72-channel EEG (NeurOne system, Mega Electronics Ltd) and 272-channel MEG (Omega, 2000; CTF Systems) throughout all experiments at 10,000 Hz and 2343.8 Hz sampling rate, respectively. EEG electrodes were positioned based on the 10-10 electrode system using an EEG cap (EC80, EASYCAP). All signals were in the dynamic ranges of the recording systems and no clipping was observed for either EEG or MEG signals.

EEG electrodes were attached using Abralyt 2000 conductive gel and impedances were kept below 2.5 kΩ for most electrodes. In the main experiment, we referenced EEG electrodes to FCz, while in the control experiment with large rubber electrodes signals were referenced to Fz, because of the placement of the stimulation rubber electrodes. The ground electrode was positioned on the right forearm, except for one control experiment with 10 min of ground electrode placement on the forehead. We did not apply any offline re-referencing to the EEG recordings. Along with EEG and MEG, we recorded the stimulation (injected) current, vertical EOG (two electrodes above an below the right eye), ECG, and respiratory movements using bipolar channels of the EEG system. The injected current was measured by recording the voltage drop across a 200 Ω resistor positioned in series to the head. The ECG was recorded through 2 electrodes placed below the right clavicle and below the left pectoral muscle. Respiration was continuously recorded with a piezo respiratory belt transducer (Vermed-Medizintechnik).

2.4. Eye blinks

We applied a zero-phase 6th order Butterworth low-pass filter at 4 Hz to the difference of the vertical EOG channels, and visually inspected the result to find the moments of eye blinks. Application of a low-pass filter was necessary, because during 11 Hz tACS strong stimulation artifacts mask the effect of eye blinks. All intervals with eye blinks were removed from the phase signals.

2.5. Artifact phase shift

For each EEG and MEG channel, we defined the temporal artifact phase-shift signal as the phase shift between each channel's signal and the injected current. As the injected current was recorded with the EEG system, for calculating the phase shift of the MEG channels, we used an MEG-synchronized version of the injected current (see below). The original injected current recorded with the EEG system was used for the EEG channels. We first band-pass filtered the signals using a 6th-order zero-phase Butterworth filter centered at the stimulation frequency of interest with a pass-band of ±5 Hz. After band-pass filtering, we down-sampled signals to 1 000 Hz and 781.25 Hz, respectively for EEG and MEG, and applied the Hilbert transform to obtain phase signals. Finally, we subtracted the un-wrapped phase of the injected current form the un-wrapped phase of each channel. For all comparisons between sham and tACS conditions, we used the filter and injected current of the corresponding tACS condition. To test the significance of the phase shift of each channel, we calculated phase shifts of 1 000 white noise signals with the same procedure as applied to the recorded signal for the corresponding condition, and compared the circular standard deviation of each channel's phase shift over time with the population of circular standard deviations of the noise phase signals.

EEG recordings corresponding to the reference channel by definition contain only measurement noise. Therefore, we excluded this channel from all following analyses.

2.6. Phase deflection

For each channel, we calculated the circular mean of the phase shift over time and defined the phase deflection as the smallest value among the phase mean subtracted by 0, π and -π.

To test the significance of the phase deflection of each channel, we applied a permutation test. First, we calculated the phase deflection from 0, π or -π at each time point (the temporal average of this signal is the phase deflection, as defined above). Band-pass filtering around the stimulation frequency induces a dependency of phases at nearby time points. To take into account this dependency, we re-sampled the phase deflection signal at 2 Hz, i.e. substantially below the bandwidth of the pass-band (±5 Hz). We then computed the p-value of the null-hypothesis of zero phase deflection, by comparing the absolute of the temporal average of this signal against the distribution of the absolute of temporal averages of 1 000 random phase deflection signals. These random signals were generated by randomly assigning a sign to the phase deflection at each time point.

We defined the effective strength of phase deflections as the strength of a sine signal that could have generated these phase deflections, when added to a sinusoidal artifact with no phase deflection. To find such a sine signal, for each channel and each stimulation frequency, we calculated the difference between a sine wave with zero-phase and a sine wave with

the observed phase deflection, and multiplied the result with the mean artifact amplitude. Finally, we calculated the standard deviation of this signal and compared it against the standard deviation of sham recordings (the sham signal was band-passed filtered with a 6th order Butterworth filter centered at the stimulation frequency of interest with a pass-band of ±5 Hz). We applied a similar procedure to quantify the effective strength of phase jitters over time. We calculated the difference between a sine wave with zero-phase and a sine wave with mean-removed phase signal (i.e. containing only the phase jitter) of each channel, multiplied the result with the mean artifact amplitude of each channel, and divided the variance of this signal by the variance of the sham recording.

To test the effect of tACS frequency on phase deflections, for each channel, we calculated the ratio between the absolute value of phase deflections of the two stimulation conditions, found the median across all channels and subjects, and compared this value to the distribution of 1 000 randomly generated values. These random values were generated by applying the same procedure with condition labels randomly assigned to the phase deflections.

2.7. MEG-synchronized injected current

Because the stimulation current was recorded with the EEG system, we generated the MEG-synchronized version of the stimulation current by estimating and correcting the differences in system clocks and temporal offsets between the MEG and EEG systems based on trigger codes that were simultaneously sent to both systems. We first generated two time vectors, representing moments that triggers were received by EEG and MEG systems. Next, we performed a linear regression to find the best scale and shift parameters that map MEG time to EEG time. Using these parameters, we estimated the corresponding EEG time points for the moments at which the MEG system sampled the data, and finally resampled the injected current at these time points to find the rate-corrected version of the injected current.

This procedure corrected for the difference between EEG and MEG clock rates, and most of the temporal offset between the two systems. However, the resulted rate-corrected injected current still contained a small temporal offset relative to the MEG signals. This offset was either due to a difference of hardware-induced delays between EEG and MEG signals (e.g. due to anti-aliasing filters), or due to a small difference in how fast MEG and EEG hardware register the received trigger codes. We estimated this temporal offset based on the increase in the phase difference between the rate-corrected injected current and MEG signals from 6.99° to 38.85° (median across channels and subjects), when the stimulation frequency increases from 11 Hz to 62 Hz. These phase values correspond to a temporal offset of 1.7 ms between the MEG signals and the rate-corrected injected current. Therefore, we generated the MEG-synchronized injected current by shifting the rate-corrected injected current by 1.7 ms.

2.8. Temporal analyses

To find the effect of heartbeats on artifact phase signals, we first found the R-peaks of each subject's simultaneous ECG, defined 4 s long segments of the phase shift signal centered on the R-peaks, and averaged all these segments. To assess the significance of each subject's heartbeat related modulation, for each channel we calculated the power of the average heartbeat-locked phase signal at the frequency of the subject's average heart rate by means of the discrete-time Fourier transform. Next, we assigned a p-value to this power value based on the histogram of 1 000 power values generated with the same procedure but using random R-peak moments. The resulting p-values were corrected for false discovery rate (FDR; Benjamini and Hochberg, 1995). We studied the temporal dynamic of the heartbeat-locked phase modulations by means of PCA. PCA was applied only to the average heartbeat-locked phase modulation of those channels that showed significant heartbeat-locked phase modulations. Finally, we estimated the effective strength of these phase modulations. For each channel, we generated two 4 s long sinusoids, one with no phase modulation and the other one with the measured average heartbeat-locked phase modulation, subtracted them from each other, multiplied the result with the channel's average artifact strength (the standard deviation of each channel's signal over time), and compared the standard deviation of this residual signal with the standard deviation of the sham recordings.

We applied the same procedure to check the effect of respiration on 8 s long segments centered on inspiration endpoints.

2.9. Spectral analyses

We estimated the power spectra of sham and tACS conditions on 4 s long segments. We first split the data in 4 s long segments, applied a Hanning window to each segment, computed the Fourier transform of each segment, and calculated the average power across segments. To study the influence of the artifact's phase modulation on the artifact's power spectrum (Fig. 3e, j), we first estimated the average heartbeat-locked phase modulation as explained above. Then we constructed two 4 s long 62 Hz sine waves: one without phase modulation and one with the average heartbeat-locked phase modulation. We scaled both sine waves with the average artifact strength of the relevant channel. Finally, to check the influence of the phase modulation on the power spectrum, we subtracted the non phase-modulated signal from the phase-modulated signal and calculated the power of the Fourier transform of the residual.

2.10. Influence of pure amplitude modulation

Heartbeat and respiration strongly modulate the strength of artifact signals (Noury et al., 2016). To make sure that these amplitude modulations do not influence Hilbert transformation and phase estimations in a way that leads to the observed heartbeat and respiration locked phase effects, we repeated the temporal analysis on a fake phase signal. For each channel and each stimulation condition, we excluded the actual phase of signals and generated waveforms that only reflected the amplitude modulations of the recordings. This was done by calculating each signal's amplitude by means of Hilbert transform and multiplying it with the injected current. Finally, we obtained the fake phase signals by estimating phase of the resulted waveforms.

2.11. Heartbeat simulation

We checked if a combination of EEG referencing, small random phase shifts on each EEG electrode (i.e. the random capacitive effect), and heartbeat-locked artifact amplitude modulations might generate heartbeat-locked artifact phase modulations (Fig. 5c). We first re-referenced EEG recordings to average reference to estimate the tACS artifact of each EEG electrode prior to referencing to Fcz. By means of Hilbert transform, we found the artifact amplitude at each EEG electrode, segmented it into 4 s long pieces centered at each ECG R-peak, and computed the average heartbeat-locked artifact amplitude modulation at each EEG electrode. For each electrode, we then multiplied this amplitude signal onto a 4 s long sine wave at 11 Hz, which had a small constant random phase drawn from a uniform distribution from 0 to 0.05 radians. This specific interval was chosen because the absolute value of phase deflections of the 10 percent of channels with strongest artifact amplitudes were lying in an interval of about 0.05 radians. The rational behind this selection is that, based on the model presented in Fig. 5a, phase deflections of channels with strong artifacts should mostly reflect the capacitive effect of the EEG electrodes. Next, we simulated the effect of referencing by simply subtracting the signal of the desired reference electrode from all other electrodes. Finally, for each channel we estimated the temporal phase modulation by means of Hilbert transformation, and quantified the modulation strength as the temporal standard deviation of the phase modulation in radians. We repeated this

simulation 100 times and calculated the mean across all simulations.

2.12. Heartbeat and respiration frequencies

For each subject, heartbeat and respiration rates were defined as the inverse of the median of the temporal intervals between successive ECG R-peaks and inspiration endpoints, respectively.

2.13. Analysis software

All data analyses were performed in Matlab (MathWorks) using custom scripts, the open source toolbox Fieldtrip (Oostenveld et al., 2011), and the circular statistics toolbox (Berens, 2009).

2.14. Raw data

The raw data analyzed here is the same as the data analyzed in our previous study (Noury et al., 2016), and is available by contacting: noury.siegel.2017@gmail.com.

3. Results

3.1. Anti-phase regions of artifact

We recorded EEG and MEG during 11 Hz tACS, 62 Hz tACS, and sham stimulation in 4 subjects. Stimulation currents were injected through two Ag/AgCl electrodes with 1 mA peak-to-peak strength (Fig. 1a). EEG was recorded through the 72 remaining electrodes of the 10-10 electrode system, along with 272 MEG channels. Throughout the experiment, we also recorded the electrocardiogram (ECG) and respiration of subjects.

The stimulation current leaves one tACS electrode, runs through the entire head, and reaches the other tACS electrode. Therefore, all EEG electrodes experience strong sinusoidal stimulation artifact. The artifact's amplitude topography reflected the location of the stimulation and reference electrodes (top topographies in Fig. 1b and c). This is because, for each EEG channel, the EEG device measures the voltage difference between that EEG electrode and the reference electrode. Due to this subtraction, one expects that the artifact phase divides EEG channels into two anti-phase groups. To test this, we calculated the phase difference between each EEG signal and the stimulation current. All channels showed significant phases relative to the stimulation current and, as

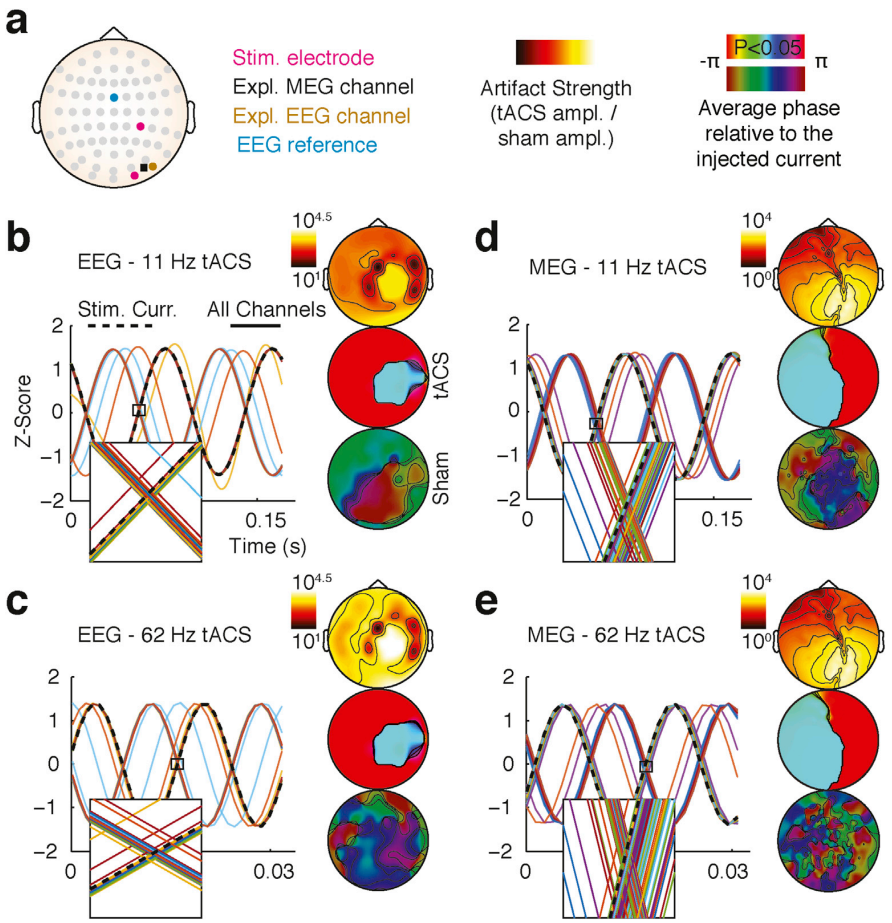

Fig. 1. tACS experiment and artifact phase. (a) 74 Ag/AgCl electrodes were placed according to the 10-10 system. Two electrodes (purple circles) were used for tACS stimulation and the all other electrodes were used for EEG measurement. The brown circle and black square indicate the channels used for demonstrating the EEG (O9) and MEG (MLT31) results in the next figures, respectively. The blue circle shows the reference EEG electrode. (*b*) Typical EEG and (*d*) typical MEG recordings during 11 Hz tACS. Time domain plots show 2 cycles of normalized signals of all channels (solid lines) and stimulation current (dashed lines). Subplots show the zero-crossing moment. Notably, different channels cross the zero line at different moments. The top topography shows the artifact strength relative to sham recordings, i.e. the standard deviation of signals recorded during tACS divided by the standard deviation of sham recordings, in logarithmic scale. Middle and bottom topographies depict the average phase shift of each channels signal relative to the stimulation current. Bright colors indicate regions with significant phase shift. (*c*) and (*d*) show recordings during 62 Hz tACS. The data shown is from the first subject.

expected, the phase topography reflected two anti-phase regions (Fig. 1b and c, blue and red regions in middle topographies).

For the MEG, the main sources of artifacts are the inward and outward currents running through the stimulation cables and the scalp. Due to the opposite current direction of inward and outward currents, artifact phase should be divided into two anti-phase regions. Indeed, similar to EEG, all MEG channels showed significant phase shifts relative to the stimulation current, and the phase topography was divided into two anti-phase regions (middle topographies in Fig. 1d and e). As a simple control, we checked whether band-passed sham recordings show any significant stable phase throughout the experiment. We did not find a significant phase in any EEG or MEG channel during sham condition (bottom topographies in Fig. 1b, c, d, e).

3.2. Artifact phase deflections in EEG and MEG

If EEG and MEG signals at the stimulation frequency were reflecting a purely linearly transformed version of the stimulation current, each channel's signal had to be on average either an in-phase (0° phase shifted) or an anti-phase (180° phase shifted) version of the stimulation current. To test this, we quantified each channel's phase deflection from such a pure in-phase or anti-phase signal (Materials and Methods). For almost all EEG and MEG channels this revealed an average phase deflection that was significantly different from 0° or 180° with small jitters over time (subplots in Figs. 1 and 2a, d, $p < 0.05$ Bonferroni-corrected for multiple comparisons across channels, for properties of phase jitter see Supplementary Fig. 1).

Do these average phase deflections from pure linear artifacts reflect the effect of tACS on brain activity, or are they due to nonlinear technical artifacts? We hypothesized that if the observed phase deflections were due to technical artifacts, their value should be related to the artifact's strength. Indeed, for both, EEG and MEG and for both tACS conditions, we found a significant negative correlation between the strength of the tACS artifact and strength of the phase deflection (Fig. 2b, e; Spearman correlation (r) of −0.32 and −0.26, for EEG, and −0.51 and −0.61, for MEG, $p < 1e^{-6}$, pooled across subjects and channels). To further address this question, for each channel we quantified the effective strength of phase deflections as the smallest sinusoidal signal that, when added to an artifact with no phase deflection (pure in-phase or anti-phase), could lead to the observed phase deflection (Materials and Methods). Next, we compared the strength of these sinusoids to the strength of sham recordings in the same frequency band (Fig. 2c, f). For most of the channels the sinusoids that would have to be added to a purely linear artifact were more than 10 times bigger that the normal EEG and MEG signals (79% and 94% of EEG channels and 18% and 69% of MEG channels for 11 Hz and 62 Hz tACS, respectively). As none of the subjects experienced phosphenes or other sensations during the experiment, we concluded that the brain could not have generated such strong sinusoids. We concluded that the observed phase deflections are part of the stimulation artifacts (see the next section for a third observation supporting this conclusion).

We tested if the phase deflections of the two stimulation conditions were related to each other. In both EEG and MEG, phase deflections of 11 Hz and 62 Hz tACS artifacts were strongly correlated across sensors (Spearman correlation (r) of 0.79 and 0.85 for EEG and MEG, respectively; both $p < 10^{-16}$). Next, we investigated if the strength of phase deflections changes with tACS frequency. For both, EEG and MEG we found a significant change in phase deflections by increasing the stimulation frequency from 11 Hz to 62 Hz. For EEG, the median of ratios of absolute phase deflections (62 Hz divided by 11 Hz) across channels was 0.84, suggesting a general decrease of phase deflections, while the median of ratios across MEG channels was 1.32, suggesting an increase in phase deflections ([10th, 90th] percentile of [0.4, 1.39] and [0.56, 4.48] for EEG and MEG, respectively; all $p <$ 1e-3, permutation test, Materials and Methods).

3.3. Heartbeat-locked phase modulations

Heartbeats move the head and EEG electrodes and influence the electrical properties of the body (Kristiansen et al., 2005; Nyboer et al., 1950; Pinheiro et al., 2010). Consequently, heartbeats modulate the amplitude of tES stimulation artifacts for EEG and MEG (Noury et al., 2016). Therefore, we hypothesized that heartbeats also modulate the phase of the stimulation artifact. To test this, in each subject we checked whether the artifact phase in EEG and MEG shows a rhythmic modulation locked to the subject's ECG R-peak (Materials and Methods). Indeed, in all subjects and for both, 11 Hz and 62 Hz tACS, most channels showed a significant rhythmic modulation of their artifact phase ($P <$ 0.05, FDR

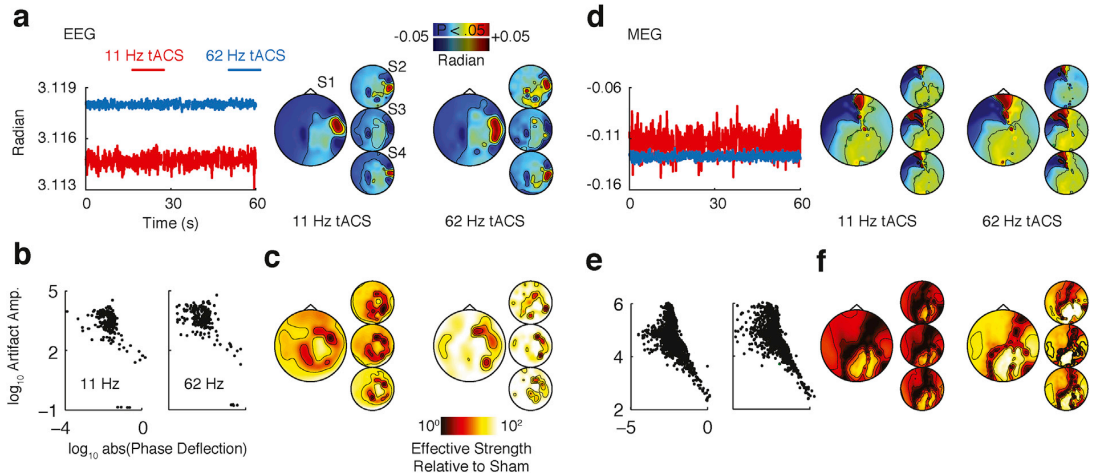

Fig. 2. Artifact phase deflection. (*a*) Artifact phase deflection in EEG. Time domain plot shows 1 min of artifact phase shift relative to the stimulation current during 11 Hz (red) and 62 Hz (blue) tACS (channel O9 of the first subject). Topographies show the phase deflection for each channel in radians. Almost all channels show significant phase deflections (non-significant regions are masked at P = 0.05 corrected). (*b*) Relation between artifact strength (standard deviation of signals during tACS) and absolute value of phase deflection in log-log scale. Data from all subjects is shown. Each point corresponds to a single channel in one subject. (*c*) Effective strength of phase deflections relative to sham recordings. Topographies show, in logarithmic scale, how big the signal is that results from the artifact deflection from pure in-phase or anti-phase linear artifacts, relative to the signal during sham recordings. (*d-f*) Artifact phase deflection properties in MEG. Same conventions as in (*a-c*). The time domain plot in (*d*) shows results from channel MTL31 in the first subjects. Bigger topographies correspond to the first subject (S1) and smaller topographies correspond to all other subjects (S2-S4).

corrected, Fig. 3a, b, f, g). Heartbeat-locked phase modulations were clearer for 62 Hz tACS as compared to 11 Hz (topographies in Fig. 3a, b, f, g), which might be due to weaker physiological signals mixing with the artifact at 62 Hz. In the frequency domain, these phase modulations spread the stimulation artifact beyond the stimulation frequency (Fig. 3e, j). This is because frequency is proportional to the temporal derivative of phase. Due to the heartbeat-locked phase modulations, the temporal derivative of the artifact's phase is not constant. Therefore, in the frequency domain, several frequencies are contaminated with the stimulation artifact. In other words, similar to the influence of the artifact's amplitude modulation (Noury et al., 2016), the artifact's phase modulation results in broadband artifacts.

To characterize the temporal dynamic of the spatial pattern of heartbeat-locked modulations, in each subject we applied PCA to the average heartbeat-locked phase modulations (Fig. 3c, h, Materials and Methods). In each subject, at least 2 of the first 3 PCs showed rhythmic dynamics and the first 3 PCs explained more than 99% and 97% of the variance for EEG and MEG, respectively. Consequently, the spatial pattern of phase modulations is not constant over time, but shows rhythmic temporal changes. Moreover, this suggests that for simulating tES artifacts, simulated phase modulations should contain at least 2 PCs.

The strength of heartbeat-locked phase modulations tended to be stronger for channels with bigger artifact phase deflections. For both EEG and MEG, we found a strong positive correlation between the modulation strength and absolute value of the artifact phase deflection (spearman correlation (r) of 0.56 and 0.64, for EEG, and 0.5 and 0.5, for MEG, for 11 Hz and 62 Hz tACS, respectively; all $p < 10^{-9}$). Furthermore, we found that for both, MEG and EEG and for both stimulation frequencies across channels, the strength of the heartbeat-locked phase-modulation was negatively correlated with the overall strength of tACS artifacts (spearman correlation (r) of −0.78 and −0.55, for EEG, and −0.85 and −0.69 for MEG, for 11 Hz and 62 Hz tACS, respectively; all $p < 10^{-16}$). These effects provide additional evidence for the interpretation that the observed phase deflections are caused by nonlinear artifacts, and not by brain activity.

Heartbeat-induced phase modulations were in the range of milliradians (Fig. 3a, b, f, g). Therefore, we asked if the effect of these small phase modulations is negligible, or if they should be considered in design and evaluation of artifact removal techniques. To answer this, we quantified each channel's modulation strength, in analogy to how we quantified the effective strength of average phase deflections before (Fig. 3d, i, Materials and Methods). For many channels, heart-beat locked phase modulations lead to artifact signals bigger than 10% of the EEG and MEG signals, and in some channels, in particular for MEG, the effect of heartbeat-locked phase modulations was as big as the signals recorded without stimulation. In sum, heartbeat-locked modulations of the artifact's phase induced sizable artifacts that should be accounted for in the design and evaluation of artifact removal techniques.

Heartbeats modulate artifact amplitudes in both EEG and MEG (Noury et al., 2016). Therefore, we checked if these amplitude modulations may influence our phase estimations such that the observed phase modulations may merely reflect these amplitude modulations. We simulated the case of stimulation artifacts with only amplitude modulation (Materials and Methods) and repeated the heartbeat-locked phase analysis on the estimated phase of these simulated artifacts. None of the EEG or MEG channels showed any significant heartbeat-locked phase modulation ($p > 0.05$, FDR corrected). Thus, we concluded that the observed phase-modulations did not merely reflect heartbeat locked amplitude modulations.

3.4. Respiration-locked phase modulations

Similar to the heartbeat, also respiration moves the head and EEG electrodes, modulates body impedance, and modulates tES artifact amplitudes (Dornhorst et al., 1952; Michard, 2005; Noury et al., 2016; Pinheiro et al., 2010). Thus, we expected to observe respiration-locked modulations of artifact phase, similar to heartbeat-locked effects. Indeed, for many channels, respiration-locked segments of artifact phase showed significant rhythmic modulations with sensor topographies similar to heartbeat-locked modulations (Supplementary Fig. 2). Compared to heartbeat-locked phase modulations, respiration-locked phase modulations reached significance in fewer channels, which may be due to the lower number of respirations as compared to heartbeats.

3.5. Ground electrode

We investigated whether the position of the EEG ground electrode could have generated the artifact phase-features observed in EEG recordings. To this end, in one subject we recorded two sessions of a 62 Hz tACS control experiment with EEG ground positioned either on the forearm or forehead. The two recordings showed similar artifact phase deflection and heartbeat-locked phase modulations (Supplementary Fig. 3). Thus, we concluded that artifact phase features in EEG are not related to the position of the EEG ground electrode.

3.6. Stimulation electrode size

In one subject, we performed another control experiment with big rubber stimulation electrodes to test if the observed features of the artifact phase might be due to the size of our stimulation electrodes (Fig. 4). For both, EEG and MEG and for both, 11 Hz and 62 Hz tACS, we found artifact phase deflection and phase modulations similar to the experiment with small stimulation electrodes. Thus, we concluded that the observed features are not related to the stimulation electrode size.

3.7. MEG without EEG

As the EEG cap and recording device may potentially generate noise on the MEG recordings, we checked if the artifact phase features observed in MEG were due to the simultaneous EEG measurements. In one subject, we recorded 2 min of MEG per tACS condition, without the EEG cap (Materials and Methods). We observed phase features in the recorded MEG data that were similar to the phase features observed during simultaneous MEG and EEG recordings (Supplementary Fig. 4). Thus, we concluded that the observed MEG phase effects were not related to the simultaneous EEG recordings.

4. Discussion

Here, we provide, to the best of our knowledge, the first characterization of the phase relationship between stimulation current and tACS artifacts in EEG and MEG. We show that tACS artifacts are not simple sinusoids at either 0 or 180° phase relative to the stimulation current, but that each channel shows a frequency dependent phase deflection. The magnitude of this phase deflection is negatively correlated with the amplitude of tACS artifact. Moreover, we show that the artifact phase is modulated by heartbeat and respiration. These phase modulations result in weak tACS artifacts at frequencies beyond the stimulation frequency. To facilitate research on tES artifacts and artifact rejection methods, all raw EEG and MEG data used in this study is made available online.

4.1. Artifact's bandwidth

The artifact's phase modulations spread stimulation artifacts beyond the stimulation frequency (Fig. 3e, j). This is in general similar to the effect of artifact's amplitude modulations, which result in broadband stimulation artifacts contaminating the power spectrum up to ±10 Hz beyond the stimulation frequency for a stimulation current of 1 mA peak-to-peak (Noury et al., 2016). It should be noted that the effective strength of phase modulations (Fig. 3d, i and Supplementary Fig. 2) is on average about hundred times smaller than the effective strength of amplitude modulations (Figs. 3 and 4 of Noury et al., 2016). In other words,

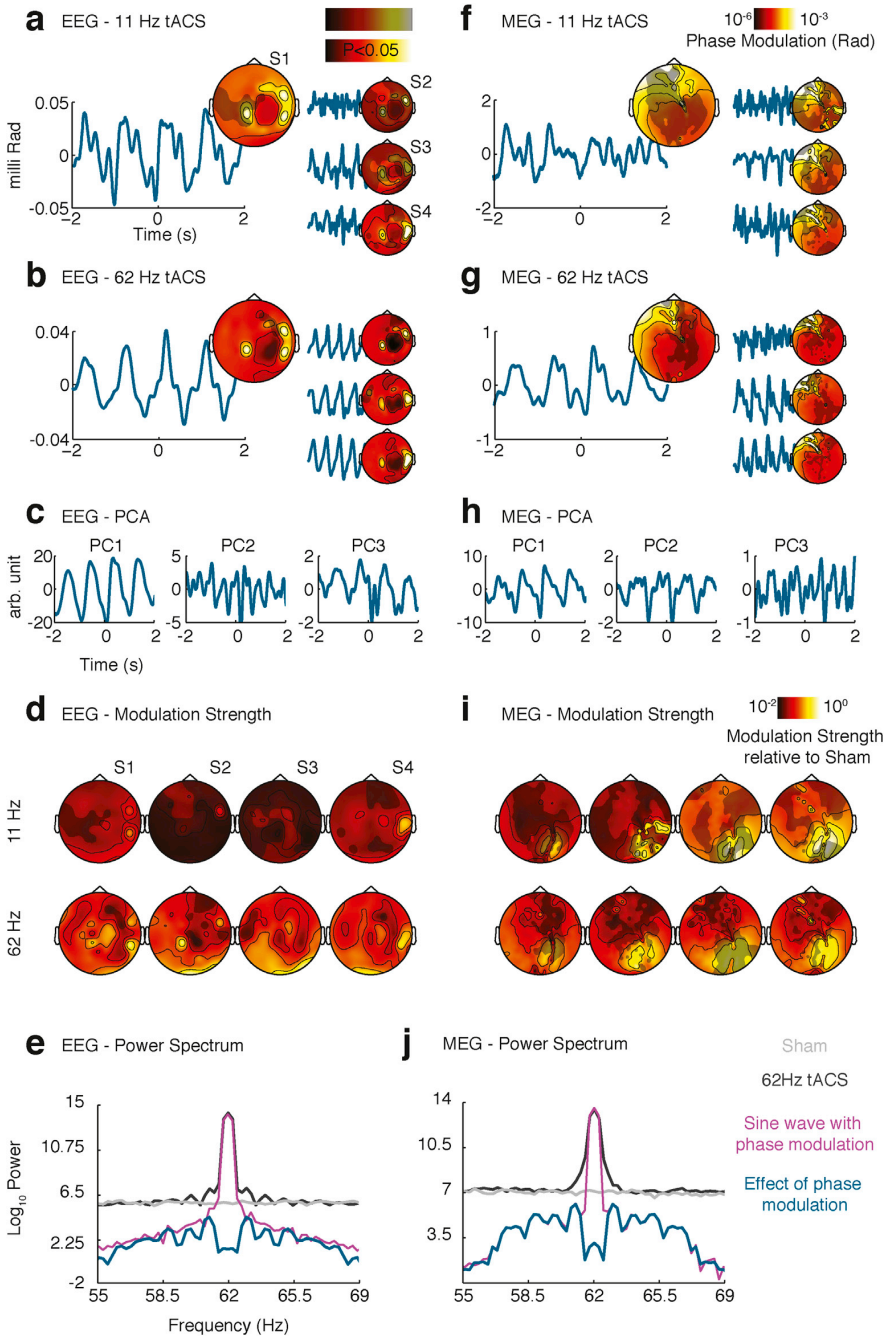

Fig. 3. Heartbeat-locked artifact phase modulation. (*a*) The time courses show how on average the EEG phase-shift relative to the stimulation current modulates around the time of heartbeats during 11 Hz tACS (signal from channel O9). The topography shows the modulation strength quantified as the decadic logarithm of the standard deviation of average heartbeat-locked phase modulation (non-significant modulations are masked at P = 0.05 corrected). The large panel shows data from subject S1. Smaller panels show all other subjects. (*b*) Similar to (*a*), but for 62 Hz tACS. (*c*) First 3 principle components (PCs) of a PCA applied to the average heartbeat-locked phase modulation. Only channels with significant heartbeat-locked modulations are included in the PCA. Data from 62 Hz tACS condition of the first subject. (*d*) Topographies show the effective strength of heartbeat-locked phase modulations, relative to the strength of sham recordings in decadic logarithmic scale. (*e*) Influence of the artifact's phase modulation on the artifact's power spectrum. Light and dark gray curves depict average power spectra of recordings from sham and 62 Hz tACS conditions, respectively (EEG channel O9). The magenta curve shows the power spectrum of a sine wave with constant amplitude and time-varying phase. The phase of this wave was set equal to the heartbeat-locked phase modulations of the same channel. The blue curve shows the effect of phase modulations in the frequency domain, i.e. the power spectrum of the residual signal, when a pure sine wave with no phase modulation is removed from the sine wave with phase modulations. (*f-j*) Same conventions as for (*a-e*), but for MEG recordings. Figures (*f, g, j*) depict results from channel MTL31.

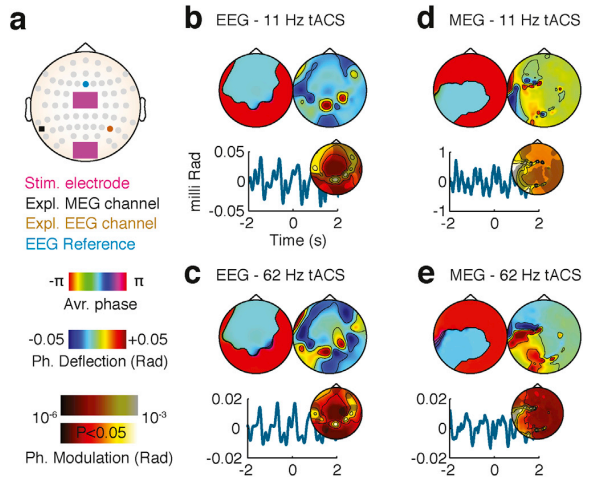

Fig. 4. tACS artifact phase properties for large stimulation electrodes. (*a*) Two large rubber stimulation electrodes (purple squares) were positioned between 62 EEG electrodes placed according to the 10–10 system. The brown circle and black square indicate the position of channels used for demonstrating EEG (P6) and MEG (MLT54) results, respectively. The blue circle shows the reference EEG electrode. (*b*) EEG artifact phase during 11 Hz tACS. The top left topography shows the average phase shift relative to the stimulation current. As expected, this topography is divided into two anti-phase regions. The top right topography shows artifact phase deflections from linear artifacts. Similar to tACS with small stimulation electrodes, different channels' artifacts deflect from linear artifacts. Bottom panel shows the heartbeat-locked phase modulation. The topography shows the standard deviation of phase modulation in decadic logarithmic scale (non-significant modulations are masked at P = 0.05 corrected). (*c*) As (*b*), but for 62 Hz tACS. (*d-e*) As (*b-c*), but for MEG recordings.

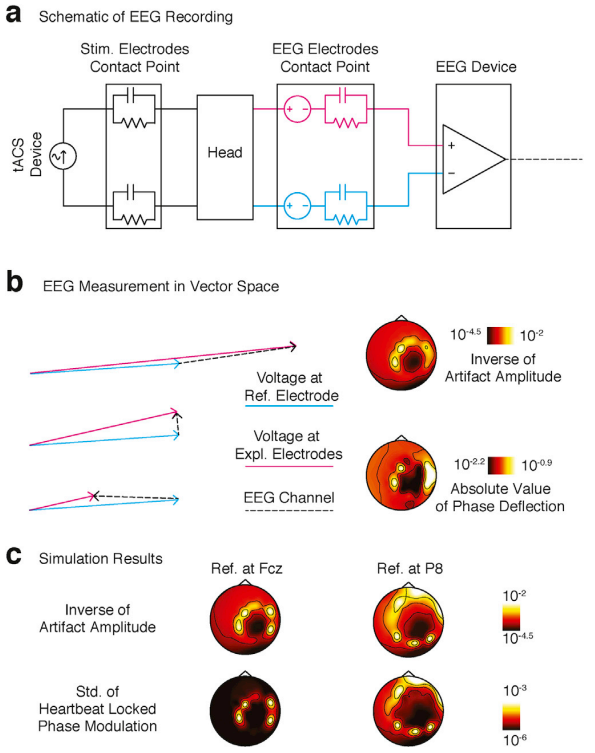

Fig. 5. EEG artifact phase. (*a*) Schematic diagram of tACS stimulation and EEG recordings. The stimulation current leaves the tACS device, flows through the head, and returns to the tACS device. The EEG device senses the voltage deference between the scalp position touched by the reference electrode (blue) and the scalp position touched by another electrode (purple). Electrochemical processes at the contact surface of electrodes and skin give rise to capacitive effects. These effects happen for both stimulation and EEG electrodes. (*b*) Schematic display of an EEG measurement in vector space. The length and phase of each vector represent amplitude and phase of the corresponding time domain signal, respectively. Blue and purple vectors correspond to the voltage sensed by the reference and example EEG electrodes, respectively. Dashed vectors represent the differential EEG signal measured for an EEG electrode, which is simply the difference between voltages sensed by that electrode (purple) and the reference electrode (blue). Capacitive effects of EEG electrodes (blue and purple in (*a*)) induce small phase shifts to the voltage sensed by each EEG electrode (non-zero phase of blue and purple vectors). This effect, together with the difference in the amplitude of voltages sensed by different electrodes, leads to various phase shifts of EEG measurements. The vector model explains the negative correlation between artifact amplitude and phase deflection, which is demonstrated in topographies. The bottom topography shows the absolute value of artifact phase deflections. The top topography shows the inverse of the artifact amplitude in decadic logarithmic scale (11 Hz tASC, averaged over subjects). (*c*) Simulating heartbeat-locked phase modulations. The vector model in (*b*) generates heartbeat-locked phase modulations, when the amplitude of each electrode's voltage is modulated by each heartbeat. Topographies show the average result of simulations with reference electrodes at Fcz (left) and P8 (right). Top topographies show inverse artifact amplitude and bottom topographies depict the standard deviation of heartbeat-locked phase modulations, in decadic logarithmic scale. Channels with smaller artifact amplitude (yellow regions in top topographies) show higher heartbeat-locked phase modulations (yellow regions in bottom topographies).

although both, phase and amplitude modulations contribute to broadband tACS artifacts, the bandwidth of tACS artifacts is practically governed by the artifact's amplitude modulations.

4.2. *Underlying mechanisms*

Capacitive effects at the contact surface of EEG electrodes and skin (Fig. 5a, Bronzino and Peterson, 2015; Tyner and Knott, 1983) induce small phase shifts to the voltages sensed by different EEG electrodes (Fig. 5b, phase of turquoise and magenta vectors). Small differences in in this capacitive effect between the reference electrode and other electrodes (Fig. 5b, phase difference of turquoise and magenta vectors), together with the variable strength of tACS artifact across electrodes (Fig. 5b, length of magenta vectors), lead to variable artifact phases across different EEG channels (Fig. 5b, phase of dashed vectors). Conceptualizing this effect in vector space explains the negative correlation between artifact amplitude and phase deflection observed for EEG (Fig. 5b). Most electrodes pick up either much stronger or much weaker artifacts relative to the reference electrode. Differential recordings from these electrodes show big artifacts with phases close to zero or 180° (Fig. 5b, first and last vector drawings). On the other hand, few electrodes experience artifacts with very similar strength as the reference electrode. Recording from these electrodes show small artifacts with phases close to either 90 or -90° (Fig. 5b, middle vector drawing). This mechanism leads to the observed negative correlation between artifact amplitude and phase deflection across channels (Fig. 2b and topographies in Fig. 5b). Furthermore, because of the capacitive effect at the contact surface, electrode impedance is frequency dependent, which explains why we observed a change in phase deflection across frequencies.

The aforementioned mechanism can not only explain the observed EEG artifact phase deflections from pure linear in-phase or anti-phase versions of the stimulation current, but it may also explain the observation of heartbeat-locked and respiration-locked artifact-phase modulations. As we have shown before (Noury et al., 2016), the artifact's amplitude is modulated by physiological processes. The artifact phases of EEG measurements depends on the electrodes' capacitive effect and the artifact amplitude at each electrode (Fig. 5b). Thus, rhythmic modulations of artifact amplitude at each electrode (amplitude modulation of magenta and turquoise vectors in Fig. 5b) could lead to observed rhythmic phase modulations of the measured artifacts (phase of dashed vectors in Fig. 5b).

We tested this idea in a simulation, in which each electrode had a small random phase shift and its amplitude was modulated by each heartbeat (Fig. 5c, Materials and Methods). This simulation confirmed

that the mentioned mechanism could lead to heartbeat-locked phase modulations. As observed in the experimental measurements (Fig. 3a and b), in the simulation heartbeat-locked phase modulations were strongest for channels on the zero isoline, i.e. channels with artifact amplitudes similar to the artifact amplitude of the reference channel (Fig. 5c). This led to a negative correlation between artifact amplitude and phase-modulation strength (Spearman correlation (r) of -0.84, $p < 10^{-16}$), as also observed in the experimental measurements.

In addition to rhythmic amplitude modulation, also rhythmic impedance changes may contribute to the observed phase-modulation. In particular, rhythmic movements of EEG electrodes induced by each heartbeat may rhythmically change capacitive and resistive electrode impedances.

Capacitive effects also affect invasive electrophysiological recordings during tACS. Thus, the abovementioned model could also explain phase properties of those recordings. In fact, a recent study (Opitz et al., 2016) reported small phase shifts in invasive recordings during tACS in the range of the phase deflections reported here. Although the authors do not statistically check the relationship between signal strength and phase shifts, they report largest phase shifts at electrodes with smallest signals, and relate this to less accurate phase estimations at these electrodes. Our model suggests that the reported phase deflections result from small capacitive effects together with referencing. Moreover, according to our model, we speculate that the phase of invasive recordings should also be rhythmically modulated by heartbeat and respiration due to small rhythmic brain movements or blood volume changes. It should be noted that these phase features happen at the measurement level. In other words, we predict that neuronal tissues experience tACS currents in-phase with the stimulation current. However, neuronal responses to these electrical currents are not necessarily in-phase with the stimulation current, and might show phase shifts that depend on different parameters, including bioelectrical features of the neurons. Detailed computer simulations and invasive recordings (Ali et al., 2013; Opitz et al., 2016) are necessary to further our understanding of the phase relationship between tACS currents and induced neuronal responses.

Our results show that phase features of MEG artifacts are generally similar to phase features of EEG artifacts. However, we are not aware of any direct counterpart of the capacitive EEG effects for SQUID-based MEG that could lead to the observed phase features of MEG artifacts. These phase features may arise from the special electronics of the MEG system. One candidate could be the flux feedback loop of the SQUID circuitry. The delay of this feedback loop could potentially generate phase delays in the recordings. Another alternative is the effect of electromagnetic waves generated by oscillating stimulation currents. Usually, it is assumed that MEG signals are measured under the quasi-static condition. This is a fair assumption when measuring brain activity, because electromagnetic waves produced by time varying brain activity are negligible. However, stimulation currents are usually much bigger than electrical currents produced by brain activity. Consequently, their produced electromagnetic waves are also several orders of magnitude bigger than electromagnetic waves produced by brain activity. These electromagnetic waves are not necessarily in-phase with stimulation currents, and therefore they could induce phase shifts in artifacts measured by MEG sensors. Pinpointing the exact mechanisms underlying observed MEG phase effects remains subject to future investigations.

4.3. Consequences for artifact rejection methods

Any sub-optimality in artifact rejection leads to a decrease in the signal to noise ratio of the recovered brain signal and residual artifacts, which, in the worst case, may lead to spurious results. This is particularly important to consider because tACS artifacts are typically several orders of magnitude larger than brain signals. Optimizing artifact rejection methods requires knowledge of the nature and characteristics of artifacts. By providing these characteristics, our results pave the way for this optimization.

Widely used EEG and MEG signal-processing methods like PCA, ICA and beamforming assume a linear and time-invariant mapping between sources (artifactual or non-artifactual) and sensors. These methods have been recently used for removing stimulation artifacts (Helfrich et al., 2014; Neuling et al., 2015). However, artifact phase and amplitude features reflect a non-linear and time-varying mapping between stimulation current and tES artifacts. During normal EEG and MEG recordings without tES, discarding non-linear and time-varying properties of source-to-senor projections leads to negligible errors, because their effective strength is small relative to brain signals. However, because tACS artifacts are several orders of magnitude larger than brain signals, small non-linear and time-varying effects cause artifact components that are well on the order of, or even larger than, brain signals (Figs. 1–3; and Noury et al., 2016). These components are hard to capture with linear and time-invariant signal processing methods. In other words, using these signal processing methods for removing stimulation artifacts result in residual artifacts (Marshall et al., 2016; Noury et al., 2016). These residual artifacts are likely to lead to higher artifactual power of the processed signal at or near the stimulation frequency compared to the sham condition. Importantly, an increase in neuronal activity at the stimulation frequency is one of the targeted physiological effects of tACS. Thus, dissociating a potential physiological signal power increase from a power increase caused by residual artifacts is challenging and requires a careful assessment of the measured power changes in comparison to the effects of potential residual artifacts. Such comparisons could be done by means of computer simulations and evaluations that are based on realistic artifact models.

Another approach to artifact rejection is to design appropriate non-linear and time-varying methods. For example, in the artifact rejection method introduced by Voss et al. (2014) an optimum phase-shift is applied to the artifact estimation of each EEG channel. Although this approach is theoretically powerful, it is not able to completely remove stimulation artifacts. The main challenge in this approach is to estimate the exact amplitude and phase of the artifact over time. This is difficult because signals recorded during tES contain both artifact and brain activity. Therefore, estimations of phase and amplitude of artifact might be sub-optimal and artifact-removed signals might contain residual artifacts. Similar to the previous approach, one might be able to deal with this problem by means of computer simulations. In other words, one could estimate the strength of residual artifacts through realistic artifact models in silico, to then quantitatively assess if the observed changes in recordings during tES relative to sham recordings could be explained by residual artifacts.

We showed that artifact phase properties in EEG and MEG depend on tACS frequency. This suggests that the performance of a single artifact rejection method may vary with stimulation frequency. Therefore, artifact rejected signals of different tACS frequencies should be compared with caution. In this context, it is also important to note that, as tDCS artifacts by definition do not have any phase shift, tES artifact removal methods may perform better for tDCS as compared to tACS.

4.4. Evaluation of artifact rejection methods in silico

Whether or not all properties of stimulation artifacts are considered in the design of artifact rejection methods, their performance needs to be evaluated. One possibility for such evaluations is to apply the artifact rejection methods to the EEG or MEG data recorded during tES, and compare the results with ground truth EEG or MEG signal. Such a ground truth, especially at the stimulation frequency, is not easy to obtain, because it is not clear how tES influences the brain activity during stimulation. The alternative is to use computer simulations to simulate artifactual signals with known ground truth. For example, Helfrich et al. (2014) simulated the artifactual signals by adding a constant 10 Hz sine wave to sham recordings, and further evaluated the performance of their artifact rejection method by applying their method to this simulated data and comparing artifact-removed results with the original sham

recordings. However, from our findings, it is clear that such a simulation does not reflect the non-linear and time-varying phase and amplitude features of tES artifacts, and thus, is not suited to assess the performance of artifact rejection method. This highlights that a necessary and critical part of such simulations is an appropriate model of stimulation artifacts that captures all relevant artifact characteristics. Our results provide the basis for such simulations by characterizing phase and amplitude features of tES artifacts, and by showing how the strength of different artifact features could be estimated from EEG and MEG recordings during tES.

4.5. A model for tES artifacts

We next suggest a complex-valued model for simulating EEG and MEG recordings during tES at frequencies close to the stimulation frequency, i.e. frequencies that do not include any stimulation harmonic. This model summarizes the results presented here and in our previous paper (Noury et al., 2016):

$$Art(t) = a(t) \times e^{i\varphi(t)} \times Cur(t) \quad (1)$$

$$s(t) = Re\{Art(t)\} + b(t) \quad (2)$$

in this model, $s(t)$ is the EEG or MEG recording, $b(t)$ is the brain activity, and $Art(t)$ and $Cur(t)$ are analytic representations[1] of stimulation artifact and normalized stimulation current, respectively. $a(t)$ and $\varphi(t)$ represent each channel's time-varying artifact amplitude and phase and are defined as:

$$a(t) = a_{avr} + a_{slow}(t) + Heart(t)*h_{ah} + Resp(t)* h_{ar}(t) \quad (3)$$

$$\varphi(t) = \varphi_{avr} + \varphi_{jitter}(t) + Heart(t)*h_{\varphi h} + Resp(t)* h_{\varphi r}(t) \quad (4)$$

While a model for tACS requires both $a(t)$ and $\varphi(t)$, Eqn. (4) should be discarded for tDCS models and $\varphi(t)$ in Eqn (1) should be replaced with zero. In Eqns (3) and (4), a_{avr} and φ_{avr} represent each channel's average amplitude and average phase shift relative to the stimulation current, respectively. $a_{slow}(t)$ represents slow changes in the artifact amplitude due to slow head movements or slow changes in EEG electrode impedance. $\varphi_{jitter}(t)$ represents artifact's phase jitter, $h_{ah}(t)$ and $h_{ar}(t)$ represent mean-removed average heartbeat-locked and respiration-locked amplitude modulations, and $h_{\varphi h}(t)$ and $h_{\varphi r}(t)$ represent mean-removed average heartbeat-locked and respiration-locked phase modulations, respectively. $Heart(t)$ and $Resp(t)$ are impulse trains with impulses at moments of, respectively, ECG R-peaks and inspiration ends. In Eqns (3) and (4), * denotes temporal convolution. This operation simply applies heartbeat locked and respiration locked modulations to amplitude and phase signals with each heartbeat and respiratory effort.

To evaluate the performance of an artifact rejection method, one could first estimate the parameters of the model based on EEG or MEG signals recorded during tES. This could be done with methods presented in this and our previous papers (Noury et al., 2016). Using these parameters, a simulated version of the recorded data, $s(t)$, could be calculated. Next, the artifact rejection method should be applied to this simulated data and the results should be evaluated. It should be noted that any model parameter estimates cannot be ideal, simply because the EEG and MEG recordings that are used for estimating model parameters contain tES artifacts together with brain activity and measurement noise. That said, a versatile artifact rejection method should be able to deal with different artifact magnitudes and should not be sensitive to small changes of model parameters.

While most of the parameters in (2) and (3) could be estimated from EEG and MEG recordings, estimating $\varphi_{jitter}(t)$ is not straightforward. This is because it is not clear how much of the observed band-passed signal's phase jitter is related to the artifact and how much is related to brain activity (Supplementary Fig. 1, bottom row). Therefore, one should evaluate the performance of artifact rejection methods assuming different levels of $\varphi_{jitter}(t)$ to find the potential effect of $\varphi_{jitter}(t)$ on results of the artifact-rejection pipeline.

The abovementioned simulation could be done with different assumptions regarding the effect of tES on brain signal (i.e. $b(t)$). Four situations are possible: no effect of tES on the brain, phase-locked entrainment of brain signal, non-phase-locked increase in brain's oscillatory activity at the stimulation frequency, and a combination of the latter two cases. For the first case, $b(t)$ could be replaced with sham recordings and a simulation could be performed to check whether artifact rejected signals show any spurious effect of stimulation, i.e. a false positive result. For the other three cases, the likelihood of a false negative result could be tested by adding different levels of phase-locked or/and non-phase-locked stimulation effects to the sham recordings, applying the artifact rejection method to the simulated data (i.e. $b(t)$), and finally checking whether the induced stimulation effects are observable after the artifact removal.

It should be noted that heartbeat-locked and respiration-locked modulations of amplitude and phase might slightly vary across heartbeats and respiratory efforts. Therefore, in the case that an artifact rejection method uses heartbeat-locked and respiration-locked modulations, these variations should be estimated from recorded data and considered in simulations and evaluations. Furthermore, it should be noted that the above model only captures those aspects of tES artifacts described here and in our previous work (Noury et al., 2016). Further research should investigate if there are other artifact properties that should be incorporated into the model.

[1] The analytical representation of a signal is a complex signal with the real part equal to the signal and the imaginary part equal to signal's Hilbert transform.

Notes

N.N. and M.S. designed the research and wrote the manuscript. N.N. performed the experiments and analyzed the data.

Funding

This work was supported by the Centre for Integrative Neuroscience (Deutsche Forschungsgemeinschaft, EXC 307).

Appendix A. Supplementary data

Supplementary information related to this article can be found at http://dx.doi.org/10.1016/j.neuroimage.2017.07.010.

References

Ali, M.M., Sellers, K.K., Fröhlich, F., 2013. Transcranial alternating current stimulation modulates large-scale cortical network activity by network resonance. J. Neurosci. 33, 11262–11275. http://dx.doi.org/10.1523/JNEUROSCI.5867-12.2013.

Benjamini, Y., Hochberg, Y., 1995. Controlling the false discovery rate: a practical and powerful approach to multiple testing. J. R. Stat. Soc. Ser. B Methodol. 57, 289–300.

Berens, P., 2009. CircStat: a MATLAB toolbox for circular statistics. J. Stat. Softw.

Bronzino, J.D., Peterson, D.R., 2015. The Biomedical Engineering Handbook, fourth ed. CRC Press, Boca Raton, FL. Four Volume Set, 4 edition.

Dornhorst, A.C., Howard, P., Leathart, G.L., 1952. Respiratory variations in blood pressure. Circulation 6, 553–558. http://dx.doi.org/10.1161/01.CIR.6.4.553.

Fertonani, A., Miniussi, C., 2016. Transcranial electrical stimulation: what we know and do not know about mechanisms. Neurosci. Rev. J. Bringing Neurobiol. Neurol. Psychiatry. http://dx.doi.org/10.1177/1073858416631966.

Helfrich, R.F., Schneider, T.R., Rach, S., Trautmann-Lengsfeld, S.A., Engel, A.K., Herrmann, C.S., 2014. Entrainment of brain oscillations by transcranial alternating current stimulation. Curr. Biol. 24, 333–339. http://dx.doi.org/10.1016/j.cub.2013.12.041.

Kristiansen, N.K., Fleischer, J., Jensen, M.S., Andersen, K.S., Nygaard, H., 2005. Design and evaluation of a handheld impedance plethysmograph for measuring heart rate variability. Med. Biol. Eng. Comput. 43, 516–521.

Kuo, M.-F., Nitsche, M.A., 2012. Effects of transcranial electrical stimulation on cognition. Clin. EEG Neurosci. 43, 192–199. http://dx.doi.org/10.1177/1550059412444975.

Marshall, T.R., Esterer, S., Herring, J.D., Bergmann, T.O., Jensen, O., 2016. On the relationship between cortical excitability and visual oscillatory responses - a concurrent tDCS-MEG study. NeuroImage 140, 41–49. http://dx.doi.org/10.1016/j.neuroimage.2015.09.069.

Michard, F., 2005. Changes in arterial pressure during mechanical ventilation. Anesthesiology 103, 419–428 quiz 449–445.

Neuling, T., Ruhnau, P., Fuscà, M., Demarchi, G., Herrmann, C.S., Weisz, N., 2015. Friends, not foes: magnetoencephalography as a tool to uncover brain dynamics during transcranial alternating current stimulation. NeuroImage 118, 406–413. http://dx.doi.org/10.1016/j.neuroimage.2015.06.026.

Nitsche, M.A., Paulus, W., 2000. Excitability changes induced in the human motor cortex by weak transcranial direct current stimulation. J. Physiol. 527, 633–639. http://dx.doi.org/10.1111/j.1469-7793.2000.t01-1-00633.x.

Noury, N., Hipp, J.F., Siegel, M., 2016. Physiological processes non-linearly affect electrophysiological recordings during transcranial electric stimulation. NeuroImage 140, 99–109. http://dx.doi.org/10.1016/j.neuroimage.2016.03.065.

Nyboer, J., Kreider, M.M., Hannapel, L., 1950. Electrical impedance plethysmography a physical and physiologic approach to peripheral vascular study. Circulation 2, 811–821. http://dx.doi.org/10.1161/01.CIR.2.6.811.

Oostenveld, R., Fries, P., Maris, E., Schoffelen, J.-M., 2011. FieldTrip: open source software for advanced analysis of MEG, EEG, and invasive electrophysiological data. Comput. Intell. Neurosci. 2011, 156869. http://dx.doi.org/10.1155/2011/156869.

Opitz, A., Falchier, A., Yan, C.-G., Yeagle, E.M., Linn, G.S., Megevand, P., Thielscher, A., Deborah, A.R., Milham, M.P., Mehta, A.D., Schroeder, C.E., 2016. Spatiotemporal structure of intracranial electric fields induced by transcranial electric stimulation in humans and nonhuman primates. Sci. Rep. 6, 31236. http://dx.doi.org/10.1038/srep31236.

Pinheiro, E., Postolache, O., Girão, P., 2010. Theory and developments in an unobtrusive cardiovascular system representation: ballistocardiography. Open Biomed. Eng. J. 4, 201–216. http://dx.doi.org/10.2174/1874120701004010201.

Soekadar, S.R., Herring, J.D., McGonigle, D., 2016. Transcranial electric stimulation (tES) and NeuroImaging: the state-of-the-art, new insights and prospects in basic and clinical neuroscience. NeuroImage 140, 1–3. http://dx.doi.org/10.1016/j.neuroimage.2016.08.020.

Soekadar, S.R., Witkowski, M., Cossio, E.G., Birbaumer, N., Robinson, S.E., Cohen, L.G., 2013. In vivo assessment of human brain oscillations during application of transcranial electric currents. Nat. Commun 4. http://dx.doi.org/10.1038/ncomms3032.

Thut, G., Bergmann, T.O., Fröhlich, F., Soekadar, S.R., Brittain, J.-S., Valero-Cabré, A., Sack, A.T., Miniussi, C., Antal, A., Siebner, H.R., Ziemann, U., Herrmann, C.S., 2017. Guiding transcranial brain stimulation by EEG/MEG to interact with ongoing brain activity and associated functions: a position paper. Clin. Neurophysiol. 128, 843–857. http://dx.doi.org/10.1016/j.clinph.2017.01.003.

Tyner, F.S., Knott, J.R., 1983. Fundamentals of EEG Technology: Basic Concepts and Methods. Lippincott Williams & Wilkins.

Voss, U., Holzmann, R., Hobson, A., Paulus, W., Koppehele-Gossel, J., Klimke, A., Nitsche, M.A., 2014. Induction of self awareness in dreams through frontal low current stimulation of gamma activity. Nat. Neurosci. Adv. Online Publ. http://dx.doi.org/10.1038/nn.3719.

Witkowski, M., Garcia-Cossio, E., Chander, B.S., Braun, C., Birbaumer, N., Robinson, S.E., Soekadar, S.R., 2016. Mapping entrained brain oscillations during transcranial alternating current stimulation (tACS). NeuroImage, Transcranial Electr. Stimul. (tES) Neuroimaging 140, 89–98. http://dx.doi.org/10.1016/j.neuroimage.2015.10.024.

Supplementary Information

Phase properties of transcranial electrical stimulation artifacts in electrophysiological recordings

Nima Noury[1, 2] and Markus Siegel[1]

[1] Centre for Integrative Neuroscience & MEG Center, University of Tübingen, Germany

[2] IMPRS for Cognitive and Systems Neuroscience, Tübingen, Germany

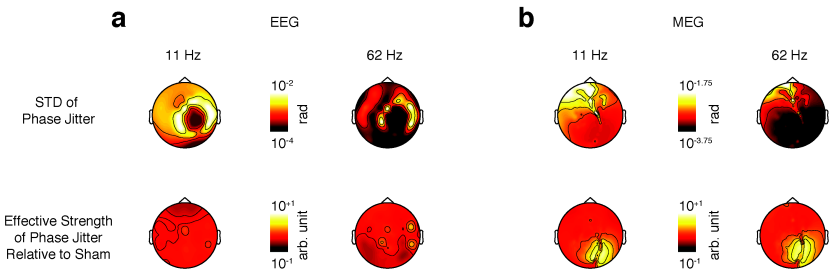

Supplementary Figure 1. Phase jitter of recordings during tACS. (*a*) EEG phase jitter. Top topographies depict standard deviation of temporal jitters of the phase shift between EEG recordings and the stimulation current (in decadic logarithmic scale). Bottom topographies show effective strength of the signals that when added to artifacts without phase jitter, would result in signals with the observed phase jitters in recordings. Bottom topographies show the effective strength of phase jitters relative to sham recordings in decadic logarithmic scale. The effective strength is quantified as the difference between each channels signal and the same signal without phase jitter. The left column corresponds to 11 Hz tACS and the right column to 62 Hz tACS. (*b*) Similar to (*a*), but for MEG recordings. In both EEG and MEG, phase jitter's effective strength in most channels is comparable with the strength of sham recordings. Therefore, in most channels, phase jitters reflect brain signals and not jitters in the phase of artifact.

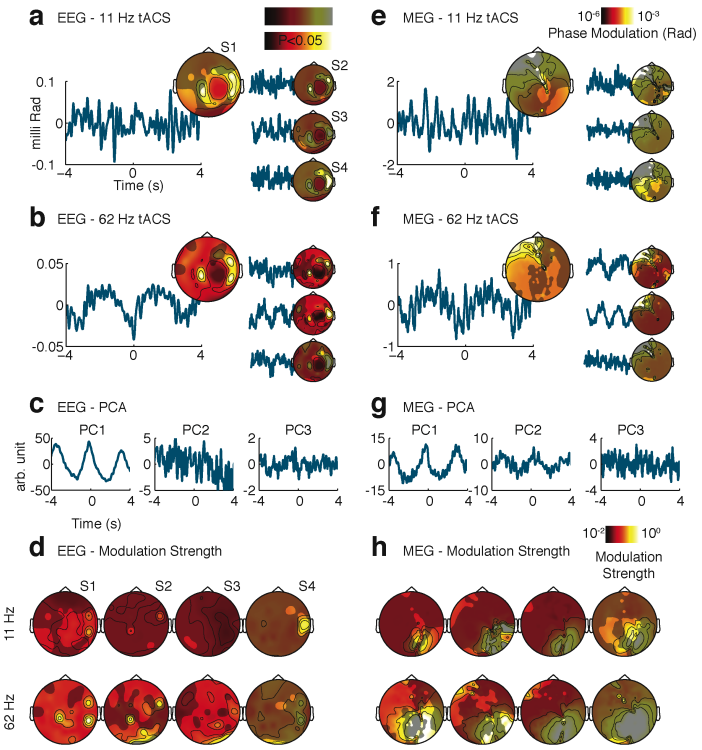

Supplementary Figure 2. Respiration-locked artifact phase modulation. (*a*) Time courses depict how on average the EEG phase-shift relative to the stimulation current modulates around the time of respiratory efforts during 11 Hz tACS (signal from channel O9). The topography shows the modulation strength quantified as the decadic logarithm of the standard deviation of average respiration-locked phase modulation (non-significant modulations are masked at P = 0.05 corrected). The large panel shows data from subject S1. Smaller panels show all other subjects. (*b*) Similar to (*a*), but for 62 Hz tACS. (*c*) First 3 PCs of the PCA applied to the average respiration-locked phase modulations. Only channels with significant respiration-locked modulations are included in PCA analysis. Data from 62 Hz tACS condition of the first subject. (*d*) Topographies show effective strength of respiration-locked phase modulations, relative to the strength of sham recordings in decadic logarithmic scale. In other words, they show how big is the signal generated by phase modulations compared to sham recordings. (*e*-*h*) Similar to (*a*-*d*), but for MEG recordings. Figures (*e*-*f*) depict results from channel MTL31.

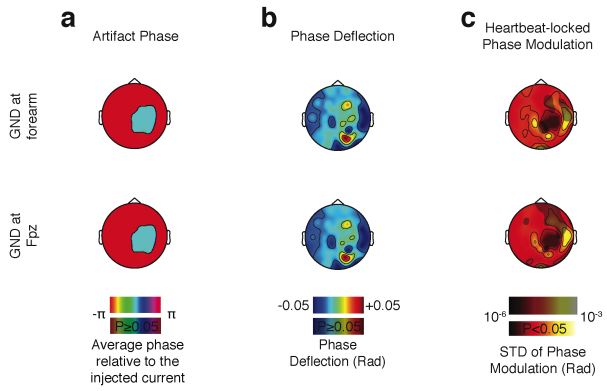

Supplementary Figure 3. Influence of EEG ground electrode on artifact phase properties. Top and bottom rows depict results from recordings during 62 Hz tACS with ground electrode positioned on, respectively, forearm and forehead (EEG channel Fpz). (*a*) Phase of artifact relative to the stimulation current. As expected, channels are divided in to anti-phase groups. (*b*) Artifact phase deflection from pure linear in-phase and anti-phase artifacts. Recordings from the two conditions show similar phase deflections. (*c*) Heartbeat-locked phase modulations. Topographies show standard deviation of temporal modulations in radian (decadic logarithmic scale). Both conditions show significant heartbeat-locked phase modulations in many channels.

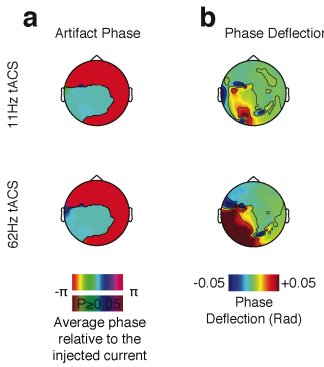

Supplementary Figure 4. Artifact phase in MEG recordings without EEG. Top and bottom rows correspond to, respectively, 11 Hz and 62 Hz tACS. Stimulation was done with large stimulation electrodes as in Fig. 4. (*a*) Artifact phase shift relative to the stimulation current. As expected, MEG channels are divided into two anti-phase groups. (*b*) Artifact phase deflections from pure linear in-phase or anti-phase artifacts. Similar to recordings done with simultaneous EEG (Fig. 4), many channels show phase deflections from pure linear artifacts. Therefore, observed phase deflections in MEG are not due to the noise of simultaneous EEG recordings.

6.3 Paper 3

Noury, N., Siegel, M., Analyzing EEG and MEG signals recorded during tES, a reply. Submitted to NeuroImage.

Statement of contributions:

Data analysis: NN.

Manuscript writing: NN and MS.

Analyzing EEG and MEG signals recorded during tES, a reply

Nima Noury[1, 2] and Markus Siegel[1]

[1] Centre for Integrative Neuroscience & MEG Center, University of Tübingen, Germany

[2] IMPRS for Cognitive and Systems Neuroscience, Tübingen, Germany

Keywords:

transcranial electric stimulation (tES), transcranial alternating current stimulation (tACS), transcranial direct current stimulation (tDCS), EEG, MEG, neural entrainment, stimulation artifacts

Correspondence:

Nima Noury (nima.noury@cin.uni-tuebingen.de) & Markus Siegel (markus.siegel@uni-tuebingen.de), Centre for Integrative Neuroscience, University of Tübingen, Otfried-Müller-Str. 25, 72076 Tübingen, Germany

Abstract

Transcranial Electric Stimulation (tES) is a widely used non-invasive brain stimulation technique. However, strong stimulation artifacts complicate the investigation of neural activity with EEG or MEG during tES. Thus, studying brain signals during tES requires detailed knowledge about the properties of these artifacts. Recently, we characterized the phase- and amplitude-relationship between tES stimulation currents and tES artifacts in EEG and MEG and provided a mathematical model of these artifacts (Noury and Siegel, 2017, and Noury et al., 2016, respectively). Among several other features, we showed that, independent of the stimulation current, the amplitude of tES artifacts is modulated time locked to heartbeat and respiration. In response to our work, a recent paper (Neuling et al., 2017) raised several points concerning the employed stimulation device and methodology. Here, we show that none of the concerns by Neuling et al. are correct or applicable to our results. Furthermore, we explain in detail the physics underlying tES artifacts, and discuss several approaches how to study brain function during tES in the presence of residual artifacts.

1. Introduction

Transcranial Electric Stimulation (tES) is a noninvasive brain stimulation technique that is widely used to manipulate brain function (Fertonani and Miniussi, 2016; Kuo and Nitsche, 2012). However, the neurophysiological mechanisms underlying tES effects are largely unknown, mainly because strong stimulation artifacts render the electrophysiological investigation of brain activity with EEG or MEG during tES challenging (Bergmann et al., 2016; Thut et al., 2017). Such simultaneous measurements may not only provide insights into the mechanisms underlying tES effects, but may also pave the way for new feedback-controlled brain stimulation protocols, in which stimulation parameters are continuously optimized based on the simultaneously recorded brain activity (Bergmann et al., 2016; Brittain et al., 2013; Lustenberger et al., 2016; Romei et al., 2016).

Despite several efforts to remove tES artifacts from simultaneously recorded EEG and MEG signals, a comprehensive artifact-removal pipeline that completely removes artifacts is still missing (Helfrich et al., 2014; Neuling et al., 2015; Soekadar et al., 2013; Voss et al., 2014). This is at least partly because the employed methods have been designed and used without considering the properties of tES artifacts. Recently, we characterized both, amplitude (Noury et al., 2016) and phase (Noury and Siegel, 2017) properties of tES artifacts for EEG and MEG. We suggested a mathematical model for the transfer function that defines the relationship between the stimulation current and tES artifacts and may be used for simulating tES artifacts (Noury and Siegel, 2017). We showed that the mapping between stimulation current and tES artifacts is non-linear and time-varying. The non-linearity manifests itself in the amplitude and phase of stimulation artifacts. Moreover, both, phase and amplitude of artifacts are rhythmically modulated time-locked to heartbeats and respiration, due to body resistance changes and head movements. These modulations have a time-varying spatial pattern, which makes the transfer function time-varying. We used the rhythmic modulation of artifact amplitudes as landmarks of tES artifacts to quantify their bandwidth in the frequency domain, and to detect the presence of artifacts at different stages of available artifact-removal pipelines. We showed

that none of the available artifact-removal pipelines is able to completely remove stimulation artifacts. Therefore, we concluded that residual artifacts need to be considered to prevent false positive results and wrong conclusions (Noury et al., 2016).

In response to our work regarding the amplitude of tES artifacts (Noury et al., 2016), a recent paper (Neuling et al. 2017) raised several concerns. First, Neuling at al. argued that the amplitude modulations reported by us were due to a malfunction of our stimulation device. Second, they suggested that wrong parameters in our beamforming pipeline led to residual artifacts in our source-level estimations. Critically, the authors made both claims without applying any of the critical analyses suggested in our paper to their own data. Furthermore, the authors ignored several findings in our previous paper that already ruled out the raised concerns. Thus, we suspect that these concerns may be based on a misunderstanding of our results and of the physics underlying tES artifacts. Therefore, in the following we first discuss in detail the physics behind amplitude modulations of tES artifacts and explain our previous findings in more detail. We then systematically go through all sections of Neuling et al. (2017) and show that none of the raised points are correct or relevant to our results. Finally, we point out several approaches and directions on how brain signals recorded during tES can be studied.

2. Materials and Methods

2.1. Participants and experimental protocol

All experiments were conducted in 3 healthy male participants. All subjects gave written informed consent before participating. All experiments were conducted in accordance with the Declaration of Helsinki and approved by the local ethics committee. Two of the subjects participated in a transcranial alternating current stimulation (tACS) experiment. One of the two received stimulation with large rubber electrodes and the other one received stimulation with small Ag/AgCl electrodes (same data previously used in Noury et al. (2016)). This experiment included 6 experimental runs, and each run consisted of the following sequential conditions: sham, tACSa, tACSb, sham, tACSb, and tACSa. Each condition lasted 66

seconds. For each run, 11 Hz tACS and 62 Hz tACS were randomly assigned to tACSa and tACSb conditions to avoid any potential sequence effects. Subject fixated a central fixation spot at the center of a blank monitor (60 Hz refresh rate), except from runs 3 and 6, in which subject kept his eyes closed. Before start of the experiment, subject was habituated to transcranial electric stimulation. In another experiment, one subject's head movement during an MEG experiment was continuously measured for 10 minutes using MEG head localization coils. The subject was fixating at rest.

2.2. Transcranial electric stimulation

Stimulation currents were applied with an IZ2h stimulator (Tucker Davis Technologies Inc.). Stimulation amplitude was 0.5 mA (i.e., 1 mA peak-to-peak for tACS) and did not induce flicker percepts. In the experiment with large rubber electrodes (35 cm^2 MR-compatible, neuroConn GmbH), electrodes were placed over occipital and frontal lobes underneath the EEG cap. In the experiment with small stimulation electrodes, two Ag/AgCl electrodes were used for the stimulation over right occipital and right parietal areas (electrodes O10 and CP4 of the 10–10 electrode system). Stimulation electrodes were attached using Ten20 conductive paste (Weaver and Company) and their impedance was kept below 2.5 kΩ. To minimize magnetic artifacts produced by the stimulation current, we carefully twisted the stimulation cables.

2.3. Data acquisition and preprocessing

We simultaneously recorded the EEG (NeurOne system, Mega Electronics Ltd) and 272-channel MEG (Omega 2000, CTF Systems) throughout the tACS experiment at 10,000 Hz and 2,343.8 Hz sampling rate, respectively. Due to the placement of stimulation electrodes, the EEG was recorded with 62 and 72 electrodes in the experiments with large and small stimulation electrodes, respectively. EEG electrodes were positioned based on the 10–10 electrode system using an EEG cap (EC80, Easycap). All signals were in the dynamic range of the recording systems. No clipping was observed for either EEG or MEG signals. Due to the interference between stimulation currents and electrical currents of the head-positioning circuits of the MEG system, we could not monitor head movement continuously during the stimulation experiments.

EEG electrodes were attached using Abratyl 2000 conductive gel and impedances were kept below 2.5 kΩ for most electrodes. We referenced EEG electrodes to FCz and positioned a ground electrode on the right forearm. EEG signals were re-referenced to average reference offline. Along with EEG and MEG, we recorded the injected current, the ECG and respiratory movements using bipolar channels of the EEG system. The injected current was indirectly measured by recording the voltage drop across a 200 Ω resistor positioned in series to the head. The ECG was recorded through 2 electrodes placed below the right clavicle and below the left pectoral muscle. Respiration was continuously recorded with a piezo respiratory belt transducer (Vermed-Medizintechnik).

In the second experiment, the head localization system of the MEG device was used to continuously measure 10 minutes of one subject's head movement. The head position relative to the MEG sensors was measured using three head localization coils (nasion, left/right preauricular points) with the sampling rate of 24.4 Hz. The subject's ECG was simultaneously recorded as explained above.

2.4. Sinusoidal model subtraction

To remove an optimal sinusoidal model from artifactual signals, we fitted the amplitude, frequency and phase of a sinusoid to the MEG and EEG data and subtracted it from the data. For this, it is important to estimate the stimulation frequency with μHz accuracy. This is because, if the internal clocks of the stimulation and recording systems are not synchronized, as in the present case, even small errors of the estimated stimulation frequency lead to strong residual artifacts around the main peak. To this end, we first chose 20 MEG channels with strongest tACS artifacts and split their data into 33 s long segments on which we fitted amplitude, frequency and phase of a sinusoidal model separately for each channel. We estimated the stimulation frequency as the median across all segments and channels (standard deviation of 8.50 and 4.85 μHz, for 11 Hz and 62 Hz tACS, respectively). Next, we defined a new sinusoidal model fixing its frequency at the estimated stimulation frequency. We then separately fitted amplitude and phase of this new model to each segment and channel and removed it from the data.

We followed a similar strategy for EEG. As we also recorded the injected current with the EEG system, this allowed for estimating the stimulation frequency based on the injected current. This is more accurate than estimation based on the EEG signal, because the injected current does not include any brain signals. As for the MEG, we split the injected current into 33 s long segments and estimated the stimulation frequency for each piece. We estimated the stimulation frequency as the median across all segments (standard deviation of 0.10 and 0.66 μHz, for 11 Hz and 62 Hz tACS, respectively).

2.5. Spectral analyses

To estimate the high-resolution power spectral density (PSD), we first split the data into 33 s segments. Then, we applied a Hanning window to each segment and computed its Fourier transform. Finally, we calculated the average power across all segments and scaled the results to PSD (μV^2/Hz and fT^2/Hz for EEG and MEG, respectively). The power spectrum of the beamformed data was calculated analogously on 5 s segments.

The PSD of the mean-removed head movement was calculated as above, using 30 s segments (M^2/Hz). For simulating the effect of amplitude modulation using head movement signal, we multiplied the normalized head movement signal (x axis) with a sinusoid of amplitude one. As the sampling rate of the MEG was not an integer number, signal segments were not exactly 30 s long. Therefore, to avoid power leakage of the main peak to nearby frequencies, we set the sinusoid's frequency equal to the sampled FFT frequency that was closest to 11 Hz.

Heartbeat and respiration rates were defined as the inverse of the median of temporal intervals between successive ECG R-peaks and respiration ends, respectively.

2.6. Head movement

The MEG's localization coil movement data were converted to head movements using the method presented in Stolk et al. (2013).

2.7. Beamforming

We applied adaptive linear spatial filtering (beamforming) (Van Veen et al., 1997) to the MEG data of the experiment with small stimulation electrodes and 11 Hz tACS. The procedure was exactly as explained in Noury et al. (2016). Data were band-passed using a 6th-order zero-phase Butterworth high-pass filter at 2 Hz and a low-pass filter at 90 Hz. Then, we notch filtered line noise by means of a 6th-order zero-phase Butterworth band-stop filter from 49.8 Hz to 50.2 Hz band. We down-sampled the data to 585.94 Hz and calculated the covariance matrix based on the concatenated data of the 11 Hz tACS and sham conditions of both runs. Importantly, as explained in Noury et al. (2016), during application of tACS the high signal power caused by the stimulation artifact makes it difficult to determine the cutoff between brain signals and sensor noise. Thus, we set the regularization factor (λ), which is an estimate of measurement noise, based on sham recordings only. To this end, we applied PCA on the sham recordings, and set the regularization factor equal to the Eigenvalue of the PC at which the cumulative explained variance reached 99% of the total variance. Finally, based on the covariance matrix of pooled sham and stimulation data and on the regularization factor based only on sham data, for each source location, we calculated three orthogonal filters (one for each spatial dimension) and linearly combined them to a single filter in the direction of maximum variance.

To check the effect of the regularization factor on the beamforming results (Fig. 4), we also estimated source level activity using λ values of 0%, 1e-7%, 5%, 15%, 100%, 300% and 600%. These values were defined as percentages relative to the average power of MEG sensor-level signals during pooled sham and tACS conditions.

2.8. Source locations and physical forward model

We performed beamforming for a regular three-dimensional grid that covered the entire brain with 1-cm spacing in MNI space (2982 source locations). We nonlinearly transformed source locations into the individual head space using each participants' individual T1-weighted structural MRI. MEG sensors were aligned to the head geometry based on three fiducial points (nasion, left ear, right ear) that were registered before and after the MEG acquisition by three

head localization coils. To derive the physical relation between sources and sensors (leadfield), we employed a single-shell head model (Nolte, 2003).

2.9. Analysis software

All data analyses were performed in Matlab (MathWorks) using custom scripts and the open source toolbox Fieldtrip (Oostenveld et al., 2011).

3. tES artifacts

3.1. Physics underlying amplitude modulations of tES artifacts

EEG measures the voltage difference between a reference electrode and electrodes placed at different points on the head as defined by Ohm's law:

$$\Delta V = -\int \rho\, J.dl \qquad (1)$$

$$\Delta V_{eeg} = \alpha\ .\ \Delta V$$

Considering tES artifacts, ΔV stands for the voltage difference between two points on the body, ΔV_{eeg} is the voltage that the EEG device reports, α is a scale factor (close to one) that depends on electrode impedances, which may induce phase-shifts through capacitive effects, and on the input resistance of the EEG amplifier, J is the stimulation current density vector on the head (in A/m^2), ρ is the head's electrical resistivity (in Ω.m), dl is a path element, and the integral is along the path from the skin underlying the reference EEG electrode to the skin underlying a specific EEG electrode.

MEG, on the other hand, measures the magnetic fields generated by current sources mainly inside the MEG room. Under the quasi-static condition (Baillet et al., 2001), the magnetic field is defined by the Biot-Savart law:

$$B = \frac{\mu}{4\pi}\iiint_V \frac{(J\, dV)\times \acute{r}}{|\acute{r}|^3} \qquad (2)$$

For the case of tES artifacts, B is the artifactual magnetic field sensed by an MEG sensor, J is the stimulation current density vector in stimulation wires, stimulation electrodes, and on the head, $\acute{r}$ is the distance vector between the position of the electrical current and the MEG sensor, μ is the magnetic

permeability, and dV is the volume element. It is worth noting that recent findings indicate small phase shifts of tACS artifacts relative to the stimulation current, which may be due to the influence of time-varying electromagnetic waves produced by tACS currents (see Noury and Siegel, 2017 for more information on phase features of tES artifacts). In other words, the quasi-static estimation of magnetic fields during tACS (i.e. equation 2) may not reflect all aspects of the stimulation artifacts. However, the influence of such time-varying electromagnetic fields should be small, and thus, equation (2) can be used to explain the basic features of the stimulation artifact's amplitude.

From equations (1) and (2), it follows that the stimulation current linearly scales tES artifacts. Therefore, to identify the origin of any observed electromagnetic effect during tES, it is necessary to first closely examine the waveform of the injected current. In other words, one must make sure that the observed effects do not already exist in the output current of the stimulation device. In particular, it is necessary to rule out wrong conclusion resulting from a malfunction of the stimulation device (Noury et al., 2016). The stimulation current can be measured by recording the voltage drop across a small resistance positioned in series to the head by means of an EEG amplifier. Importantly, this resistance needs to be small enough that the produced voltage drop does not exceed the dynamic range of the EEG device.

TES artifacts would only linearly reflect the injected current, if except from the stimulation current no other part of the equations (1) and (2) was time varying. However, the EEG electrode impedance, the body's resistivity (i.e. ρ) (Fisch, 1999), and head position (i.e. $\acute{r}$) (Stolk et al., 2013) are all time varying. From equations (1) and (2) it follows that any change in the spatial pattern of the body's resistivity or electrode impedance, and any change in the distance between the stimulation current and the MEG sensors, results in a change of the observed tES artifact for EEG and MEG. In other words, because of the multiplications in equations (1) and (2), changes in α, ρ and $\acute{r}$ over time result in modulations of the amplitude of stimulation artifacts. For EEG, this is simply because any change in impedance changes the voltage drop measured by the EEG device. For MEG, moving a current source closer to an MEG sensor increases

the magnetic field that is sensed by that MEG sensor. It is worth noting that, as the stimulation current (J) is orders of magnitude bigger than normal physiological currents, the multiplications in (1) and (2) have magnifying effects such that even very small changes of α, ρ and $\acute{r}$ can lead to tES artifact modulations comparable to the strength of physiological signals of interest at the sensor level.

The above-mentioned amplitude modulation (AM) of stimulation artifacts in the time domain has a direct influence on the power spectrum of stimulation artifacts in the frequency domain. Because multiplication in the time domain translates to convolution in the frequency domain (Oppenheim and Schafer, 2009), amplitude modulation of artifacts, in the frequency domain leads to artifacts with symmetric power spectra and a wider bandwidth compared to the bandwidth of the injected current. In case of a stimulation current with a sharp main peak at f_{stim} and a modulation waveform with bandwidth W, the resulting tES artifact will have a bandwidth of $2W$ (i.e. the frequency band from $f_{stim} - W$ to $f_{stim} + W$), and a symmetric power spectrum that contains normal and mirrored versions of the spectrum of the modulation waveform around the main stimulation peak (Fig. 1). For the special case of tDCS, the artifact will occupy the frequency band from 0 to W.

Apart from the symmetricity of tES artifacts in the frequency domain, the artifacts' power spectra have other general features that derive from properties of the body's resistivity (ρ) and head position ($\acute{r}$). In general, temporal changes in ρ and $\acute{r}$ include both slow non-rhythmic components like sweating (for ρ) and head drift (for $\acute{r}$), and rhythmic components like eye blinks (for ρ), heartbeats, and respiration (for both ρ and $\acute{r}$, Dornhorst et al., 1952; Kristiansen et al., 2005; Michard, 2005; Nyboer et al., 1950; Pinheiro et al., 2010; Stolk et al., 2013). In the frequency domain, power spectra of these modulations have a general 1/f appearance due to the arrhythmic components, with several local peaks at frequencies of rhythmic variations and/or their harmonics (Fig. 2A). Therefore, as a results of the AM mechanism explained above, artifacts at the sensor level have a symmetric power spectrum that decays at frequencies away from the stimulation frequency, and shows symmetric local side peaks at the stimulation

frequency ± the fundamental and harmonic frequencies of rhythmic variations of ρ and $\acute{r}$ (Fig. 2B).

It is important to note that both, non-rhythmic and rhythmic components of the artifact amplitude modulation should be removed from the data before attempting to assess brain activity. However, a major problem for this is that no ground truth is currently available for evaluating the output of artifact cleaning methods. As suggested in Noury et al. (2016), in the absence of ground truth, one possibility is to use the known features of artifacts to test the presence of residual artifacts at different stages of artifact cleaning pipelines. Notably, because of the lack of information about specific features of non-rhythmic artifact modulations, it is particularly difficult to track and dissociate these non-rhythmic artifact modulations from brain activity. Nevertheless, the broadband symmetricity of the spectrum, and peaks related to heartbeat and respiration induced artifact modulations are two critical artifact features that can be used for such tests. Based on these two features, in Noury et al. (2016), we presented several methods for detecting and tracking artifacts in time, frequency and space, which we briefly present in the following.

3.2. Detecting artifacts in raw recordings

Prior to the application of artifact cleaning methods and in each subject, heartbeat and respiration-induced modulations of artifacts can be well detected in the time domain by analyzing each channel's artifact amplitude, time-locked to heartbeats and respiration. Another way is to determine local peaks of the high-resolution spectrum at frequencies around the stimulation frequency and to check if they match the predicted frequencies for artifactual side peaks based on the AM model as explained above. Compared to the time domain analysis, this is a less sensitive method, because it does not use all the information about the timing of heartbeats and respiration. Furthermore, in the frequency domain, several confounds may hinder the detection of rhythmic artifact modulations (Noury et al., 2016). In particular, power leakage of the main stimulation peak, strong non-rhythmic artifact modulation, and overlapping brain activity are three confounds that we briefly explain next.

Power leakage

If stimulation and recording devices share the same clock, the power spectrum is estimated with high resolution, and the data is segmented properly, the main peak at the stimulation frequency will be sharp and will not leak to nearby frequencies (Fig. 2B). However, normally this is not the case and, even after appropriate windowing, the strong peak at the stimulation frequency leaks to nearby frequencies, which may mask important details of the spectrum. As explained in Noury et al. (2016), to solve this problem and to uncover details of the power spectrum, one needs to first remove a non-linearly fitted sine model of the stimulation artifact from the recorded signal of each channel. This procedure not only substantially reduces the stimulation peak itself, but also its spectral leakage, which helps to uncover artifact peaks at frequencies close to the stimulation frequency (compare dark gray vs. magenta curves in Fig. 3C-F).

Non-rhythmic components

As explained above, non-rhythmic components of artifact modulations generate a symmetrical 1/f decay of the power spectrum around the stimulation frequency. In particular close to the stimulation frequency, this may mask artifactual peaks. As this contamination decays away from the stimulation frequency, side peaks related to harmonics of rhythmic modulations may be easier to detect than the side peaks at the fundamental frequency of rhythmic modulations (Fig. 3F).

Overlapping brain activity

Power spectra of M/EEG during tACS reflect both, brain activity and stimulation artifacts. Therefore, strong brain activity at the stimulation frequency may mask details of the artifact's spectrum and may influence its symmetric appearance (Fig. 3C, F). As the power of brain signals generally decays at higher frequencies, stimulation artifacts at higher frequencies are generally easier to observe (artifacts are easier observable in Fig. 3D, F than in Fig. 3C, E). Therefore, control stimulation conditions at high frequencies (for example in the high gamma range or higher) may be useful for revealing the spectral features of stimulation artifacts.

3.3. Detecting residual artifacts

The above-mentioned tools for detecting stimulation artifacts prior to application of artifact-cleaning methods may not be able to detect residual artifacts after artifact cleaning. As detailed in Noury et al. (2016), this is mainly due to two reasons. First, artifact-cleaning methods strongly attenuate artifacts. Therefore, brain activity may mask the spectral and temporal landmarks of residual artifacts. Second, artifact-cleaning methods (e.g., template subtraction) may destroy the consistent pattern of rhythmic artifactual modulations.

Importantly, difficulty in detecting the residual artifacts does not imply that they do not exist in the data. Therefore, ad-hoc tests are required to carefully evaluate how clean the output of an artifact-cleaning pipeline is. In Noury et al. (2016), we devised and applied several methods for evaluating the output of different artifact-cleaning methods based on the artifact features explained above. Relevant to the present paper, for beamforming we suggested to investigate the spatial distribution of power of the beamformed data at different frequencies. The stimulation artifact leads to a non-physiological relation between the stimulation frequency and AM-related side-peak frequencies. We argued that, for artifact free beamformed data, there should be no significant relation between signals at these frequencies. Therefore, we suggested to test if the spatial distribution of power at the stimulation frequency is significantly correlated to the spatial distribution of power at side peak frequencies (i.e., stimulation frequency ± heartbeat and respiration related frequencies). In case of a significant correlation, the beamformed data contains residual artifacts at the stimulation and side peak frequencies (see Figure 8e in Noury et al. 2016).

4. Reply to Neuling et al.

A recent paper (Neuling et al., 2017) claimed that the features of stimulation artifacts described in Noury et al. (2016) are merely due to technical problems of the stimulator or of the applied methods, and that these artifacts are largely absent in recordings of Neuling et al. Unfortunately, Neuling et al., (2017) made these claims without applying any of the critical artifact-detection tests that we suggested in Noury et al. (2016) to their data. In the following, we go through all

sections of Neuling et al. (2017), and show that none of their points are correct or applicable to our results.

4.1. Reply to "the origin of the nonlinear artifacts"

The central claim of this section of Neuling et al. (2017) is that the amplitude modulations reported in Noury et al. (2016) are due to technical problems of the stimulation device. This claim is wrong.

If the stimulation device is used beyond its technical limits, the output current of the stimulator may be non-sinusoidal, i.e. show increased harmonics, and may become time-varying, which leads to artifacts at frequencies surrounding the stimulation frequency. We carefully ruled this out for all our experiments. First, we directly measured the stimulation current generated by our stimulation device and ensured that this current was sinusoidal. According to the Biot-Savart law (eq. 2), direct evaluation of the stimulation current is the necessary and sufficient control analysis to rule out any technical issue related to the stimulation device. Unfortunately, Neuling et al. did not provide measurements or analyses of the applied stimulations currents for any of their work (Neuling et al. 2015, 2017). We showed that the stimulation current recorded during our experiments displayed neither any modulations locked to heartbeat or respiration in the time domain, nor side peaks at relevant frequencies in the frequency domain (Supplementary Figure 1 of Noury et al. 2016). Moreover, by fit and removal of a single sinusoidal model, we showed that at the stimulation and nearby frequencies, the output of our stimulation device was almost a pure sinusoid (Fig. 3A, B and Figure 2 of Noury et al. 2016). Thus, in contrast to the claim of Neuling et al. (2017), we did not reach the technical limits of our stimulator and none of the results presented in our paper can be attributed to a dysfunction of the stimulation device.

It should be noted that our experimental procedures were carefully designed to prevent any technical problems caused by using the stimulator beyond its technical limits. We kept each stimulation electrode's resistance below 2.5 K Ohm (Noury et al. 2016). Consequently, the stimulator had to produce less than 5 Volt peak-to-peak sine waves to drive a stimulation current of 1 mA peak-to-peak. In contrast to the claim of Neuling et al. (2017), this is far below the

dynamic range of the used stimulator (24 Volt and 6 mA peak-to-peak output voltage and output current, respectively).

Three, more points about this section of Neuling et al. (2017) should be addressed. First, as correctly pointed out by the authors, in their phantom experiments, their stimulation device failed to produce a single sinusoidal output with constant amplitude. This can be inferred from the fact that, although the melon phantom did not move during the experiment (i.e. constant $\acute{r}$ in eq. 2), the power spectrum of the magnetic field at the sensor level (i.e. B in eq. 2) shows more than one peak, which speaks for a non-sinusoidal stimulation current (i.e. J in eq. 2). This may have happened because of the 20 K Ohm electrode resistance of their tACS electrodes, which is much higher than the 2.5 K Ohm electrode resistance in our experiments (Noury et al., 2016).

The second point is related to the claim of Neuling et al. (2017) that, for their data, only 6 out of 17 subjects showed side peaks at the sensor level, and therefore data from most of their subjects were not contaminated with non-linear artifacts. This claim is not supported by sufficient evidence, because the authors did not apply any of the critical tests to detect artifacts. As we pointed out before (Noury et al., 2016) and above, it is important to first eliminate the spectral leakage of the main stimulation peak by fit and removal of a sine model for each sensor, before being able to assess the details of the spectrum. Unfortunately, Neuling et al. did not perform this critical analysis step. Moreover, averaging over sensors blurs details of the spectra. However, even under this condition, all power spectra presented in Figure 1a of Neuling et al. (2017) are highly symmetric around the stimulation frequency, which is a strong indication for a potential amplitude modulation of the tACS artifact. Even if after careful evaluation of the power spectrum, heartbeat and respiration-related side peaks are not present, a simple heartbeat or respiration-locked time-domain analysis of the artifact envelope must be applied, before concluding the absence of artifact modulations. Unfortunately, Neuling et al. (2017) did not perform this critical analysis.

Third, Neuling et al. assessed source level power spectra to evaluate how clean the beamformed data was. As explained in the previous section, this test is not

sufficiently sensitive. We also did not observe clear side peaks in our data at the source level (Fig. 4A). Therefore, in our original paper (Noury et al., 2016), we suggested and demonstrated the use of a cross-frequency spatial correlation analysis to investigate the presence of residual artifacts at the source level. Again, unfortunately, Neuling et al. (2017) did not perform this critical analysis.

4.2. Reply to "methodological concerns"

In this section, Neuling et al. (2017) claim that tES artifact modulations may be related to the use of small stimulation electrodes in Noury et al. (2016), and question if artifact modulations also hold for big stimulation electrodes. This claim is wrong and surprising, because in our original paper, we already provided results of a control experiment with big stimulation electrodes that clearly showed strong heartbeat and respiration-related artifact modulations (Figure. 6 of Noury et al., 2016). To further investigate this, we re-calculated the power spectra of this control experiment with higher spectral resolution (Fig. 3). In accordance with our previous results (Figure 6 of Noury et al., 2016) and in contrast to the claim of Neuling et al. (2016), high-resolution power spectra showed clear side peaks at heartbeat and respiration frequencies as well as at their harmonic frequencies. Notably, in accordance with our findings, another recent tDCS study with large stimulation electrodes by an independent group of researchers (Marshall et al., 2015) also showed heartbeat-induced nonlinear stimulation artifacts at sensor and source levels. In sum, these results falsify the claim of Neuling et al. (2017) and show amplitude modulations of tACS artifacts for both, small and large stimulation electrodes.

4.3. Reply to "the real tACS signal"

This section of Neuling et al. (2017) again builds on the wrong assumption that the non-linear artifact modulations shown in our paper (Noury et al. 2016) are due to a stimulator dysfunction and non-sinusoidal stimulation currents. As discussed above, evidence presented in our original and current paper clearly falsifies this assumption and shows that stimulation currents were sinusoidal (Fig. 3A, B and Figure 2 of Noury et al. 2016).

If the stimulation current that is generated by the stimulator is not modulated, but the measured EEG voltages show modulations, what does this imply for the

effect of tES on neurons? The effect on neurons depends only on the current that reaches them. In the present situation, the sum of stimulation currents flowing through the head is constant, i.e. equal to the stimulation current generated by the stimulator. But, the way that the current flows are distributed through the head may vary over time. For example, these variations could result from changes of the relative resistivity of the skull and the scalp, or of the relative resistivity of different parts of the scalp. Neurons experience such rhythmic and non-rhythmic modulations only if the spatial pattern of tES current flows varies in such a way that the currents that reach neurons are modulated. Our PCA analysis suggests that rhythmic changes in the spatial distribution of the stimulation currents indeed happen, but that these rhythmic variations are about 1000 times smaller than the average tES current (Figures 3 and 4 of Noury et al., 2016). Thus, future simulation studies and invasive recordings are required to clarify to what extent rhythmic as well as non-rhythmic changes in current distribution reach neurons, and if neural responses are affected by these modulations (Ali et al., 2013; Fröhlich and McCormick, 2010; Huang et al., 2017; Opitz et al., 2016, 2015).

4.4. Reply to "regularization impedes beamforming performance"

In this section, Neuling et al. claim that the regularization factor (λ) used in our original paper (Noury et al. 2016) was not optimal. This claim is wrong.

Figure 2 of Neuling et al. (2017) shows the effect of λ on beamforming of tACS-MEG data. The figure shows that the strength of residual artifacts, i.e. the peak at the stimulation frequency, monotonically increases with increasing λ. In this figure, the peak of the curve that is claimed to correspond to our method is bigger than the peak of the curve for a λ of 100 % of the average MEG power. However, the average regularization factor that we used in Noury et al. (2016) was 2.5e-6 % of the average MEG power (4e-7 % STD across subjects). Thus, it follows that Neuling et al. did not correctly apply our method, but mistakenly assigned a λ bigger that 100% to our method. To correct this mistake of Neuling et al., we replicated their analysis with the correct λ for our method and found that, as expected, the results for our method were indistinguishable from the results for a λ of zero or 7e-7 %. In sum, Neuling et al. applied a wrong (too high)

regularization parameter for what was claimed to be 'our method'. Our results were not affected by such a wrong regularization.

Furthermore, related to this section of Neuling et al. (2017), it should be pointed out again that average power spectra, as provided by Neuling et al., are insufficient to conclude that source-level data is artifact free. As mentioned above, we also did not observe side peaks in the averaged source level power spectrum (Fig. 4A). In fact, in our paper we did not make any claims concerning the appearance of the source level power spectrum. But, as explained before, difficulty in detecting artifactual side peaks in spectrum does not imply that the source level data is artifact free, especially because side peaks only represent the rhythmic part of artifact modulations. Therefore, we introduced a more sensitive test, which is evaluating the spatial distribution of power at different frequencies. Unfortunately, Neuling et al. (2017) did not perform this analysis.

5. Discussion

Here, we discussed the physics underlying amplitude modulations of tES artifacts in EEG and MEG. These amplitude modulations are independent of the stimulation device or electrode size, and contain both non-rhythmic and rhythmic components. Both components should be removed from data before investigating brain activity. Rhythmic components generate landmarks in the data, and thus, provide opportunities to detect and track tES artifacts at different processing stages. We went through all points raised in Neuling et al. (2017) and showed that none of these points are correct or applicable to our results.

Stimulation artifacts in EEG and MEG are orders of magnitude larger than brain signals and have complex phase and amplitude features. However, it should be emphasized that it may still be possible to investigate brain activity during tES.

One approach is to employ new stimulation protocols that prevent tES artifacts in the frequency band of interest (Witkowski et al., 2016). The potential of such new stimulation protocols to manipulate brain activity should be thoroughly investigated (Chander et al., 2016). Another approach is to use established stimulation protocols, and employ artifact-removal pipelines to suppress stimulation artifacts strongly enough to be able to study brain activity in

presence of residual artifacts. For this approach, it should be noted that all available artifact-cleaning pipelines, including beamforming, strongly attenuate tES artifacts. Therefore, it may be possible to devise specific measures or control experiments to check for the influence of residual artifacts. In the following, we first discuss why beamforming is unable to completely remove stimulation artifacts, and then provide ideas on how to account for residual artifacts and study brain activity in their presence.

5.1. Beamforming as an artifact removal method

Although beamforming strongly reduces tES artifacts, it cannot completely remove them. Beamformed data contains residual artifacts (Marshall et al., 2015; Noury et al. 2016). We suggest that this is largely due to time varying (Noury et al. 2016) and phase-shifted (Noury and Siegel, 2017) artifact-leadfields. The former factor is a result of artifact amplitude modulations caused by head movements and body impedance changes. This leads to time varying pattern of tES artifacts at the sensor level. Therefore, a time invariant beamforming filter is not able to remove tES artifacts at all time points. The latter factor manifests itself in artifact phase deflections at the sensor level (Noury and Siegel, 2017). For both, EEG and MEG, tACS artifacts are not pure in-phase or anti-phase sinusoids, but have different phase shifts relative to the stimulation current, which is probably due to capacitive effects and time varying electromagnetic fields for EEG and MEG, respectively (see Noury and Siegel, 2017 for more information on phase features of tES artifacts). Theoretically, both factors can be modeled as artifact sources that are not 100% correlated with each other. Consequently, beamforming results contain residual artifacts that result from to the uncorrelated part of stimulation artifact (Mäkelä et al., 2017). In sum, beamforming results contain residual artifacts that should be accounted for. Next, we present some ideas how to cope with residual artifacts.

5.2. Artifact-sensitive control experiments

TES artifacts are easier observable at higher frequencies, for which MEG and EEG contain weaker physiological signals. Therefore, artifact-sensitive control experiments with high stimulation frequencies may be used to evaluate the strength and effects of residual artifacts. This is particularly useful when the

tACS frequency of interest is in the alpha range or below, because at these low frequencies, strong brain signals mask the detectable features of tES artifacts, which in turn complicates estimating the strength of residual artifacts. Although tES may influence brain signals at any frequency, it seems unlikely that the very same physiological effects can be produced by stimulating at very different frequencies. Thus, one can compare the observed effects of tES at the main stimulation frequency of interest with effects at tES at a higher artifact-sensitive control frequency to check if residual artifacts could drive the effects observed at the main tES frequency of interest.

5.3. Event related responses

Residual artifacts have little effect on event related potentials and fields. If tES waves are not time-locked to stimuli, and physiological processes do not become time-locked to either stimuli or tES waves, averaging brain responses time-locked to stimuli cancels out tES artifacts. In this situation, residual artifacts merely increase the noise level of trials. Therefore, the number of trials needed to obtain specific results will be larger than for experiments without tES.

5.4. Contrasting two populations under the same tES condition

If two signal populations contain the same amounts of tES artifacts, one can subtract their mean values from each other to cancel the effect of tES artifacts and to quantify the difference of brain activity between the two populations during tES. For example, these populations can be obtained from M/EEG signals at two different trial time-points, or from M/EEG signals of two different cognitive states. Importantly, both populations should be measured under the exact same tES condition. Furthermore, to ensure the same average residual artifacts for both populations, it needs to be ensured that the two populations have the same physiological states (heart rate, respiratory rate, body resistance etc.).

To give an example, one may ask if alpha power decrease or gamma power increase due to visual stimulation differs between sham and tES conditions. If there was no temporal relationship between tES waves and visual stimuli, and visual stimulation did not affect the physiological states of subjects, one may

assume the same levels of residual tES artifacts before and after stimulation onset. Under this condition, the average power of these time points could be subtracted from each other, and the results from sham and tES conditions could be compared. However, it is important to note that during tES, the power at each time point contains residual tES artifacts. Therefore, non-linear contrasts like "percent change relative to baseline" cannot be compared between sham and stimulation conditions, simply because the baseline during tES contains residual artifacts, which is not the case for the sham condition.

5.6. Simulation

Another approach would be to quantitatively evaluate the performance of an available artifact-cleaning pipeline, and to check if the observed M/EEG effects could be attributed to residual artifacts. Currently, no phantom is available that reflects all features of tES artifacts. However, computer simulations could be used for such evaluations (Noury and Siegel, 2017). First, different features of tES artifacts can be estimated from sensor level recordings. Based on these features, simulated tES artifacts could be added to sham data. Then, the effect of artifact-cleaning of this simulated data could be compared to the results of artifact-cleaning of the real tES data to estimate if the observed effects could be accounted for by residual artifacts.

Acknowledgements

This work was supported by the Centre for Integrative Neuroscience (Deutsche Forschungsgemeinschaft, EXC 307). We thank Marcus Siems for providing the MEG head movement recordings, and Florian Sandhäger and Marcus Siems for their valuable comments on the manuscript.

References

Ali, M.M., Sellers, K.K., Fröhlich, F., 2013. Transcranial Alternating Current Stimulation Modulates Large-Scale Cortical Network Activity by Network Resonance. J. Neurosci. 33, 11262–11275. doi:10.1523/JNEUROSCI.5867-12.2013

Baillet, S., Mosher, J.C., Leahy, R.M., 2001. Electromagnetic brain mapping. IEEE Signal Process. Mag. 18, 14–30. doi:10.1109/79.962275

Bergmann, T.O., Karabanov, A., Hartwigsen, G., Thielscher, A., Siebner, H.R., 2016. Combining non-invasive transcranial brain stimulation with neuroimaging and electrophysiology: Current approaches and future perspectives. NeuroImage 140, 4–19. doi:10.1016/j.neuroimage.2016.02.012

Brittain, J.-S., Probert-Smith, P., Aziz, T.Z., Brown, P., 2013. Tremor suppression by rhythmic transcranial current stimulation. Curr. Biol. CB 23, 436–440. doi:10.1016/j.cub.2013.01.068

Chander, B.S., Witkowski, M., Braun, C., Robinson, S.E., Born, J., Cohen, L.G., Birbaumer, N., Soekadar, S.R., 2016. tACS Phase Locking of Frontal Midline Theta Oscillations Disrupts Working Memory Performance. Front. Cell. Neurosci. 120. doi:10.3389/fncel.2016.00120

Dornhorst, A.C., Howard, P., Leathart, G.L., 1952. Respiratory Variations in Blood Pressure. Circulation 6, 553–558. doi:10.1161/01.CIR.6.4.553

Fertonani, A., Miniussi, C., 2016. Transcranial Electrical Stimulation: What We Know and Do Not Know About Mechanisms. Neurosci. Rev. J. Bringing Neurobiol. Neurol. Psychiatry. doi:10.1177/1073858416631966

Fisch, B., 1999. Fisch and Spehlmann's EEG Primer: Basic Principles of Digital and Analog EEG, 3e, 3 edition. ed. Elsevier, Amsterdam; New York.

Fröhlich, F., McCormick, D.A., 2010. Endogenous Electric Fields May Guide Neocortical Network Activity. Neuron 67, 129–143. doi:10.1016/j.neuron.2010.06.005

Helfrich, R.F., Schneider, T.R., Rach, S., Trautmann-Lengsfeld, S.A., Engel, A.K., Herrmann, C.S., 2014. Entrainment of Brain Oscillations by Transcranial Alternating Current Stimulation. Curr. Biol. 24, 333–339. doi:10.1016/j.cub.2013.12.041

Huang, Y., Liu, A.A., Lafon, B., Friedman, D., Dayan, M., Wang, X., Bikson, M., Doyle, W.K., Devinsky, O., Parra, L.C., 2017. Measurements and models of electric fields in the in vivo human brain during transcranial electric stimulation. eLife 6, e18834. doi:10.7554/eLife.18834

Kristiansen, N.K., Fleischer, J., Jensen, M.S., Andersen, K.S., Nygaard, H., 2005. Design and evaluation of a handheld impedance plethysmograph for measuring heart rate variability. Med. Biol. Eng. Comput. 43, 516–521.

Kuo, M.-F., Nitsche, M.A., 2012. Effects of transcranial electrical stimulation on cognition. Clin. EEG Neurosci. 43, 192–199. doi:10.1177/1550059412444975

Lustenberger, C., Boyle, M.R., Alagapan, S., Mellin, J.M., Vaughn, B.V., Fröhlich, F., 2016. Feedback-Controlled Transcranial Alternating Current Stimulation Reveals a Functional Role of Sleep Spindles in Motor Memory Consolidation. Curr. Biol. 26, 2127–2136. doi:10.1016/j.cub.2016.06.044

Mäkelä, N., Sarvas, J., Ilmoniemi, R.J., 2017. Proceedings #17. A simple reason why beamformer may (not) remove the tACS-induced artifact in MEG. Brain Stimulat. 10, e66–e67. doi:10.1016/j.brs.2017.04.110
Marshall, T.R., Esterer, S., Herring, J.D., Bergmann, T.O., Jensen, O., 2015. On the relationship between cortical excitability and visual oscillatory responses - A concurrent tDCS-MEG study. NeuroImage. doi:10.1016/j.neuroimage.2015.09.069
Michard, F., 2005. Changes in arterial pressure during mechanical ventilation. Anesthesiology 103, 419–428; quiz 449–445.
Neuling, T., Ruhnau, P., Fuscà, M., Demarchi, G., Herrmann, C.S., Weisz, N., 2015. Friends, not foes: Magnetoencephalography as a tool to uncover brain dynamics during transcranial alternating current stimulation. NeuroImage 118, 406–413. doi:10.1016/j.neuroimage.2015.06.026
Neuling, T., Ruhnau, P., Weisz, N., Herrmann, C.S., Demarchi, G., 2017. Faith and oscillations recovered: On analyzing EEG/MEG signals during tACS. NeuroImage 147, 960–963. doi:10.1016/j.neuroimage.2016.11.022
Nolte, G., 2003. The magnetic lead field theorem in the quasi-static approximation and its use for magnetoencephalography forward calculation in realistic volume conductors. Phys. Med. Biol. 48, 3637. doi:10.1088/0031-9155/48/22/002
Noury, N., Hipp, J.F., Siegel, M., 2016. Physiological processes non-linearly affect electrophysiological recordings during transcranial electric stimulation. NeuroImage 140, 99–109. doi:10.1016/j.neuroimage.2016.03.065
Noury, N., Siegel, M., 2017. Phase properties of transcranial electrical stimulation artifacts in electrophysiological recordings. NeuroImage 158, 406–416. doi:10.1016/j.neuroimage.2017.07.010
Nyboer, J., Kreider, M.M., Hannapel, L., 1950. Electrical Impedance Plethysmography A Physical and Physiologic Approach to Peripheral Vascular Study. Circulation 2, 811–821. doi:10.1161/01.CIR.2.6.811
Opitz, A., Falchier, A., Yan, C.-G., Yeagle, E.M., Linn, G.S., Megevand, P., Thielscher, A., Deborah A., R., Milham, M.P., Mehta, A.D., Schroeder, C.E., 2016. Spatiotemporal structure of intracranial electric fields induced by transcranial electric stimulation in humans and nonhuman primates. Sci. Rep. 6, 31236. doi:10.1038/srep31236
Opitz, A., Paulus, W., Will, S., Antunes, A., Thielscher, A., 2015. Determinants of the electric field during transcranial direct current stimulation. NeuroImage 109, 140–150. doi:10.1016/j.neuroimage.2015.01.033
Oppenheim, A.V., Schafer, R.W., 2009. Discrete-Time Signal Processing, 3 edition. ed. Pearson, Upper Saddle River.
Pinheiro, E., Postolache, O., Girão, P., 2010. Theory and Developments in an Unobtrusive Cardiovascular System Representation: Ballistocardiography. Open Biomed. Eng. J. 4, 201–216. doi:10.2174/1874120701004010201
Romei, V., Thut, G., Silvanto, J., 2016. Information-Based Approaches of Noninvasive Transcranial Brain Stimulation. Trends Neurosci. 39, 782–795. doi:10.1016/j.tins.2016.09.001
Soekadar, S.R., Witkowski, M., Cossio, E.G., Birbaumer, N., Robinson, S.E., Cohen, L.G., 2013. In vivo assessment of human brain oscillations during

application of transcranial electric currents. Nat. Commun. 4. doi:10.1038/ncomms3032
Stolk, A., Todorovic, A., Schoffelen, J.-M., Oostenveld, R., 2013. Online and offline tools for head movement compensation in MEG. NeuroImage 68, 39–48. doi:10.1016/j.neuroimage.2012.11.047
Thut, G., Bergmann, T.O., Fröhlich, F., Soekadar, S.R., Brittain, J.-S., Valero-Cabré, A., Sack, A.T., Miniussi, C., Antal, A., Siebner, H.R., Ziemann, U., Herrmann, C.S., 2017. Guiding transcranial brain stimulation by EEG/MEG to interact with ongoing brain activity and associated functions: A position paper. Clin. Neurophysiol. 128, 843–857. doi:10.1016/j.clinph.2017.01.003
Van Veen, B.D., van Drongelen, W., Yuchtman, M., Suzuki, A., 1997. Localization of brain electrical activity via linearly constrained minimum variance spatial filtering. IEEE Trans. Biomed. Eng. 44, 867–880. doi:10.1109/10.623056
Voss, U., Holzmann, R., Hobson, A., Paulus, W., Koppehele-Gossel, J., Klimke, A., Nitsche, M.A., 2014. Induction of self awareness in dreams through frontal low current stimulation of gamma activity. Nat. Neurosci. advance online publication. doi:10.1038/nn.3719
Witkowski, M., Garcia-Cossio, E., Chander, B.S., Braun, C., Birbaumer, N., Robinson, S.E., Soekadar, S.R., 2016. Mapping entrained brain oscillations during transcranial alternating current stimulation (tACS). NeuroImage, Transcranial electric stimulation (tES) and Neuroimaging 140, 89–98. doi:10.1016/j.neuroimage.2015.10.024

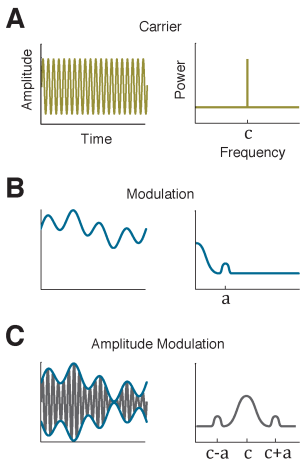

Figure 1. Schematic illustration of amplitude modulation (AM) in the time (left) and frequency (right) domain. In this example, the carrier signal (A) is a pure sinusoidal wave with constant amplitude. The ideal estimation of the power spectrum of such a signal contains only a sharp peak at the carrier frequency *c*. A modulation wave shows slow variations over time (B left). These variations can be rhythmic or arrhythmic. Rhythmic variations correspond to a peak in the power spectrum at frequency *a*, and non-rhythmic variations correspond to a power increase at low frequencies (B right). Multiplying the carrier signal with the modulation wave yields the amplitude-modulated signal (C left). Multiplication in the time domain corresponds to convolution in the frequency domain. Therefore, the power spectrum of the amplitude-modulated signal is symmetric, with the power spectrum of the modulation wave and its mirrored version around the carrier frequency.

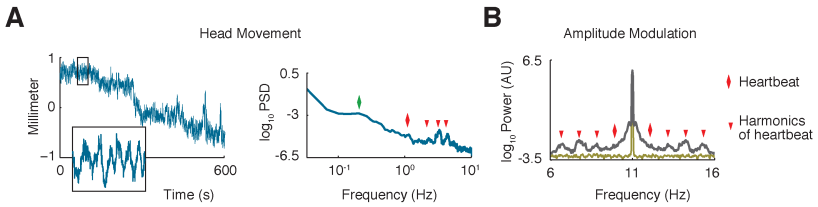

Figure 2. (A) The left panel shows, ten minutes of a healthy subject's head movement in the MEG system. Head movements contain both, rhythmic and non-rhythmic components. The inset shows 30 s of rhythmic head movements. The right panel shows the power spectrum of the same head-movement data. While non-rhythmic movements have a 1/f power spectrum, rhythmic movements lead to observable peaks in the power spectrum. In particular, heartbeats lead to rhythmic head movements. The red rhombus indicates the heartbeat frequency and red triangles indicate its harmonics. (B) Modulating the amplitude of an 11 Hz sinusoid with the normalized head movement signal yields a symmetric power spectrum. Heartbeat related peaks are symmetric around the 11 Hz peak. Also the 1/f head-movement component is reflected symmetrically around the 11 Hz peak.

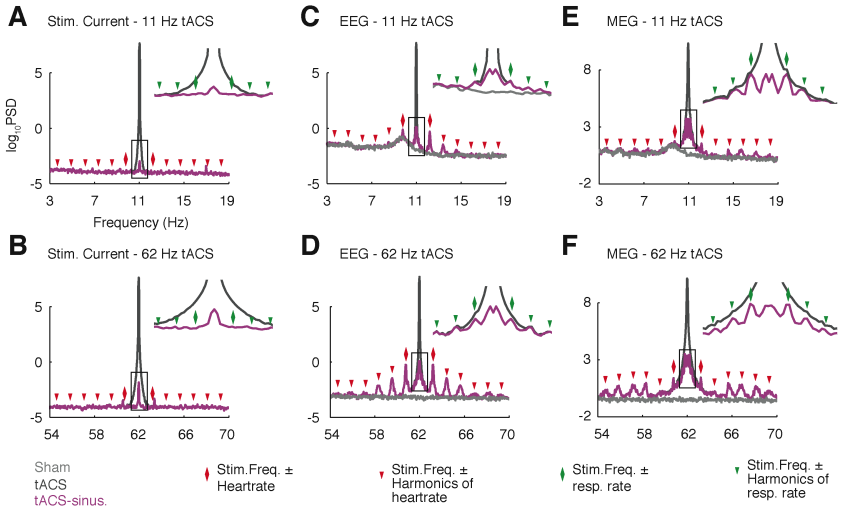

Figure 3. Stimulation artifacts in the frequency domain for tACS experiment with large rubber stimulation electrodes. (A, B) High resolution power spectral density of the stimulation current (gray) around the stimulation frequency for 11 Hz and 62 Hz tACS. Smaller subplots show the power spectra zoomed into the stimulation frequency ± 1 Hz. Importantly, subtracting a sinusoidal model from the stimulation current (magenta) removes almost all power of the stimulation current. This shows that the technical limits of the stimulator were not reached, and that the stimulator successfully generated a pure sinusoidal output current at the stimulation frequencies. (C, D) EEG power spectral density around the stimulation frequency during sham and tACS, with and without removal of a sinusoidal artifact model. (E, F) MEG power spectra for sham and tACS. Red and green rhombuses mark the stimulation frequency ± individual average heartbeat and respiration frequencies, respectively. Triangles mark harmonics of heartbeat and respiration frequencies. Peaks of EEG and MEG power are at the frequencies related to physiological processes. Subtracting the sinusoidal artifact uncovers details of the power spectrum for frequencies close to the stimulation frequency. In addition to side peaks, power spectra contain symmetric 1/f components, which likely reflect arrhythmic artifactual amplitude modulations. EEG and MEG data show channels CPz and MRT34, respectively.

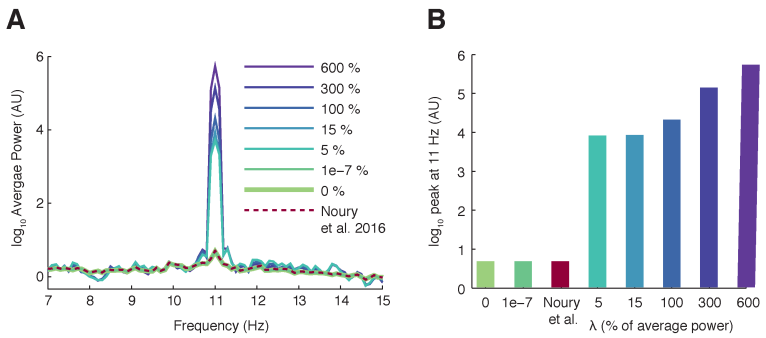

Figure 4. Influence of the regularization factor (λ) on beamforming results. (A) Average source level power at the stimulation and nearby frequencies in one subject. Each curve corresponds to beamforming with a specific λ. Percentage is relative to the average MEG power during both sham and tACS. Darker curves have higher λ values. Note that some of the curves overlap with each other. The red dashed line corresponds to the λ used in Noury et al. (2016) (0.0000032% for this subject). (B) The average power at the stimulation frequency (11 Hz) is monotonically related to λ.

Acknowledgment

I would like to thank all current and previous members of the **Siegellab**, especially for all the inspiring discussions during our marathon all2all journal clubs! Among them, a special thanks to **Jörg Hipp**, who was not only a great colleague with good ideas, but also a reliable friend and belayer. Thank you, **Constantin von Nicolai** for your friendship and of course for the proof reading. Thanks to **Marcus Siems** and **Constantin von Nicolai** for being patient subjects and letting me decrease the EEG electrode impedances as much as I want. A big thanks to my supervisor **Markus Siegel**, especially for trusting me at the very beginning! Working with you was a valuable experience. I learned a lot and always enjoyed discussing scientific and non-scientific issues and topics with you. Thanks for all the moments that you devoted to me and to my project, even during your vacations!

Thank you to all the people at the other side of the corridor. I really enjoyed hearing you laugh every now and then. Thanks for tasty pastas and warm coffees. Thank you, **Christoph Braun,** for being a nice Boss and employing all these friendly people.

I also want to thank my advisory board members, i.e., **Peter Thier**, **Bin Yang** and **Markus Siegel** for the time they devoted to my project and their feedback. Thank you, **Bin Yang,** for traveling from Stuttgart to Tübingen for each meeting!

Finally, I want to truly thank my family and friends. First of all, thanks to my dear parents, **Razieh Tavassoli** and **Asghar Noury** for all their love for me, and all the sacrifices they made for me! You mean a lot to me! Thanks to **Pirkko Jahn** for all her love and support! There would have been no Germany, no Tübingen, and maybe no PhD for me without you. Thanks for all the new windows you added to my life, and thanks for helping me to go out of my room and take a walk in the woods! Thanks a lot, **Farhad Meysami**. I will never forget all the inspiring moments we spent together. Thanks for always having a cup of Iranian tea for me! I would also like to thank **Oma**, i.e. **Sophie Jahn** for her hospitality in the first months that I arrived in Germany. Thanks for taking me to the train station every time that I was late!